

Alma Mater Studiorum – Università di Bologna

DOTTORATO DI RICERCA IN

Meccanica e Scienze Avanzate dell'Ingegneria
Prog.3 Meccanica Applicata

Ciclo: XXIV

Settore Concorsuale di afferenza: 09/A2

Settore Scientifico disciplinare: ING-IND/13

A Design Method for Flexure-Based Compliant Mechanisms on the Basis of Stiffness and Stress Characteristics

Presentata da:

Ing. Qiaoling Meng

Coordinatore Dottorato:

Prof. Vincenzo Parenti Castelli

Relatore:

Prof. Vincenzo Parenti Castelli

Correlatori:

Dr. Giovanni Berselli

Dr. Rocco Vertechy

To my father



Abstract

Geometric nonlinearities of flexure hinges introduced by large deflections often complicate the analysis of compliant mechanisms containing such members, and therefore, Pseudo-Rigid-Body Models (PRBMs) have been well proposed and developed by Howell [29] to analyze the characteristics of slender beams under large deflection. These models, however, fail to approximate the characteristics for the deep beams (short beams) or the other flexure hinges. Lobontiu's work [46] contributed to the diverse flexure hinge analysis building on the assumptions of small deflection, which also limits the application range of these flexure hinges and cannot analyze the stiffness and stress characteristics of these flexure hinges for large deflection.

Therefore, the objective of this thesis is to analyze flexure hinges considering both the effects of large-deflection and shear force, which guides the design of flexure-based compliant mechanisms. The main work conducted in the thesis is outlined as follows.

- Three popular types of flexure hinges : (circular flexure hinges, elliptical flexure hinges and corner-filletted flexure hinges) are chosen for analysis at first.
 - Commercial software (Comsol) based Finite Element Analysis (FEA) method is then used for correcting the errors produced by the equations proposed by Lobontiu when the chosen flexure hinges suffer from large deformation.
 - Three sets of generic design equations for the three types of flexure hinges are further proposed on the basis of stiffness and stress characteristics from the FEA results.
 - A flexure-based four-bar compliant mechanism is finally studied and modeled using the proposed generic design equations. The load-displacement relationships are verified by a numerical example. The results show that a maximum error about the relationship between moment and rotation deformation is less than 3.4% for a flexure hinge, and it is lower than 5% for the four-bar compliant mechanism compared with the FEA results.
-

Contents

| | | |
|----------|---|-----------|
| 1 | Introduction | 17 |
| 1.1 | The Role of Flexure-Based Compliant Mechanisms(FCMs) | 17 |
| 1.2 | Motivation | 19 |
| 1.3 | Contribution of the Thesis | 21 |
| 1.4 | Thesis Outline | 22 |
| 2 | Flexure Hinges and Beam Theory | 25 |
| 2.1 | Flexure Hinges | 25 |
| 2.2 | Beam Theory | 30 |
| 2.3 | PRBM | 32 |
| 2.3.1 | Brief literature review about PRBM | 32 |
| 2.3.2 | Beam theory in PRBM | 34 |
| 3 | Stiffness-Based Design of Flexure Hinges | 37 |
| 3.1 | Stiffness Mathematical Formulas for Small Deformation | 37 |
| 3.1.1 | Circular flexure hinges | 39 |
| 3.1.2 | Elliptical flexure hinges | 40 |
| 3.1.3 | Corner-filletted flexure hinges | 41 |
| 3.2 | Stiffness Mathematical Formulas for Large Deflection | 42 |
| 3.2.1 | Circular flexure hinges | 43 |
| 3.2.2 | Elliptical flexure hinges | 46 |
| 3.2.3 | Corner-filletted flexure hinges | 50 |
| 4 | Stress-Based Design of Flexure Hinges | 57 |
| 4.1 | Circular Flexure Hinges | 58 |
| 4.1.1 | Capacity of rotation | 58 |
| 4.1.2 | Material characteristic | 60 |
| 4.1.3 | Geometric characteristic | 60 |

| | | |
|----------|---|------------|
| 4.2 | Elliptical Flexure Hinges | 62 |
| 4.2.1 | Capacity of rotation | 62 |
| 4.2.2 | Material characteristic | 63 |
| 4.2.3 | Geometric characteristic | 64 |
| 4.3 | Corner-Filletted Flexure Hinges | 65 |
| 4.3.1 | Capacity of rotation | 65 |
| 4.3.2 | Material characteristic | 67 |
| 4.3.3 | Geometric characteristic | 67 |
| 5 | Discussion and Error Analysis | 69 |
| 5.1 | Evaluation of Stiffness Generic Design Equations | 70 |
| 5.1.1 | Circular flexure hinges | 70 |
| 5.1.2 | Elliptical flexure hinges | 71 |
| 5.1.3 | Corner-filletted flexure hinges | 72 |
| 5.2 | Evaluation of Stress Generic Design Equations | 74 |
| 5.2.1 | Circular flexure hinge | 75 |
| 5.2.2 | Elliptical flexure hinge | 76 |
| 5.2.3 | Corner-filletted flexure hinge | 78 |
| 6 | Flexure-Based Compliant Mechanisms | 81 |
| 6.1 | Design of a Flexure-Based Compliant Mechanism | 81 |
| 6.2 | Analysis and Evaluation for the Generic Design Equations in FFCMs | 84 |
| 6.2.1 | Flexure-based four-bar compliant mechanisms(FFCMs) | 84 |
| 6.2.2 | Analysis and evaluation of the generic design equations | 87 |
| 7 | Conclusions | 101 |

List of Abbreviations

| | |
|-------------|--|
| FCM | Flexure-Based Compliant Mechanism |
| FEA | Finite Element Analysis |
| FFCM | Flexure-based Four-bar Compliant Mechanism |
| PRBM | Pseudo-Rigid-Body Model |
| R | Revolute |

List of Figures

| | | |
|-----|--|----|
| 1.1 | Rigid-body mechanism(a) and Flexure-based compliant mechanism (b) | 18 |
| 1.2 | Flexure-based compliant mechanisms in a wide variety of applications | 24 |
| 2.1 | Main classes of flexure hinge | 26 |
| 2.2 | Notch-type flexure hinges | 28 |
| 2.3 | A small length straight beam | 29 |
| 2.4 | Two axes flexure and multiple axes flexure hinges | 29 |
| 2.5 | Complex flexure hinges | 29 |
| 2.6 | Euler-Bernoulli Beam | 31 |
| 2.7 | Timoshenko Beam | 32 |
| 2.8 | Error associated with the small-length flexural pivot approximation . | 35 |
| 3.1 | Main free-end loading in a single-axis, constant-width flexure hinge . | 38 |
| 3.2 | A circular flexure hinge | 39 |
| 3.3 | An elliptical flexure hinge | 40 |
| 3.4 | A corner-filletted flexure hinge | 41 |
| 3.5 | Part A: Comparison of the moment-rotation relationships obtained by FEA and small deformation stiffness equation for circular flexure hinges | 44 |
| 3.6 | Part B: Comparison of the moment-rotation relationships obtained by FEA and small deformation stiffness equation for circular flexure hinges | 45 |
| 3.7 | The $\Gamma - \theta$ relationship for circular flexure hinges | 47 |
| 3.8 | The $\Gamma - h/l$ relationship for circular flexure hinges | 48 |
| 3.9 | Part A: Comparison of the moment-rotation relationships obtained by FEA and small deformation stiffness equation for elliptical flexure hinges | 49 |

| | | |
|------|--|----|
| 3.10 | Part B: Comparison of the moment-rotation relationships obtained by FEA and small deformation stiffness equation for elliptical flexure hinges | 50 |
| 3.11 | The $\Gamma - \theta$ relationship for elliptical flexure hinges | 51 |
| 3.12 | The $\Gamma - h/l$ relationship for elliptical flexure hinges | 52 |
| 3.13 | Part A: Comparison of the moment-rotation relationships obtained by FEA and small deformation stiffness equation for corner-filletted flexure hinges | 53 |
| 3.14 | Part B: Comparison of the moment-rotation relationships obtained by FEA and small deformation stiffness equation for corner-filletted flexure hinges | 54 |
| 3.15 | The $\Gamma - \theta$ relationship for corner-filletted flexure hinges | 55 |
| 3.16 | The $\Gamma - h/l$ relationship for corner-filletted flexure hinges | 55 |
| 4.1 | The relationship between $\bar{\sigma}$, θ and h/l for ten circular flexure hinges . | 59 |
| 4.2 | The relationship between θ , $\bar{\sigma}$ and h/l for ten circular flexure hinges . | 59 |
| 4.3 | The relationship between h/l , θ and $\bar{\sigma}$ for ten circular flexure hinges . | 61 |
| 4.4 | The relationship between $\bar{\sigma}$, θ and h/l for ten elliptical flexure hinges | 62 |
| 4.5 | The relationship between θ , $\bar{\sigma}$ and h/l for ten elliptical flexure hinges | 63 |
| 4.6 | The relationship between h/l , θ and $\bar{\sigma}$ for ten elliptical flexure hinges | 65 |
| 4.7 | The relationship between $\bar{\sigma}$, θ and h/l for ten corner-filletted flexure hinges | 66 |
| 4.8 | The relationship between θ , $\bar{\sigma}$ and h/l for ten corner-filletted flexure hinges | 66 |
| 4.9 | The relationship between h/l , θ and $\bar{\sigma}$ for ten corner-filletted flexure hinges | 68 |
| 5.1 | Comparison results and fitting errors for the generic stiffness design equation with nonlinear modified coefficient equation for circular flexure hinges | 71 |
| 5.2 | Comparison results and fitting errors for the generic stiffness design equation with linear modified coefficient equation for circular flexure hinges | 71 |
| 5.3 | Comparison results and fitting errors for the generic stiffness design equation with nonlinear modified coefficient equation for elliptical flexure hinges | 72 |

| | | |
|------|--|----|
| 5.4 | Comparison results and fitting errors for the generic stiffness design equation with linear modified coefficient equation for elliptical flexure hinges | 73 |
| 5.5 | Comparison results and fitting errors for the generic stiffness design equation with nonlinear modified coefficient equation for corner-filletted flexure hinges | 73 |
| 5.6 | Comparison results and fitting errors for the generic stiffness design equation with linear modified coefficient equation for corner-filletted flexure hinges | 74 |
| 5.7 | Comparison results and fitting errors for the $\theta_{z,max}$ design equation for circular flexure hinges | 75 |
| 5.8 | Comparison results and fitting errors for the $\bar{\sigma}$ design equation for circular flexure hinges | 76 |
| 5.9 | Comparison results and fitting errors for the h/l design equation for circular flexure hinges | 77 |
| 5.10 | Comparison results and fitting errors for the $\theta_{z,max}$ design equation for elliptical flexure hinges | 77 |
| 5.11 | Comparison results and fitting errors for the $\bar{\sigma}$ design equation for elliptical flexure hinges | 78 |
| 5.12 | Comparison results and fitting errors for the h/l design equation for elliptical flexure hinges | 78 |
| 5.13 | Comparison results and fitting errors for the $\theta_{z,max}$ design equation for corner-filletted flexure hinges | 79 |
| 5.14 | Comparison results and fitting errors for the $\bar{\sigma}$ design equation for corner-filletted flexure hinges | 80 |
| 5.15 | Comparison results and fitting errors for the h/l design equation for corner-filletted flexure hinges | 80 |
| 6.1 | Design flow chart for designing a FCM | 82 |
| 6.2 | Design flow chart for designing a flexure hinge | 83 |
| 6.3 | A FFCM | 84 |
| 6.4 | The equivalent pseudo rigid body model for the FFCM | 85 |
| 6.5 | A couple of forces loaded on FCM | 89 |
| 6.6 | Refined mesh for a FFCM | 89 |
| 6.7 | The moment-rotation relationship of link 2 | 91 |

| | | |
|------|---|----|
| 6.8 | The moment-rotation profile of FFCM with four corner-filletted flexure hinges | 93 |
| 6.9 | The moment-rotation relationship of link 2 | 94 |
| 6.10 | The moment-rotation relationship of link 2 | 95 |
| 6.11 | Comparison for the obtained moment-rotation relationship | 99 |
| 6.12 | Error analysis diagram | 99 |

List of Tables

| | | |
|-----|---|----|
| 3.1 | h/l and θ | 43 |
| 3.2 | The coefficients of the modified linear/nonlinear coefficient equations | 46 |
| 3.3 | The coefficients of the modified linear/nonlinear coefficient equations | 48 |
| 3.4 | The coefficients of the modified linear/nonlinear coefficient equations | 52 |
| 4.1 | Parameters for rotation design equation of circular flexure hinges . . . | 60 |
| 4.2 | Parameters for material characteristic equation of circular flexure hinges | 60 |
| 4.3 | Parameters for geometric characteristic equation of circular flexure hinges | 61 |
| 4.4 | Parameters for rotation design equation of elliptical flexure hinges . . | 63 |
| 4.5 | Parameters for material characteristic equation of elliptical flexure hinges | 64 |
| 4.6 | Parameters for geometric characteristic equation of elliptical flexure hinges | 64 |
| 4.7 | Parameters for rotation design equation of corner-filletted flexure hinges | 67 |
| 4.8 | Parameters for material characteristic equation of corner-filletted flexure hinges | 67 |
| 4.9 | Parameters for geometric characteristic equation of corner-filletted flexure hinges | 68 |
| 6.1 | Configuration of the desired FFCM | 88 |
| 6.2 | Geometries of a flexure hinge(slender beam) | 91 |
| 6.3 | Geometries of a corner-filletted flexure hinge | 92 |
| 6.4 | Geometries of a circular flexure hinge | 93 |
| 6.5 | Geometries of an elliptical flexure hinge | 95 |
| 6.6 | Designed flexure hinges (Generic design equations) | 97 |
| 6.7 | Designed flexure hinges (Small deflection design equations) | 98 |

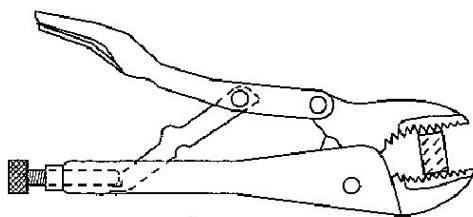
Chapter 1

Introduction

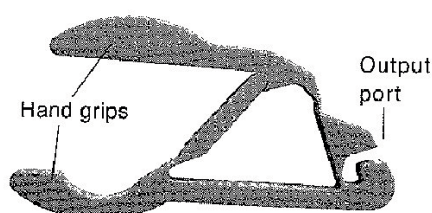
This chapter simply introduces the concept of flexure-based compliant mechanisms (FCMs), the advantages of FCMs and their applications in various fields. Then, the motivation for studying FCMs based on stiffness and stress characteristics is emphasized. The main contribution of the thesis is finally exposed together with the outline.

1.1 The Role of Flexure-Based Compliant Mechanisms (FCMs)

A traditional rigid mechanism consists of rigid links and joints that are utilized to connect rigid links and make the mechanism movable. For example, a Vise Grip pliers is shown in Figure 1.1(a). This mechanism implements a output force that is larger than the input force since energy is conserved between the input and output. Recent research efforts have been directed towards mechanical design of macro, micro and nano manipulation mechanisms and systems. Such traditional rigid mechanisms, however, exhibit problems such as assembling problem, friction and lubrication. Among the approaches of solving these problems, the study of using flexure-based compliant mechanism (FCM), where conventional kinematic pairs are replaced by flexure hinges [84], instead of traditional rigid mechanism became popular increasingly in mechanical design of macro, micro and nano manipulation



(a) Vise Grip Pliers (Rigid body mechanism)



(b) Crimping mechanism (Compliant mechanism)

Figure 1.1: Rigid-body mechanism(a) and Flexure-based compliant mechanism (b)

mechanisms and systems. Such a compliant mechanism that uses flexure hinges as link joints to implement mechanical functions is called a FCM [9, 34, 72]. Most of existing designs belong to FCMs. When a FCM is loaded, the major part of the compliant mechanism undergoes rigid-body movement, with energy and force transmitted through the bending of the hinges [57]. As an example, a counterpart of a FCM crimping mechanism is shown in Figure 1.1(b). Unlike rigid mechanisms, however, compliant mechanisms are monolithic and gain at least some of their mobility from the deflection of flexible members rather than from movable joints only [24]. Such compliant mechanisms promote the performances of mechanisms and extend their application range.

FCMs have many potential advantages compared to traditional rigid mechanisms [65,87]. These advantages can fall into two categories [10]: Cost reduction and increased performance. In terms of cost reduction, the advantages are part-count reduction, reduced assembly time, simplified manufacturing processes. On the other hand, the superiorities on increased precision, increased reliability, reduced wear, re-

duced weight and reduced maintenance also raise the performance of machines. Due to these advantages, FCMs are currently employed in a wide range of industrial applications at macroscale systems, microscale systems and nanotechnology where precision of motion, reliability, ease of fabrication, compactness [43, 44, 85] are required. In macroscale systems, for instance, displacement/force amplifiers/deamplifiers, positioning devices, and manipulators use such mechanisms to implement their target functions [19, 22, 43, 52, 57]. FCMs, especially, are applied in microscale systems. For example, FCMs are used to increase the sensitivity of resonant accelerometers [5, 20] among the sensor applications. On the other hand, most of the microsystems have been focusing on three critical assembly components that determine the accomplishment of microassembly procedure namely the development of high precision positioning devices [11, 13, 25, 32, 36, 38–41, 58, 61, 71, 81]. In addition, there are other applications such as compact *XY* flexure stages [27, 28, 53, 81] that provide large range of motion, microactuators that form drive systems for microelectromechanical systems (MEMS), microleverage mechanisms attract the attention of a number of researchers to achieve mechanical or geometric advantages [3, 6, 26, 33, 37, 78]. In terms of nanotechnology applications, a typical example is the ultra-precision manipulation, which consists of sliding/rolling guides and servomotors [85]. Examples of implementation of these mechanisms are numerous and they can be found in the field of precision engineering, metrology, automotive, aerospace, bio-medicine, telecommunications, medical, optics and computer industries micro-manufacturing, X-ray lithography, micro/nano surgery, nano-metrology, scanning tunnel microscopy, atom force microscopy, nanoimprint lithography, and micro/nano surface metrology and characterization, etc. [14, 46, 55, 60, 63, 64, 82, 84, 86]. Some typical examples mentioned above are shown in Figure 1.2.

1.2 Motivation

Despite FCMs have been used in the field of robotics and mechatronics for a long time, the problem of designing a compliant mechanism accurately and conveniently remains crucial. The key to design a FCM is the design of flexure hinges. It is well-known that deflection curves for flexible beams can be obtained by solving the exact form of the Euler-Bernoulli beam equation [2, 24], which states that the bending moment at any point on the beam is proportional to its curvature and can be written as:

$$M_E = EI \frac{d\theta}{ds} = EI \frac{\frac{d^2y}{dx^2}}{\left(1 + \left(\frac{dy}{dx}\right)^2\right)^{3/2}} \quad (1.1)$$

where M is the moment, $d\theta/ds$ is the rate of change of angular deflection (slope) along the beam length, y is the transverse deflection, x is the coordinate along the undeflected axis, E is the Young's modulus of material and EI is the flexural rigidity of the beam.

The $(dy/dx)^2$ can be neglected when the beam deflection is very small. In other words, the nonlinearities introduced due to large deflections are not taken into account. Certainly, numerous techniques are available considering the nonlinearities introduced in the beam equation. A classical solution involves the solution of a second order nonlinear differential equation using elliptic integrals of the first and the second class. Though the technique yields a closed form solution which is exact, the involved derivations are cumbersome and time consuming. Therefore, Howell et al. proposed a pseudo rigid body model (PRBM) to solve this problem. Large displacement [8,70,74] analysis of flexible beams is performed with the assumptions that the beam is rigid in shear and uniform in cross section. Based on Howell's work, many researchers studied FCMs based upon the PRBM method [2, 24, 30, 31, 65]. Despite their works, the influence of shear force produced due to the beam geometry is not taken into account due to the assumptions. Therefore, the PRBM method is limited to relatively simple geometries, namely slender beams. From what reported above, there is not a method to design the flexure hinge without any restrictive assumptions in general. Currently, researchers still ignore the nonlinear influence of changing the geometry shape of flexure hinges or limiting the deformation range of flexure hinges. Nevertheless, the geometry dimensions of a flexure hinge maybe influence the entire design of a FCM, especially in the application of micro and nano-systems. Therefore, some basic problems are improvable such the following ones:

- The need to simplify the process of design a FCM. Most compliant mechanisms are still composed of flexible of designing a flexure hinge. The definition about shape and geometry of a flexure hinge is the key to design a perfect .
 - The need to extend the application range of FCMs. The influence of shear force produced during the flexure hinge deformation should be taken into account. In fact, designers prefer to use linear design equations rather than use
-

nonlinear design equations; because the nonlinear equations are too complicated to be used in practice even though the results are more accurate than those simple ones. Therefore, the application range of FCMs are limited due to the design assumptions.

In addition, it is noted that the FCMs demonstrate a number of different characteristics compared with conventional kinematic mechanisms. The established design criteria for conventional kinematic mechanisms will suffer from shortcomings such as rotational stiffness of flexure hinges and the maximum stress level (or the yield strength) of flexure hinges. Stiffness of flexure hinges determines how much flexure deflection will occur under a given load. Such a system will demonstrate the unique characteristics in the working range. Further more, studies on strength (or stress) of flexure hinges are another important issue, strength of flexure hinge that determines how much stress can occur before the failure. The yield strength (S_Y) of a material is defined in engineering and materials science as the maximum stress (σ_{max}) of material can support. The materials with the yield strength (S_Y)-to-Young's Modulus (E) rate ($\frac{S_Y}{E}$) will allow a larger deflection before material failure. This rate ($\frac{S_Y}{E}$) is one of the most important parameter available when selecting materials for compliant mechanism applications. This thesis studies the FCMs based on both these characteristics.

1.3 Contribution of the Thesis

At first in this work, three popular types of flexure hinges (circular flexure hinges, elliptical flexure hinges and corner-filletted flexure hinges) are analyzed based on the Finite Element Analysis (FEA) method. The analyzed results are then used for correcting the errors produced by the small deformation design equations when the chosen flexure hinges suffer from large deformation. Consequently, three sets of generic design equations for the three types of flexure hinges are proposed on the basis of stiffness and stress characteristics from the FEA results. Finally, a flexure-based four-bar compliant mechanism (FFCM) is studied and modeled using the proposed generic design equations. The load-displacement relationships are verified by a numerical example.

The benefits of these generic design equations include: (a) high accuracy for large

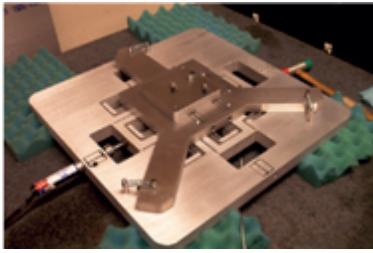
deflection flexure hinges, (b) adaptability to the cross-section shape of flexure hinges, (c) extended application range for the FCMs.

1.4 Thesis Outline

- Chapter 1 simply introduces the concept of FCM, the advantages of FCMs and their applications in various fields. Then, the motivation for studying FCMs based on stiffness and stress characteristics is emphasized. The main contribution of the thesis is finally exposed together with the outline.
 - Chapter 2 carries out a literature review concerning flexure hinges. Three common flexure hinges are chosen as the objects of study for this work. Two main beam theories, Euler-Bernoulli beam theory and Timoshenko beam theory, are briefly recalled in the part of work. Finally, a useful method, PRBM, is also stated in the chapter.
 - Chapter 3 is dedicated to defining a range of flexure hinge configurations based on their stiffness characteristics (or, conversely, compliant characteristics). Three common flexure geometries are introduced here and are characterized by closed-form stiffness equations that are obtained by modifying the Lobontiu's [34] small deformation closed-form stiffness equations based on the finite element analysis(FEA) results. Then the specific expressions are given for each individual flexure hinge.
 - Chapter 4 studies the maximum stress characteristic for the three common types of flexure hinges by means of the FEA method. For each type of flexure hinge, there are three correlated parameters, S_Y/E , h/l and the deflection rotation θ . At the end, three sets of generic design equations based on stress characteristics for each type of flexure hinge are proposed.
 - Chapter 5 discusses the characteristics of these generic design equations proposed in Chapter 3 and Chapter 4 and analyzes the errors produced by these equations compared with the FEA results. Meantime, the correctness and ap-
-

plicability for these equations are evaluated.

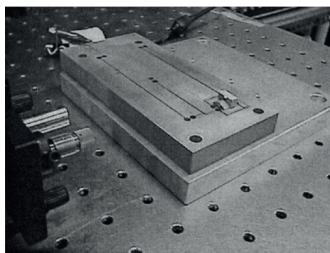
- Chapter 6 presents the design procedure for designing of a FCM. By reporting this procedure, this chapter introduces in detail the application method of the generic design equations proposed in the earlier chapters by designing a four-bar compliant mechanism. Moreover, these generic design equations are assessed again in order to verify their applicability in FCM design. Finally, a numerical example of designing a flexure-based four-bar compliant mechanism (FFCM) is presented.
 - Chapter 7 summarizes the main contributions of this thesis and reports the methods used to achieve the presented results.
-



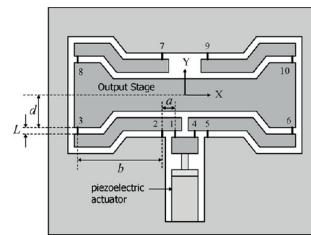
(a) X-Y Compliant Flexure mechanism XY (Ref. [55])



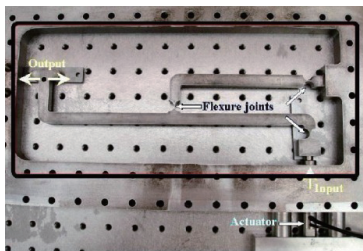
(b) Compliant Scissors for No Assembly (Courtesy of the Compliant Mechanisms Research Group, Brigham Young University)



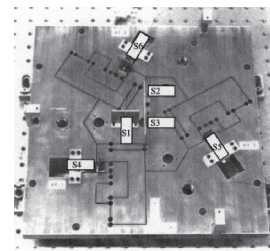
(c) The micropositioner (Ref. [58])



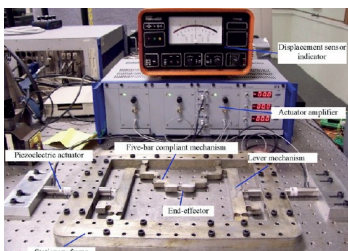
(d) Schematic of NIST 1-D mechanism (Ref. [7])



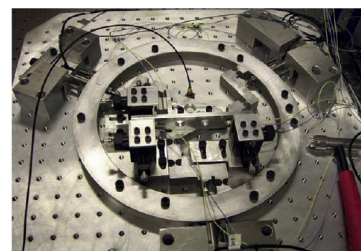
(e) the flexure-based Scott-Crossley mechanism (Ref. [85])



(f) Prototype $XY\theta$ stage and capacitance sensor position. (Ref. [27])



(g) A flexure-based five-bar mechanism (Ref. [82])



(h) 3-DOF flexure-based five-bar mechanism (Ref. [84])

Figure 1.2: Flexure-based compliant mechanisms in a wide variety of applications

Chapter 2

Flexure Hinges and Beam Theory

This chapter carries out a literature review on flexure hinges. Three common types of flexure hinges are chosen as the objects of study for this work. Two main beam theories, Euler-Bernoulli beam theory and Timoshenko beam theory, are recalled briefly in the first part of the chapter. Lastly, a useful method, the PRBM method, is also mentioned in the chapter.

2.1 Flexure Hinges

Flexure hinges are the most important components in the FCMs. A flexure hinge is a mechanical element that provides the relative rotation between adjacent rigid members through flexing (bending) instead of a conventional rotational joint [46]. Each individual flexure hinge should be accompanied by a complete set of compliances (or, conversely, stiffness) that define its mechanical response to quasi-static loading [34].

In the last 50 years, many flexible joints have been investigated and developed. Paro and Weisbord [34] first put forward the compliance-based approach to flexure hinges by giving the compliance equations and the approximate engineering formulas for symmetric circular and right circular flexure hinges in 1965. Hereafter, flexure hinges began to attract an attention of an incredible number of researchers. Many new flexure configurations are presented by using the analytical approach and refer-

ring to the results of Paros and Weisbord. For instance, the elliptical flexure hinges are presented by Smith et al. in 1997 by means of extrapolating the results from circular to elliptical [62]. Smith also presented the circular toroidal flexure hinges following the procedure used in the study of the elliptical flexure hinges. Lobontiu et al. proposed the exact compliance equations for symmetric corner-filleted flexure hinges [45,46,49] and introduced a complete form of the compliance-based approach to flexure hinges by quantifying and characterizing the capacity of rotation, precision of rotation, and stress levels [43]. With the development of flexure hinges, the flexure configurations are developed from two-dimensional to three-dimensional, as well as from simple forms to complex forms such as the cylindrical flexure hinges and cartwheel flexure hinges. Basically, a flexure hinge can be fabricated in two different ways [34]:

- Use an independently fabricated member (such as a strip or shim in two-dimensional applications or a cylinder-like part in three-dimensional applications) to connect two rigid members, which are designed to undergo relative rotation.
- Machine a blank piece of material so that a relatively thin portion is obtained, which will be the flexure hinge. Therefore, the flexure hinge is integral (or monolithic) with the parts which it connects together.

A variety of flexure hinges have been reported in years, a brief introduction about the taxonomy of flexure hinges has been discussed based on their functional principles and associated geometric configurations. At a general level, the flexure hinges can be divided into two categories: primitive flexure hinges and complex flexure hinges [75,77], as shown in Figure 2.1.

As concerning primitive flexure hinges, the flexure hinges can be separated into

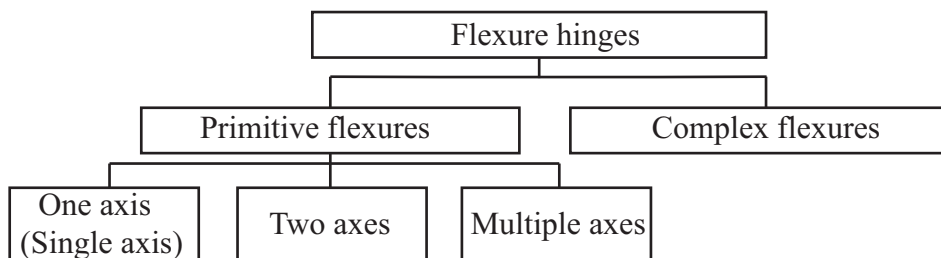


Figure 2.1: Main classes of flexure hinge

three categories based on their sensitive axis and geometric configurations. They are one axis (also called single axis, generally of constant width), two axes and multiple axes (of revolute geometry), as indicated in Figure 2.1. In general, such a single axis flexure hinge has a rectangular cross-section with constant width and variable height. This type of flexure hinges can be further classified based on the forms of their cross-section. such as notch-type flexure hinges (Figure 2.2) and small length straight beams (Figure 2.3). Notch-type flexure hinges have been widely utilized in macro/micro/nano high-precision systems. This type of flexure hinges includes circular flexure hinges [43, 49, 80], corner-filletted flexure hinges [45, 46, 49], 'V' shape flexure hinges [50, 83], elliptical flexure hinges [17, 69], right-circular elliptical flexure hinges [17], right-circular corner-filletted flexure hinges [17, 18], parabolic flexure hinges [47, 48] and hyperbolic flexure hinges [47]. The small length straight beams were widely studied since they own the simplest geometric configuration as well as all of basically characters of flexure hinges [1, 22, 24, 70, 72, 79]. Flexure hinges with two axes are sketched in Figure 2.4(a). Compared to a single axis configuration, the two axes flexure hinges will not only preferentially bend about one axis of minimum bending compliance, but also bend about the other axis. This second axis is also called the sensitive axis and lies in the cross-section of minimum thickness, it is most often perpendicular on the first sensitive axis [34]. Besides, a flexure hinge that belongs to the multiple axes category is sketched in Figure 2.4(b). This type of flexure hinge can be employed in three-dimensional applications, where the direction of the sensitive axis is not pre-specified.

As for the complex flexure hinges, they are usually the combination of two or more primitive flexures. They are also widely used in medical instrumentation and MEMS devices [54]. Up to now, there are several classes of complex flexure hinges, they are cross-axis flexural pivots [4, 23], which characterized by the connection of two rigid segments with two long flexible segments arranged in cross-shape configuration; split-tube flexural pivots incorporated by torsion as the primary mode of deformation; leaf-type isosceles-trapezoidal flexural (LITF) pivot [75], which consists of two leaf-type segments and two rigid segments; and cartwheel flexural hinges [56, 76] that can be considered as the combination of two symmetrical LITF pivots, each of which has a promising flexure since it can provide a large-deflection stroke and overcome some shortcomings of the conventional cross-axis pivot, including unavoidable assembly and relatively low rotational precision [76]. Figure 2.5 shows two typical complex flexure hinges.

As mentioned earlier, the flexure hinges can be monolithic with the rest of the mech-

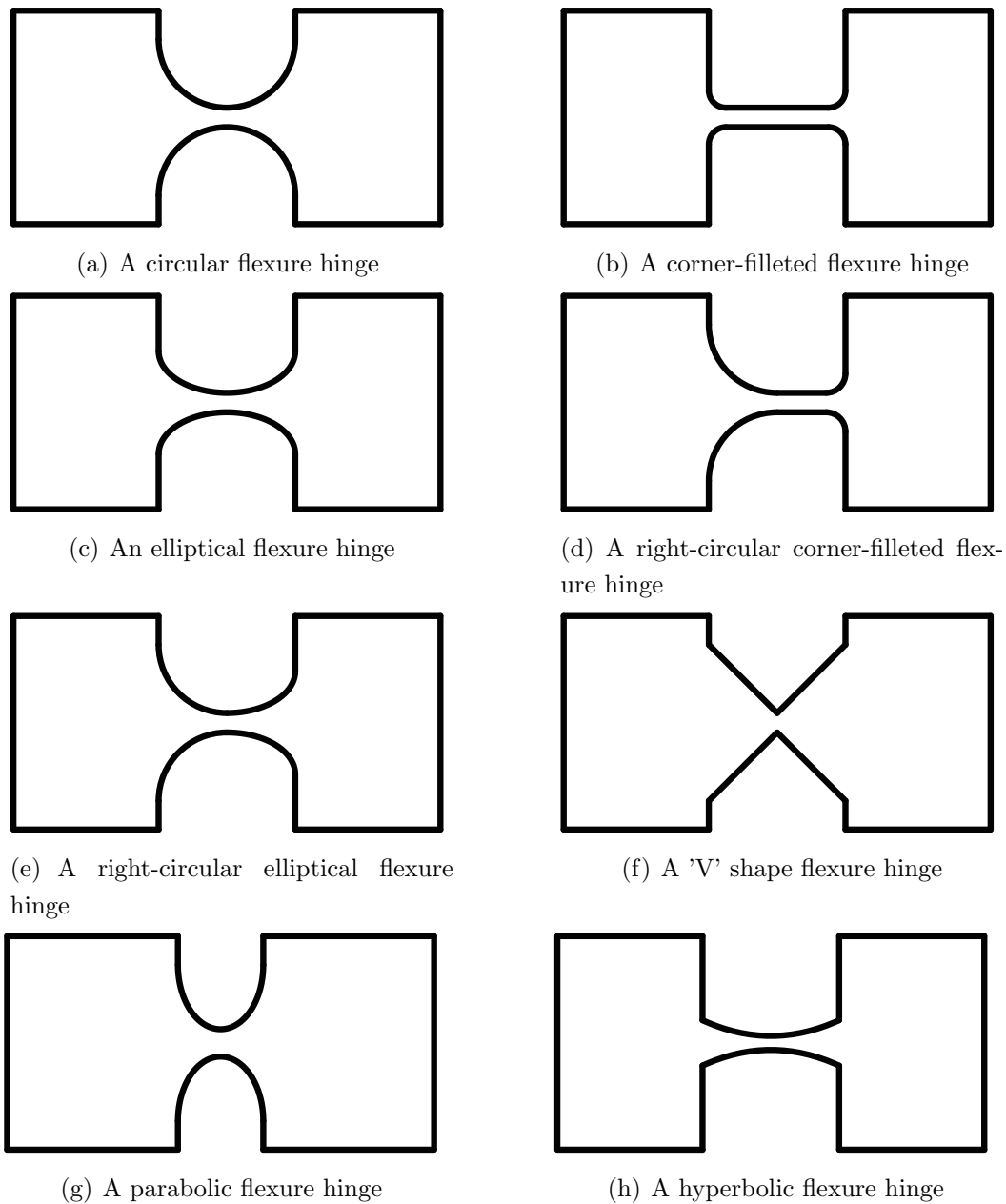


Figure 2.2: Notch-type flexure hinges

anism. They can be used in a number of applications due to their advantages over traditional rotational joints. The most notable benefits provided by flexure hinges are no friction losses, no need for lubrication, no backlash, compactness, capacity to be utilized in small-scale applications, ease of fabrication and virtually no maintenance needed [34]. Therefore, flexure hinges are increasingly popular [17, 44, 76]. The vast majority of the research reported up to now focus on applications that

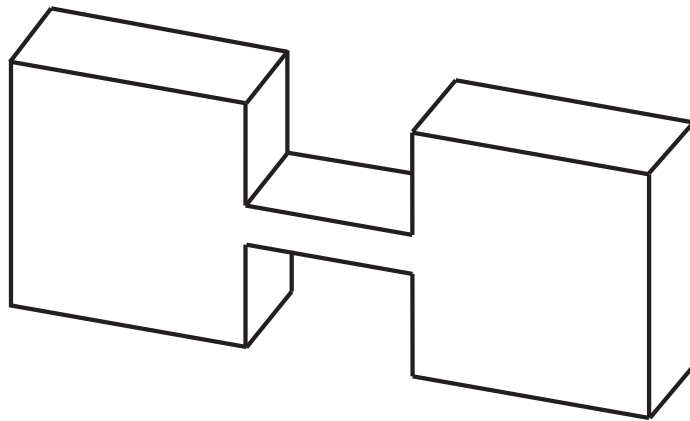
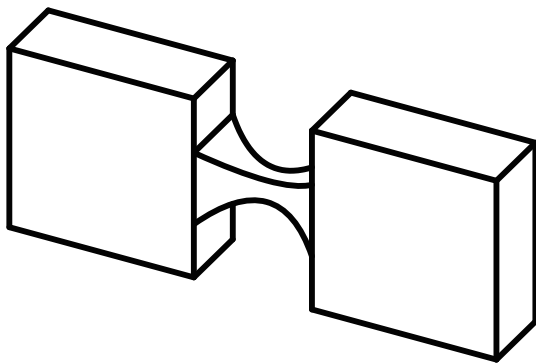
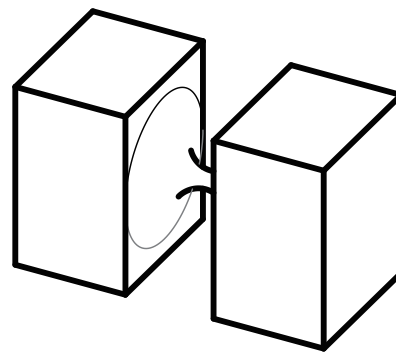


Figure 2.3: A small length straight beam

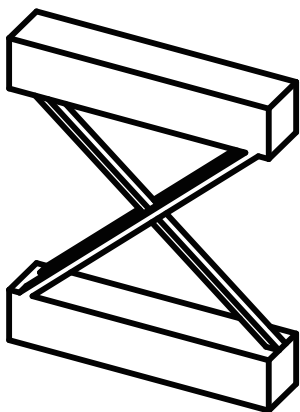


(a) Two axes flexure hinge

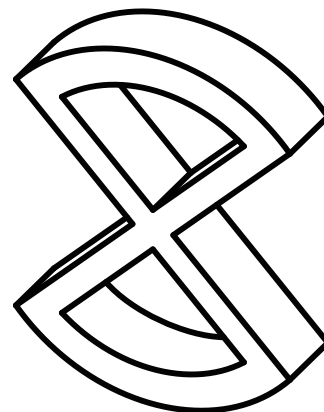


(b) Multiple axes flexure hinge

Figure 2.4: Two axes flexure and multiple axes flexure hinges



(a) Cross axis flexure hinge



(b) Cartwheel flexure hinge

Figure 2.5: Complex flexure hinges

utilize circular flexure hinges and elliptical flexure hinges and corner-filletted flexure hinges for which the analysis is performed by means of commercial finite element software. In addition, these types of flexure hinges are the prior objects considered by researchers since they can be analyzed and modeled more easily than the others complex flexure hinges.

Despite all the advantages mentioned above, there are some disadvantages associated with flexure hinges. For example, it is more complicated to model and more difficult to control the motions of flexure hinges precisely compared to conventional joints. This could be partly attributed to shear deformations of flexure hinges. Next section will introduce the basic theory and methods to face these problems.

2.2 Beam Theory

Several theories can be found in the literature representing the kinematic behavior of beams. There are two main theories, i.e. Euler-Bernoulli beam bending theory and Timoshenko beam theory, that are used in the design of flexure hinges. Since the Timoshenko beam theory is of higher order than the Euler-Bernoulli theory, it is known to be superior in predicting the transient response of the beam. The classical Euler-Bernoulli beam theory, which neglects the effect of transverse shear strain is the simplest of the both. However, the Euler-Bernoulli beam theory fails to provide accurate results when the longitudinal-transverse ratio is relatively large. In such cases, the superiority of the Timoshenko theory, which is a first shear deformation theory, is more pronounced for beams with a low aspect ratio. Besides the two basic beam theories, the refined beam theory, which can exhibit more accurate solutions, is investigated by some of researchers in [2, 21, 35, 42, 51, 59, 67, 73]. This chapter will only focus on comparing the difference between two theories is presented here.

- Euler - Bernoulli beam bending theory.

In Euler-Bernoulli beam bending theory, shear deformations are neglected, and plane sections is assumed to remain plane and normal to the longitudinal axis.

Consider a prismatic beam as shown in Figure 2.6 with length L , cross-sectional area A , second moment of area I , Young's modulus E , and shear modulus of rigidity G under any transverse loading condition. According to the Euler-Bernoulli beam theory, the force - displacement relations are given by:

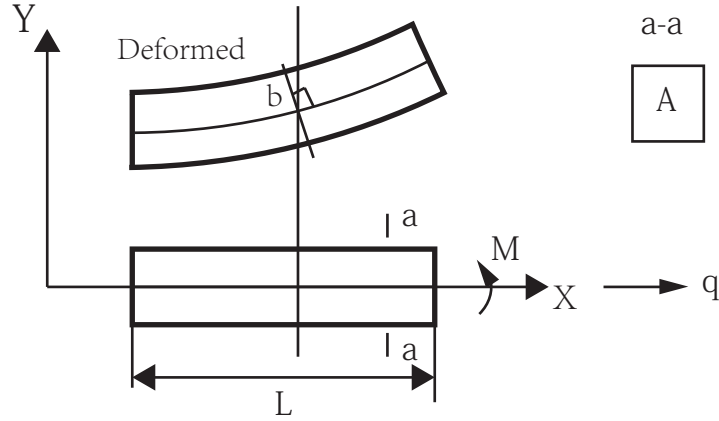


Figure 2.6: Euler-Bernoulli Beam

$$M_E = -EI \frac{d^2 w_E}{dx^2}; \quad V_E = -GI \frac{d^3 w_E}{dx^3} \quad (2.1)$$

where M_E is the bending moment of the Euler-Bernoulli beam; V_E is the transverse shearing force of the Euler-Bernoulli beam; w_E is the transverse deflection of the centroid axis of the Euler-Bernoulli beam; EI is the flexural rigidity; and x is the longitudinal coordinate measured from the left end side of the beam.

Euler-Bernoulli beam theory is a simplification of the linear theory of elasticity, which provides a means of calculating the load-deflection characteristics of beams. It covers the case for small deformations of a beam, which is subjected to lateral loads only. It is thus a special case of Timoshenko beam theory.

- Timoshenko beam bending theory.

In the Timoshenko beam theory, plane sections still remain plane but are no longer normal to the longitudinal axis [21]. Consider a model as shown in Figure 2.7. The force-displacement relations are given by:

$$M_T = -EI \frac{d^2 \Psi}{dx^2}; \quad V_T = -GAK_s \left(\Psi - \frac{dw_T}{dx} \right) \quad (2.2)$$

where M_T is the bending moment of the Timoshenko beam; V_T is the transverse shear force of the Timoshenko beam; Ψ is the rotation about y-axis; and w_T is the transverse deflection to the centroid axis of the Timoshenko beam. The subscript T denotes quantities for the Timoshenko beam. The shear correction coefficient K_s is introduced to account for the difference in the constant state of shear stress in the Timoshenko beam theory and the parabolic variation of the actual shear

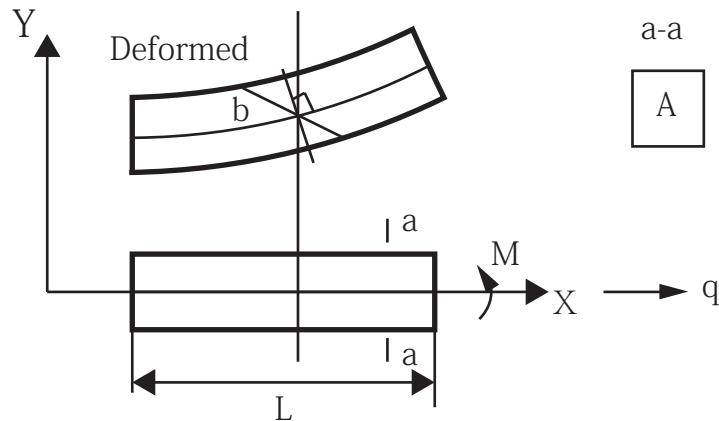


Figure 2.7: Timoshenko Beam

stress through the beam depth.

The Timoshenko model takes into account shear deformation and rotational inertia effects, making it suitable for describing the behavior of short beams. But unlike ordinary beam theory, i.e. Euler-Bernoulli beam theory, there is also a second order spatial derivative present.

2.3 PRBM

2.3.1 Brief literature review about PRBM

PRBMs have been applied in the analysis and synthesis of flexure hinges and compliant mechanisms for years. Howell and Midha [29] were the first to propose a PRBM model for solving a slender beam, which undergoes large deformations. Hereafter, the technique of PRBM was recognized and developed rapidly. Up to now, the PRBM is not only utilized in the analysis and synthesis of a flexible segment, but also in the analysis and synthesis of the whole compliant mechanisms, especially for dynamic analysis. The form of the PRB model was also extended from one revolute-like single joint to a multiple revolute like joints.

The purpose of the PRBM is to provide a simple method of analyzing systems undergoing large, nonlinear deflections. The PRBM concept is used to model the flexible members using rigid-body components that have equivalent force-deflection characteristics. Rigid-link mechanism theory may then be used to analyze compli-

ant mechanisms. In this way, the PRBM works as a bridge connecting rigid-body mechanism theory and compliant mechanism theory.

Parametric approximation for the beam tip deflection is critical for higher level design especially for design synthesis. Several PRBMs have been developed to approximate tip deflection of flexible beams for various loads. Howell and Midha proposed a PRBM 1R(revolute) model that comprised two rigid links joined at a pin joint and a torsion spring along the beam. Here 'R' represents a revolute or pin joint. They have found that the position of the pin joint was determined by the so-called characteristic radius factor ' γ ' which equals 0.85 for force applied on the end only and 0.7346 for moment applied on the end only. However this model is not appropriate for the applications where the load varies significantly and application where the mechanism undergoes exceptionally large deflection [24, 30, 31]. In order to approximate tip deflection of initially straight cantilever beams subjected to combined end force and moment, Saxaena and Kramer [2] modified the PRBM 1R model by introducing two linear springs to restrain the change of characteristic radius factor ' γ ' for different load modes.

Su et al. [65] proposed a new PRBM 3R model for initially straight cantilever beams subjected to a combined force and moment by compromising the PRBM 1R model and the FEA method. The model comprised three R joints, each one accompanied by a torsion spring. The kinematic and the mechanical parameters are loaded independently. Since the analytical inverse and forward kinematics are readily available for 3R serial chains, the kinematic and mechanical equations are relatively simple. Since PRBM is simple and accurate, a lot of researchers studied the complex flexure hinges by using this method. Pei et al. [77] proposed two PRBMs for the analysis of the moment-angle characteristics of LITF (Leaf-type Isosceles-trapezoidal Flexural) pivots. They also proposed a PRBM bar model for the cartwheel hinges. Certainly, this method can also be used in studying compliant mechanisms. Sonmez and Tutum proposed the combined use of PRBM and the elastic buckling theory to analyze a new compliant bistable mechanism design [70]. Pendleton and Jensen [68] represented the wireform mechanisms as rigid-body mechanisms using the PRBM because the mechanisms are more complex than ordinary springs. Bandopadhyaya and Njuguna [12] proposed newly variable parameters PRBM of IPMC actuator for bending resistance estimation with input voltages. Beléndenz et al. studied the deflection of a cantilever beam of linear elastic material, under the action of an external vertical concentrated load at the free end [66]. The flexure hinges studied by these researchers, however, are limited in a condition that their width must be

much less than its length, i.e. slender beams.

2.3.2 Beam theory in PRBM

The work of this part will explain the basic PRBM proposed by Howell [24]. Considered a cantilever beam shown in Figure 2.8. The beam has two segments: one is a short and flexible segment, and the other is a longer and rigid segment. If the small segment is significantly shorter and more flexible than the large segment, that is,

$$l \ll L \quad (2.3)$$

$$EI_l \ll EI_L \quad (2.4)$$

the small segment is called a short beam, or small-length beam.

For this small-length beam, the effect of the shear force can be ignored based on Euler Bernoulli beam theory because of $l \ll L$. The deflection equations for the flexible segment with a moment at the end are as follows:

$$\begin{aligned} \theta_0 &= \frac{M_0 l}{EI} \\ \frac{\delta_y}{l} &= \frac{1 - \cos\theta_0}{\theta_0} \\ \frac{\delta_x}{l} &= \frac{1 - \sin\theta_0}{\theta_0} \end{aligned}$$

This system of equation can be used to define a simple pseudo-rigid-body model for small-length flexural pivots. Since the flexible section is much shorter than the rigid section, the motion of the system may be modeled as two rigid links joined at a pin joint, called the characteristic pivot. The characteristic pivot is located at the center of the flexural pivot (Figure 2.8). This is an accurate assumption because the deflection occurs at the flexible segment and it is small compared to the length of the rigid segment. For the same reason, nearly any point along the flexible segment would represent an acceptable position for the characteristic pivot and the center point is used for convenience. The angle of the PRBM is equal to the beam end angle:

$$\Theta_0 = \theta_0 \quad (2.5)$$

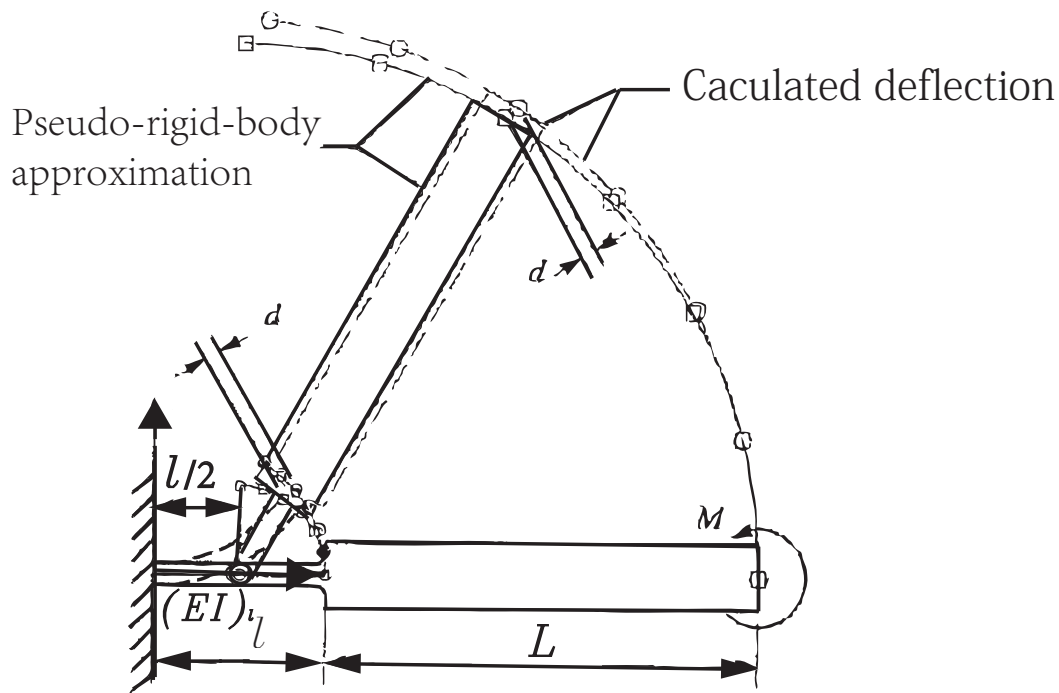


Figure 2.8: Error associated with the small-length flexural pivot approximation

To sum up, PRBM is relatively accurate correctly based on the Euler-Bernoulli beam theory. The errors of results increase with the longitudinal-transverse ratio of height and length. The Euler-Bernoulli beam theory, however, is simpler than Timoshenko beam theory regarding to the nonlinear analysis computing. Based on the considerations, this study will propose a series of equations to obtain the accurate results by comparing the FEA results and results obtained from the Euler Bernoulli beam theory results.

Chapter 3

Stiffness-Based Design of Flexure Hinges

Chapter 3 is dedicated to defining a range of flexure hinge configurations based on their stiffness characteristics (or, conversely, compliant characteristics). Three common types flexure geometries are introduced here and are characterized by closed-form stiffness equations that are obtained by modifying the Lobontiu's [34] small deformation closed-form stiffness equations based on the FEA results. Then the specific expressions are given for each individual flexure hinge.

As previously described in Chapter 1, the first important design criteria is stiffness (or, its inverse, compliance). The stiffness is subsequently used to fully study a flexure hinge by defining its capacity of producing the desired limited rotation.

3.1 Stiffness Mathematical Formulas for Small Deformation

Referring to Lobontiu's book [34], the majority of the topic on stiffness mathematical formulas for small deformation focuses on linear elastic materials and systems whose main properties are:

- The deformations (deflections or angular rotations) are small (infinitesimal).
-

- The bodies are elastic and therefore the deformations are proportional to the applied loads, according to Hooke's law.
- The bodies are homogeneous (their properties are the same at all locations within) and isotropic (their properties are identical irrespective of direction).

With a few exceptions, the generic loading for a single-axis, constant-width flexure hinge such as a circular flexure hinge, an elliptical flexure hinge or a corner-filletted flexure hinge is visualized in Figure 3.1. Only a bending moment M_Z , which has substantive effects on the flexure operation, is applied at the end of a flexure hinge. As previously shown in [34], the principal compliance can be calculated by means of the Castigliano's second theorem:

$$C_S = \frac{12}{Ew} \int_0^l \frac{dx}{t(x)^3} \quad (3.1)$$

where the subscript S denotes that the compliance equation is valid under the condition of small deformation range, and E is the elastic modulus, w is the width of a flexure hinge. $t(x)$ is the governing equation for profile of the flexure hinges.

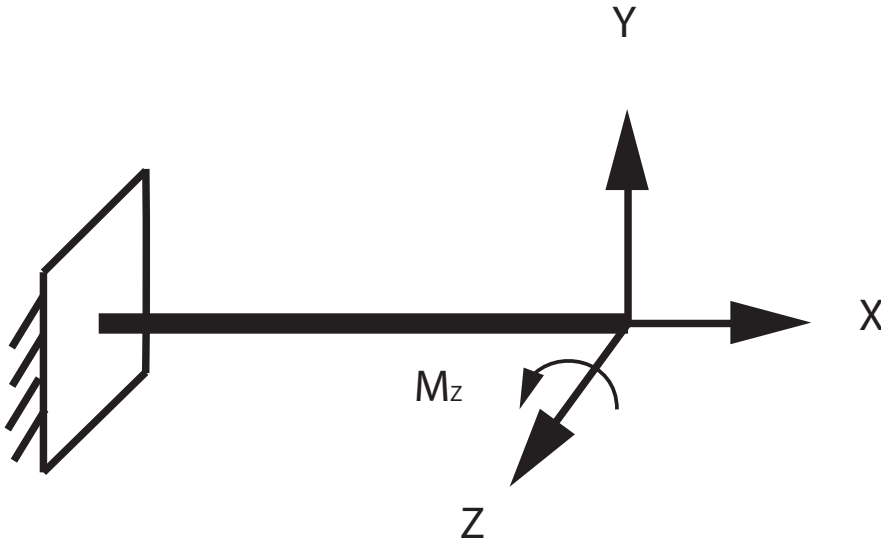


Figure 3.1: Main free-end loading in a single-axis, constant-width flexure hinge

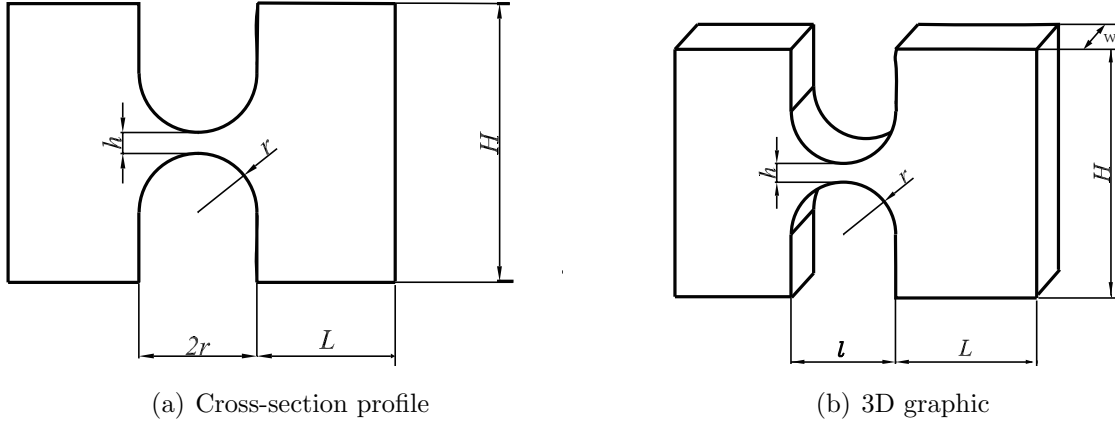


Figure 3.2: A circular flexure hinge

3.1.1 Circular flexure hinges

Circular flexure hinges will be chosen as one of the objects of study in this thesis. Especially, the symmetric circular flexure hinges are investigated in the work. The longitudinal section of a symmetric circular flexure hinge is illustrated in Figure 3.2. Here h is the minimum thickness of the circular flexure hinge, r is the radius of the circular flexure hinge, w is the width of the circular flexure hinge, H and L are the thickness and length of the rectangular parts on both the sides of the circular flexure hinge that are utilized to ensure that the analysis results could not be influenced by the loading forces. The variable thickness, $t(x)$, can be expressed in terms of the flexure geometry as:

$$t(x) = h + 2[r - \sqrt{x(2r - x)}] \quad (3.2)$$

The closed-form stiffness equation describing the capacity of rotation under the condition of small deformation range is shown as follows:

$$K_{S,C} = \frac{Ewh^3(2r + h)(4r + h)^3}{24r[h(4r + h)(6r^2 + 4rh + h^2) + 6r(2r + h)^2\sqrt{h(4r + h)}\arctan\sqrt{1 + \frac{4r}{h}}]} \quad (3.3)$$

where the subscript S, C denotes the circular flexure hinges stiffness equation is valid when the flexure hinge works under small deformation operation.

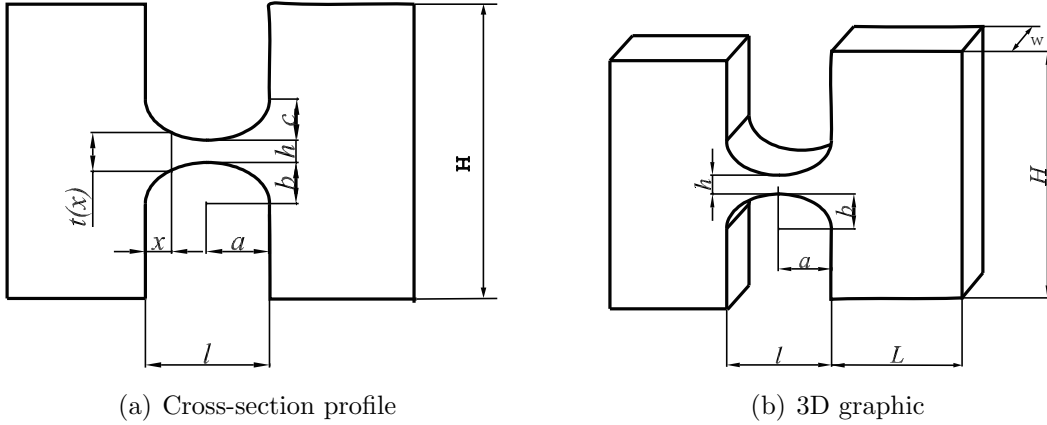


Figure 3.3: An elliptical flexure hinge

3.1.2 Elliptical flexure hinges

The flexure hinges of elliptic profile, the symmetric elliptical flexure hinges, as shown in Figure 3.3, are considered as another one of objects of study in this thesis. where h is the minimum thickness of the elliptical flexure hinge, a is the major axis of the elliptical flexure hinge, b is the minor axis of the elliptical flexure hinge, c is the distance from the point at the minimum thickness to the edge of the elliptical flexure hinge, i.e. c equals b , l is the length of the elliptical flexure hinge, i.e. l is equal to $2a$, w is the width of the elliptical flexure hinge, H and L are the thickness and length of the rectangular parts on both the sides of the elliptical flexure hinge and are utilized to ensure that the analysis results could not be influenced by the loading forces. The governing equation for the upper profile of the elliptical flexure hinges is given as follows:

$$t(x) = h + 2c \left[1 - \sqrt{1 - \left(1 - \frac{2x}{c}\right)^2} \right] \quad (3.4)$$

Even though Lobontiu also proposed the stiffness equations for elliptical flexure hinges, they are not accurate. Combining the results of Chen [16], the correct stiffness equations for elliptical flexure hinges is the following:

$$K_{S,E} = \frac{Ewh^3}{6N_E l} \quad (3.5)$$

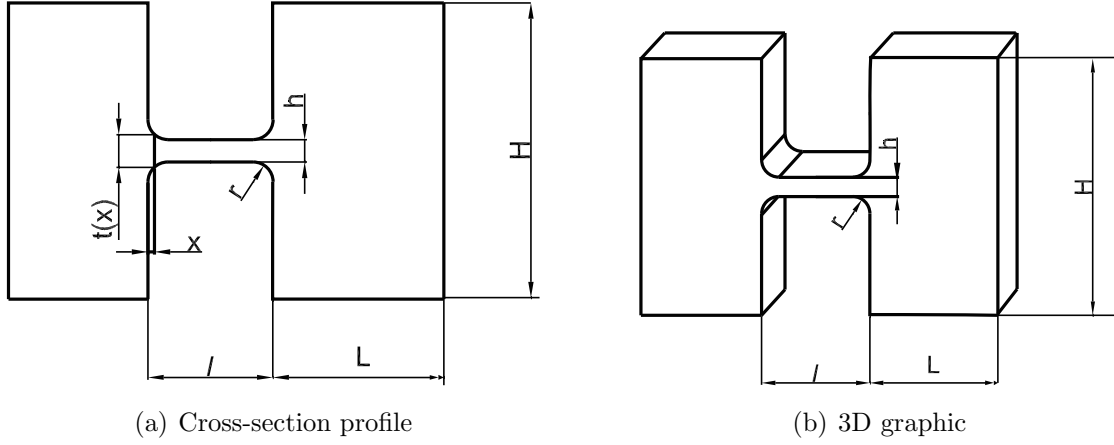


Figure 3.4: A corner-filletted flexure hinge

where the subscript S, E denotes that the stiffness equation of elliptical flexure hinges is valid under small deformation assumption. N_E is given by,

$$N_E = \frac{2 \left[\sqrt{4\left(\frac{b}{h}\right) + 1} \left(6\left(\frac{b}{h}\right)^2 + 4\left(\frac{b}{h}\right) + 1\right) \right] + 6\left(\frac{b}{h}\right)\left(2\left(\frac{b}{h}\right) + 1\right)^2 \arctan \left(\sqrt{4\left(\frac{b}{h}\right) + 1} \right)}{\left(2\left(\frac{b}{h}\right) + 1\right)\left(4\left(\frac{b}{h}\right) + 1\right)^{5/2}} \quad (3.6)$$

3.1.3 Corner-filletted flexure hinges

Corner-filletted flexure hinges are the last one to be investigated in this thesis. A longitudinally symmetric flexure hinge and its defining geometric parameters are shown in Figure 3.4, where h is the minimum thickness of the corner-filletted flexure hinge, r is the fillet radius, l is the length of the corner-filletted flexure hinge, w is the width of the corner-filletted flexure hinge and the rectangular parts, H and L are the thickness and length of the rectangular parts on both the sides of the corner-filletted flexure hinge and are utilized to guarantee that the analysis results could not be influenced by the loading forces. The governing equation for the upper profile of the corner-filletted flexure hinges is given as follows:

$$t(x) = \begin{cases} h + 2[r - \sqrt{x(2r - x)}] & x \in (0, r) \\ h & x \in (r, l - r) \\ h + 2\left\{ r - \sqrt{(l - x)[2r - (l - r)]} \right\} & x \in (l - r, l) \end{cases} \quad (3.7)$$

The situation of closed-form stiffness equation for corner-filletted flexure hinges is the same as the one for elliptical flexure hinges. The stiffness equation proposed by

Lobontiu is not correct. The right stiffness equation for corner-filletted is given by:

$$K_{S,R} = \frac{Ewh^3}{12(l + rN_R)} \quad (3.8)$$

where the subscript S, R denotes that the stiffness equation of corner-filletted flexure hinges is valid under small deformation operation. N_R can be obtained by:

$$N_R = \frac{2 \left[\sqrt{4\left(\frac{r}{h}\right) + 1} \left(6\left(\frac{r}{h}\right)^2 + 4\left(\frac{r}{h}\right) + 1 \right) \right] + 6\left(\frac{r}{h}\right) \left(2\left(\frac{r}{h}\right) + 1 \right)^2 \arctan \left(\sqrt{4\left(\frac{r}{h}\right) + 1} \right)}{\left(2\left(\frac{r}{h}\right) + 1 \right) \left(4\left(\frac{r}{h}\right) + 1 \right)^{5/2}} \quad (3.9)$$

3.2 Stiffness Mathematical Formulas for Large Deflection

As described in Chapter 2, most researchers prefer to neglect the influence of shear force produced during the flexure hinge deformation because of its complexity. Slender beams or small deformation assumptions made the study focus on research of FCMs early. Deep-beams /short-beams or large deflection operation, will extend the application range of FCMs. This thesis proposes a new method that can be utilized in more generic design for circular flexure hinges, elliptical flexure hinges and corner-filletted flexure hinges. This method corrects the stiffness mathematical formulas for small deformation by FEA method. The method is described first here.

1. Perform FEA by using COMSOL software.

In order to obtain generic stiffness design equations for the three types of flexure hinges, the ratio h/l and the deformation rotation θ are the key parameters. Therefore, the ratio h/l and the deformation rotation θ are chose as in Table 3.1. Here l equals to $2r$ (r is the radius of cross-section of a circular flexure hinge as shown in Figure 3.2(a)) for a circular flexure hinge, l equals to $2a$ (a is the major axis of an elliptical flexure hinge) for an elliptical flexure hinge, and l is the length of flexure hinge for a corner-filletted flexure hinge. Therefore, ten FEA models will be analyzed in the commercial software COMSOL for each type of flexure hinges.

2. Calculate the stiffness by using FEA and stiffness formulas for small deformation, Eq.3.3,3.5,3.8. The results of FEA will be obtained by the following equation:

$$M = K_{FEA}\theta \quad (3.10)$$

Table 3.1: h/l and θ

| | | | | | | | | | | |
|-------------------|------|-----|------|-----|------|-----|------|-----|------|-----|
| h/l | 0.1 | 0.2 | 0.3 | 0.4 | 0.5 | 0.6 | 0.7 | 0.8 | 0.9 | 1 |
| θ (radian) | 0.05 | 0.1 | 0.15 | 0.2 | 0.25 | 0.3 | 0.35 | 0.4 | 0.45 | 0.5 |

where the subscript FEA denotes the stiffness obtained by FEA data. M is a moment applied to the end of the flexure hinges, and θ is the rotational angle.

3. Compare the results obtained by FEA method with the results obtained by small deformation stiffness equations and find the difference between them. A correction factor has been defined as:

$$\Gamma = \frac{K_{FEA}}{K_S} \quad (3.11)$$

where Γ , is the correction factor influenced by shear stress. The target of this step is to get the design equations without ad hoc assumptions.

4. Fit the Γ mentioned above, and give the dimensionless stiffness equations by fitting the FEA results from the ones obtained by small deformation stiffness equations:

$$K_G = \Gamma K_S \quad (3.12)$$

where the subscription G denotes the stiffness equation is a generic equation. This generic stiffness equation can be used in the design of deep-beam or a flexure hinge undergoing large deflections.

3.2.1 Circular flexure hinges

Following the method mentioned above, the comparison graphs for circular flexure hinges are shown in Figures 3.5 and 3.6.

It can be concluded that the difference between the results obtained from the FEA and the small deformation stiffness equation increases with the deformation rotational angle θ and the ratio h/l increasing. This shows that the influence of shear force increases with the increasing deformation rotational angle θ and the ratio h/l . According to Eq. 3.11, ten sets of coefficients for ten FEA models are obtained and shown in Figure 3.7.

Following Step 3, a coefficient fitting equation for circular flexure hinges is obtained

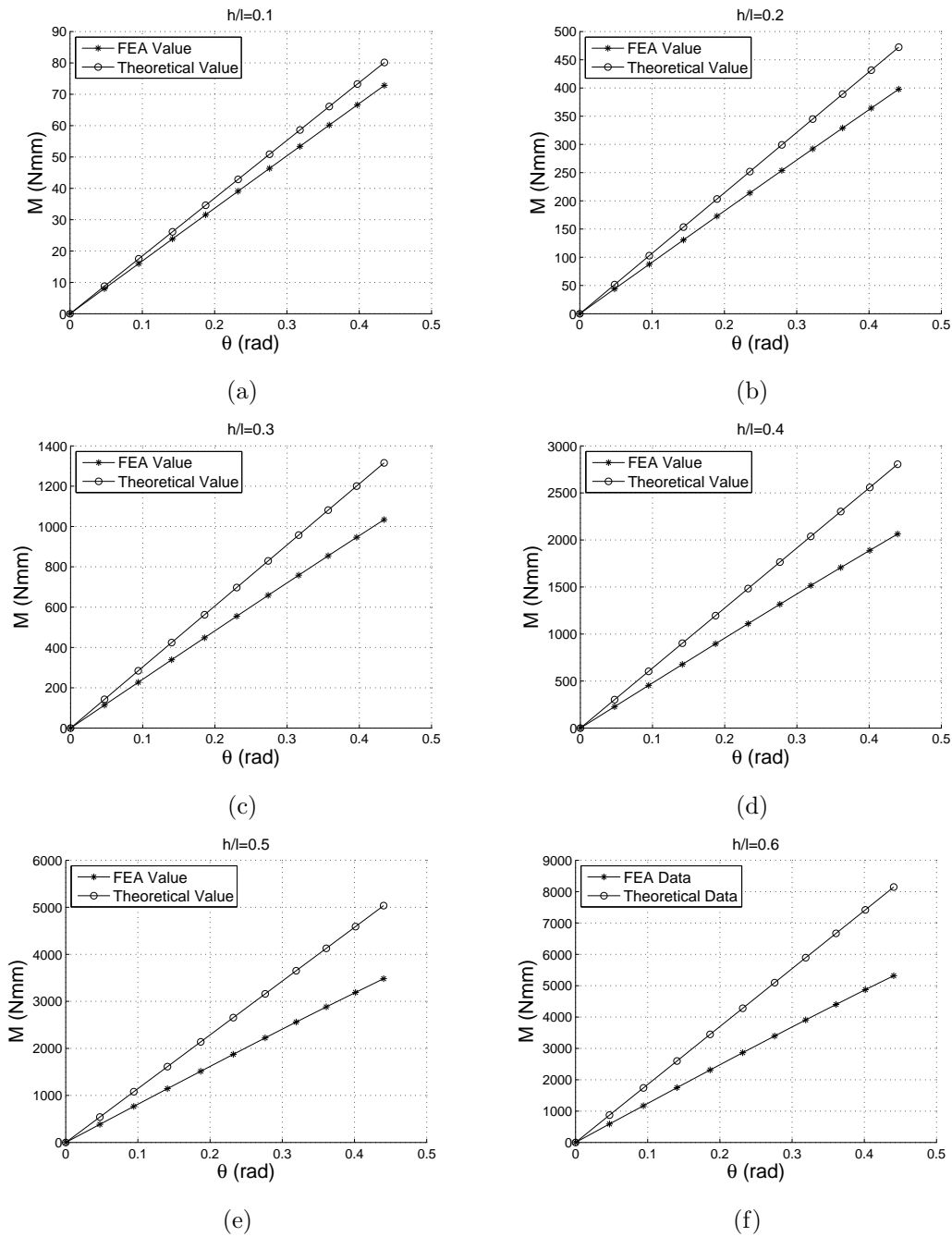


Figure 3.5: Part A: Comparison of the moment-rotation relationships obtained by FEA and small deformation stiffness equation for circular flexure hinges

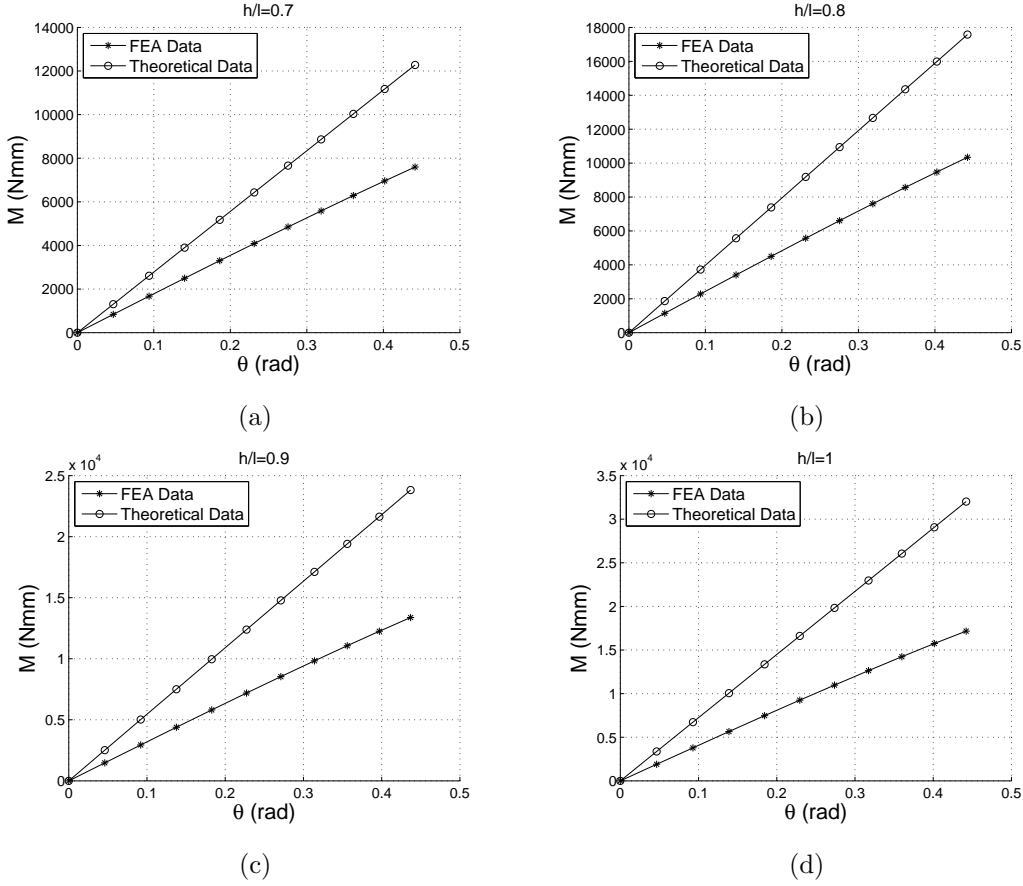


Figure 3.6: Part B: Comparison of the moment-rotation relationships obtained by FEA and small deformation stiffness equation for circular flexure hinges

by Eq. 3.13 in order to correct the small deformation stiffness equation for circular flexure hinges.

$$\Gamma_{N,C} = \sum_{i,j=0}^3 \mu_{ij} \theta^i \left(\frac{h}{l}\right)^j \quad \text{where } \mu_{ij} = 0 \text{ if } i + j \geq 4 \quad (3.13)$$

where, the subscript $\Gamma_{N,C}$ denotes the coefficients for correcting circular flexure-hinge stiffness formula for small deformation. $\mu_{i,j}$, ($i, j = 0, 1, 2, 3$) are given in Table 3.4.

The generic stiffness equation of circular flexure hinges obtained by Eq.(3.12) is:

$$K_{G,N,C} = \Gamma_{N,C} K_{S,C} \quad (3.14)$$

where the subscription G meaning is generic, N is for nonlinear, and C denotes circular flexure hinges.

Table 3.2: The coefficients of the modified linear/nonlinear coefficient equations

| Eq. 3.13 | | Eq. 3.15 | |
|------------|---------------|----------|--------------|
| μ_{00} | 0.9806483912 | ν_0 | 0.9780638940 |
| μ_{01} | -0.7188987234 | ν_1 | -0.742493327 |
| μ_{02} | 0.4226894870 | ν_2 | 0.4263492700 |
| μ_{03} | -0.1216940062 | ν_3 | -0.113300098 |
| μ_{10} | 0.0092610617 | | |
| μ_{11} | -0.0637867336 | | |
| μ_{12} | 0.0621808885 | | |
| μ_{20} | -0.0154084738 | | |
| μ_{21} | -0.1311447262 | | |
| μ_{30} | -0.0140972474 | | |

By inspection of Figure 3.7, which shows the relationship of coefficient versus rotational angle, it can be seen that the influence of the rotational angle on the coefficients is too small to be ignored. A relationship between the coefficient and the ratio h/l is shown in Figure 3.8.

By fitting the curves shown in Figure 3.8, a linear coefficient equation for correcting the small deformation stiffness equation is obtained:

$$\Gamma_{L,C} = \sum_{k=0}^3 \nu_k \left(\frac{h}{l} \right)^k \quad (3.15)$$

where the subscript L means linear, C is for circular flexure hinges. The modified coefficient equation is function of the ratio h/l only.

Therefore, the linear generic stiffness design equation is :

$$K_{G,L,C} = \Gamma_{L,C} K_{S,C} \quad (3.16)$$

The subscript G means generic, L is for linear, and C is for circular flexure hinges. ν_k , ($k = 0, 1, 2, 3$) are given in Table 3.4.

3.2.2 Elliptical flexure hinges

The analysis method of elliptical flexure hinges undergoing large deflection is performed following a similar way used in analyzing circular flexure hinges. The comparison graphs between results obtained from FEA (Eq.3.10) and small deformation

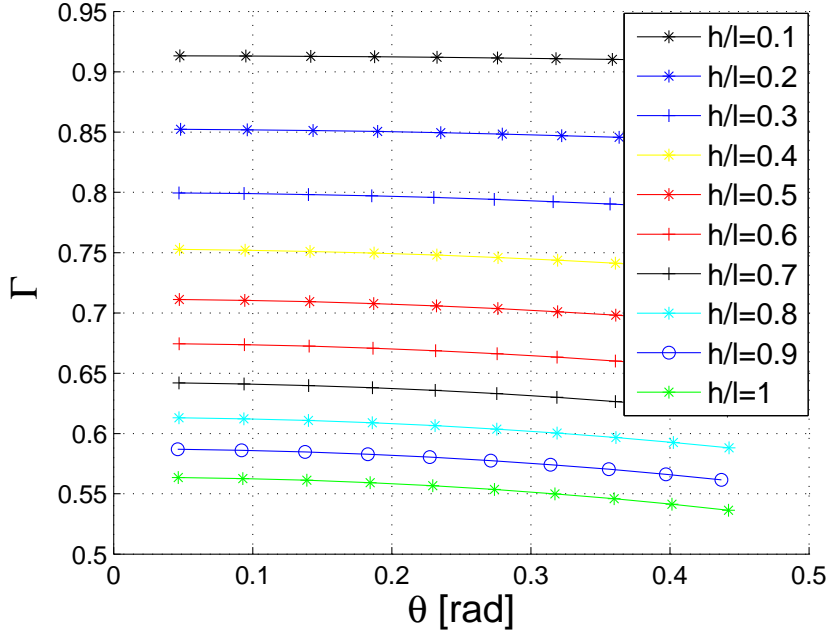


Figure 3.7: The $\Gamma - \theta$ relationship for circular flexure hinges

theory equation (Eq.3.5) for elliptical flexure hinges are shown in Figure 3.9 and Figure 3.10.

According to Eq. 3.11, ten sets of coefficients for ten FEA models are obtained and shown in Figure 3.11. Following Step 3, a coefficient fitting equation for elliptical flexure hinges is given in the following equation for correcting the elliptical flexure-hinge stiffness equation for small deformation.

$$\Gamma_{N,E} = \sum_{i,j=0}^3 \mu_{ij} \theta^i \left(\frac{h}{l}\right)^j \quad \text{where } \mu_{ij} = 0 \text{ if } i + j \geq 4 \quad (3.17)$$

$$(3.18)$$

where, the subscript N is for nonlinear, E means elliptical flexure hinges. $\mu_{i,j}$, ($i, j = 0, 1, 2, 3$) is given in Table 3.3.

The generic stiffness equation of elliptical flexure hinges is obtained by Eq.(3.12) and lead to:

$$K_{G,N,E} = \Gamma_{N,E} K_{S,E} \quad (3.19)$$

Referring to Figure 3.11, the effect of rotational angle upon the coefficient is too small to be ignored. Therefore, a relationship between the coefficient and the ratio h/l is shown in Figure 3.12.

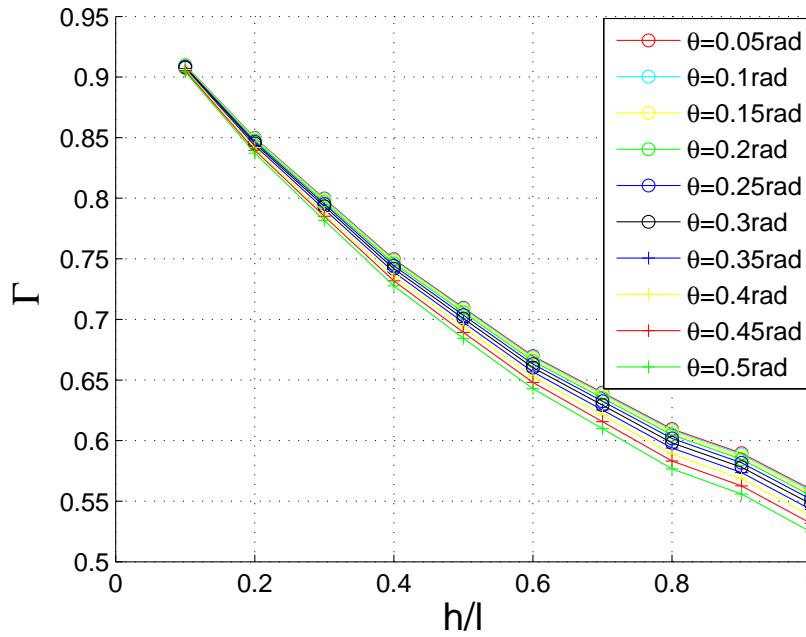


Figure 3.8: The $\Gamma - h/l$ relationship for circular flexure hinges

Table 3.3: The coefficients of the modified linear/nonlinear coefficient equations

| Eq. 3.17 | | Eq. 3.20 | |
|------------|---------------|----------|--------------|
| μ_{00} | 0.9900404617 | ν_0 | 0.983759894 |
| μ_{01} | -0.5796279622 | ν_1 | -0.564171511 |
| μ_{02} | 0.1818647630 | ν_2 | 0.12326874 |
| μ_{03} | -0.0043240000 | ν_3 | 0.034767849 |
| μ_{10} | 0.0093903912 | | |
| μ_{11} | -0.0591407532 | | |
| μ_{12} | 0.0565284698 | | |
| μ_{20} | -0.0077330730 | | |
| μ_{21} | -0.1173331034 | | |
| μ_{30} | -0.0059145774 | | |

By fitting the curves shown in Figure 3.12, a linear modified coefficient equation for correcting the small deformation stiffness equation can be obtained:

$$\Gamma_{L,E} = \sum_{k=0}^3 \nu_k \left(\frac{h}{l} \right)^k \quad (3.20)$$

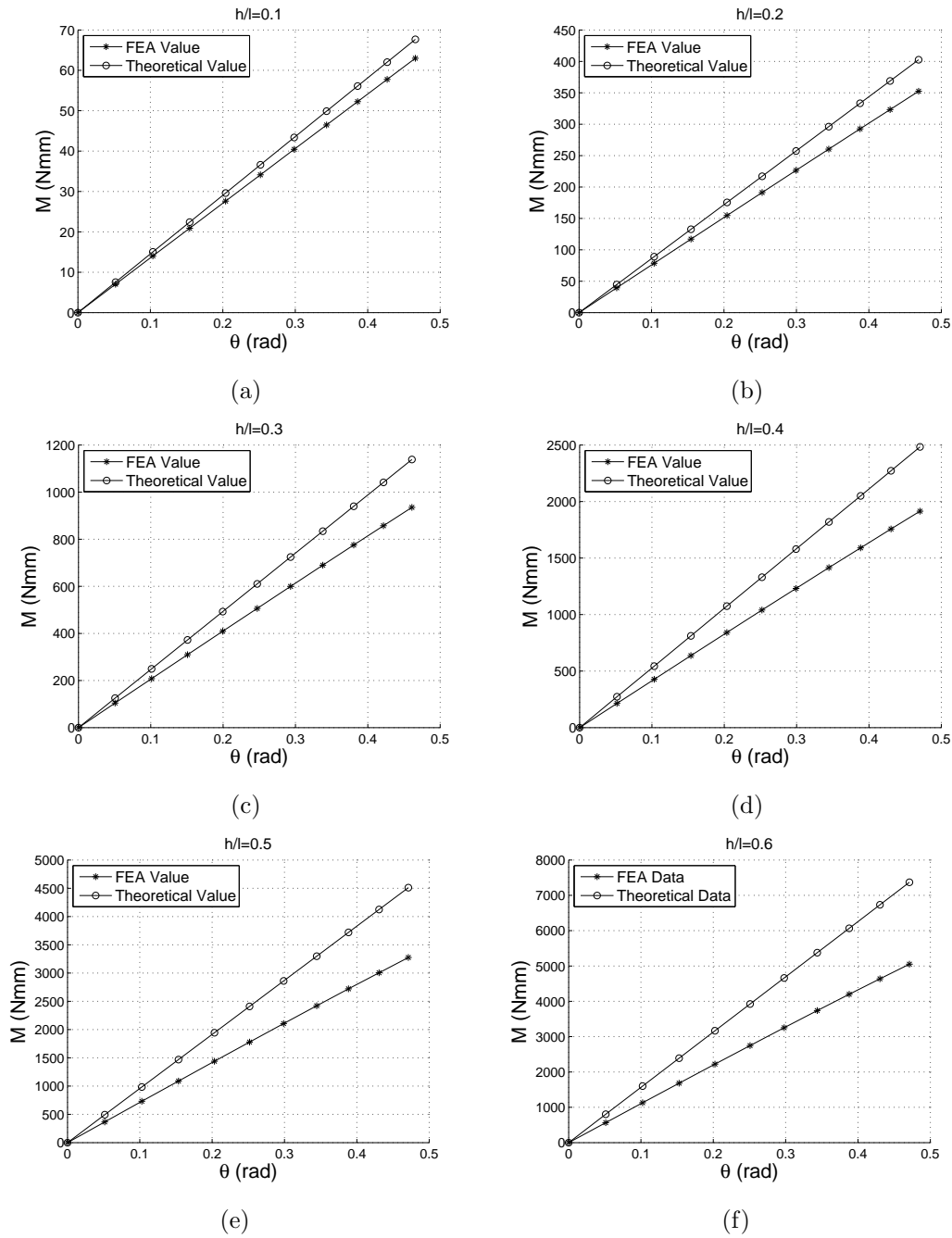


Figure 3.9: Part A: Comparison of the moment-rotation relationships obtained by FEA and small deformation stiffness equation for elliptical flexure hinges

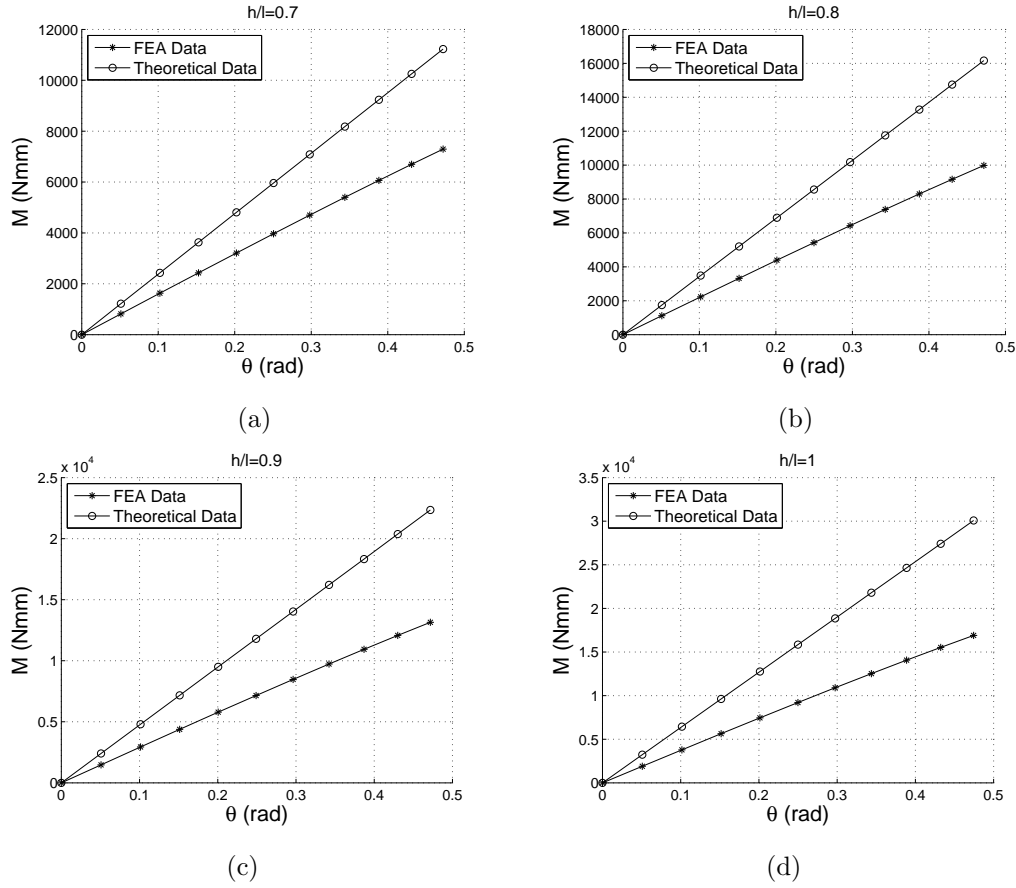


Figure 3.10: Part B: Comparison of the moment-rotation relationships obtained by FEA and small deformation stiffness equation for elliptical flexure hinges

where the subscript L denotes that the equation is linear, E is for elliptical flexure hinges. This modified coefficient equation is just the function of the ratio h/l .

Thus, the linear generic stiffness design equation is :

$$K_{G,L,E} = \Gamma_{L,E} K_{S,E} \quad (3.21)$$

The subscript Gl is for generic, L is for linear, here the meaning of linear denotes the modified coefficient equation $\Gamma_{L,E}$ is linear, E is elliptical flexure hinges.

3.2.3 Corner-filletted flexure hinges

Following a similar method as described above, the comparison graphs for corner-filletted flexure hinges are shown in Figures 3.13 and 3.14. According to Eq. 3.11, ten sets of coefficients for ten FEA models are obtained and shown in Figure 3.15.

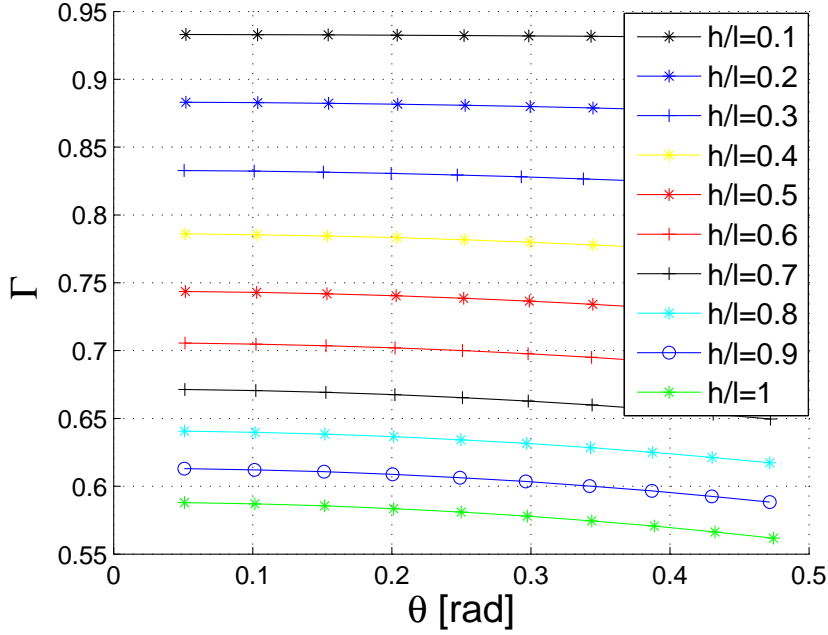


Figure 3.11: The $\Gamma - \theta$ relationship for elliptical flexure hinges

Following Step 3, a coefficient fitting equation for corner-filletted flexure hinges is produced in Eq. 3.22 for correcting the corner-filletted flexure hinges stiffness equation for small deformation.

$$\Gamma_{N,R} = \sum_{i,j=0}^3 \mu_{ij} \theta^i \left(\frac{h}{l}\right)^j \quad \text{where } \mu_{ij} = 0 \text{ if } i + j \geq 4 \quad (3.22)$$

where, the subscript N meaning is for nonlinear, and R denotes the corner-filletted flexure hinges.

The generic stiffness equation of corner-filletted flexure hinges obtained by Eq.(3.12) and lead to:

$$K_{G,N,R} = \Gamma_{N,R} K_{S,R} \quad (3.23)$$

where the subscripts G is for generic, N is for nonlinear, and R denotes the corner-filletted flexure hinges. Looking back at Figure 3.15, the influence of rotational angle on the coefficient is so tiny that it can be ignored. Therefore, a relationship between the coefficient and the ratio h/l is shown in Figure 3.16.

Obtaining the fitting equation from the curves shown in Figure 3.16, the linear modified coefficient equation is shown to be as follows:

$$\Gamma_{L,R} = \sum_{k=0}^3 \nu_k \left(\frac{h}{l}\right)^k \quad (3.24)$$

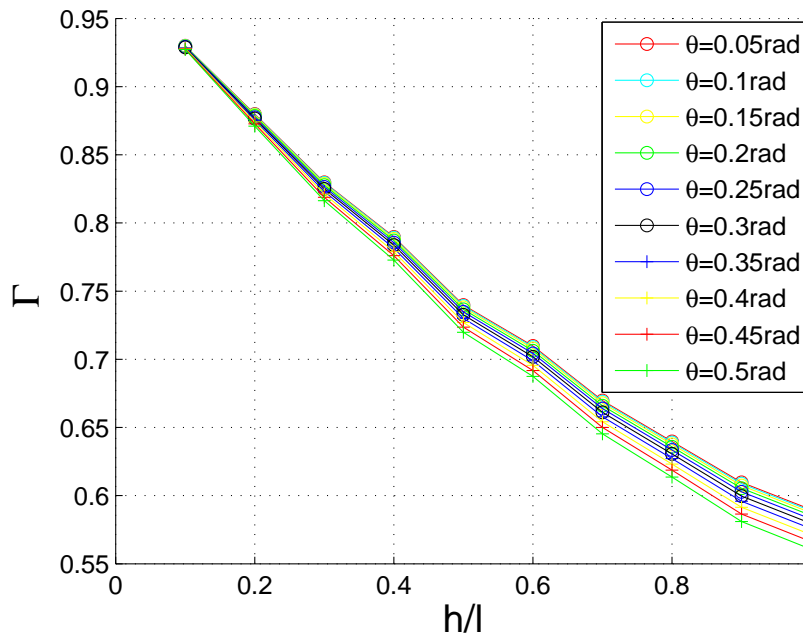


Figure 3.12: The $\Gamma - h/l$ relationship for elliptical flexure hinges

Table 3.4: The coefficients of the modified linear/nonlinear coefficient equations

| Eq. 3.22 | | Eq. 3.24 | |
|------------|---------------|----------|--------------|
| μ_{00} | 1.0160649738 | ν_0 | 1.0188556500 |
| μ_{01} | -0.6806918859 | ν_1 | -0.713718696 |
| μ_{02} | 0.2923808930 | ν_2 | 0.3505313250 |
| μ_{03} | -0.0437517603 | ν_3 | -0.081827186 |
| μ_{10} | 0.0024102766 | | |
| μ_{11} | -0.0186960657 | | |
| μ_{12} | 0.0180951590 | | |
| μ_{20} | 0.0095757216 | | |
| μ_{21} | -0.0952978063 | | |
| μ_{30} | -0.0037196879 | | |

where the subscripts L means linear, R denotes the corner-filletted flexure hinges. The linear modified equation is function of the ratio h/l only. Therefore, the linear generic stiffness design equation is :

$$K_{G,L,R} = \Gamma_{L,R} K_{S,R} \quad (3.25)$$

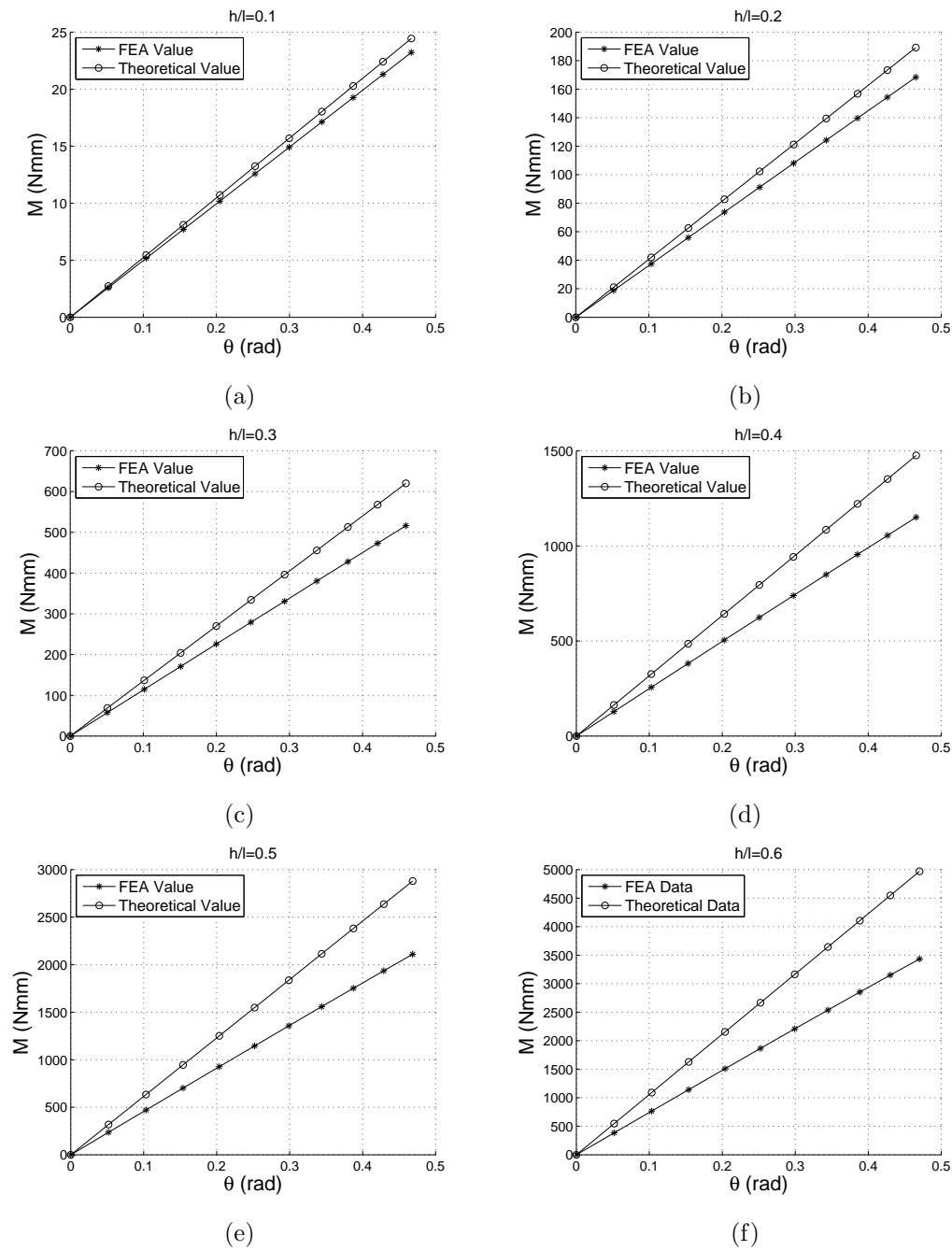


Figure 3.13: Part A: Comparison of the moment-rotation relationships obtained by FEA and small deformation stiffness equation for corner-filleted flexure hinges

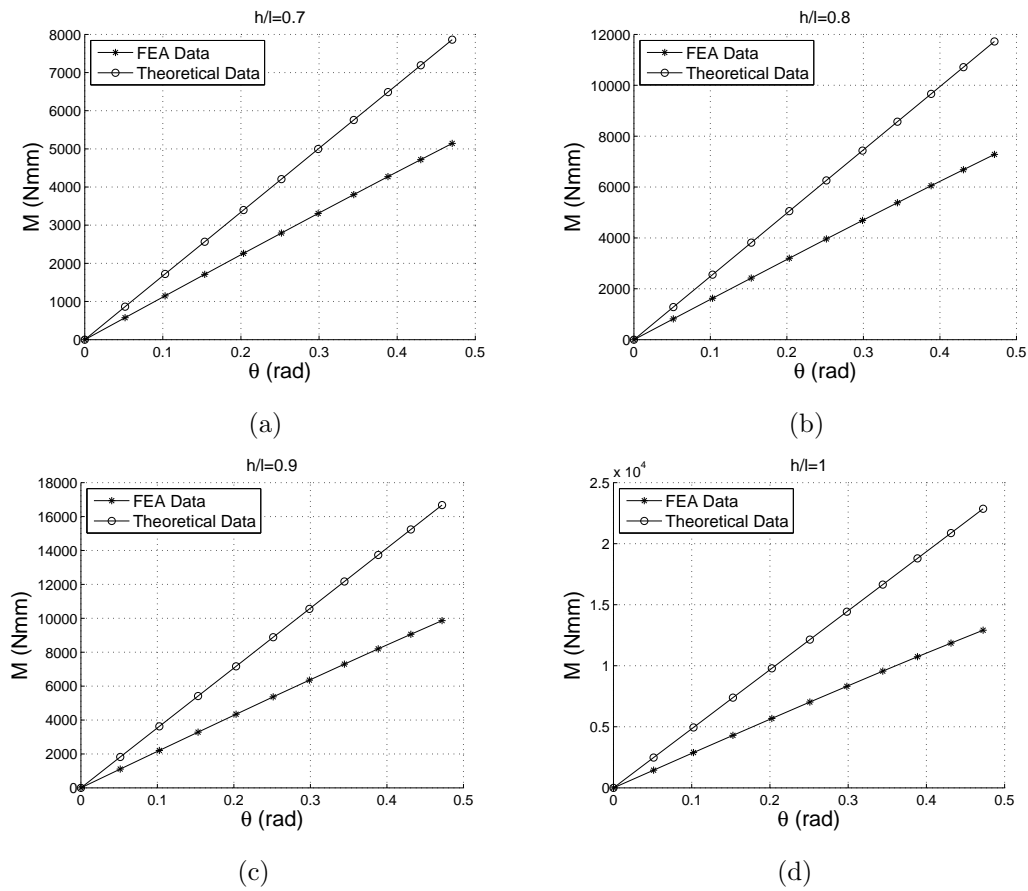


Figure 3.14: Part B: Comparison of the moment-rotation relationships obtained by FEA and small deformation stiffness equation for corner-filleted flexure hinges

The subscripts G means generic, L means linear, The modified coefficient equation is linear. R denotes the corner-filleted flexure hinges.

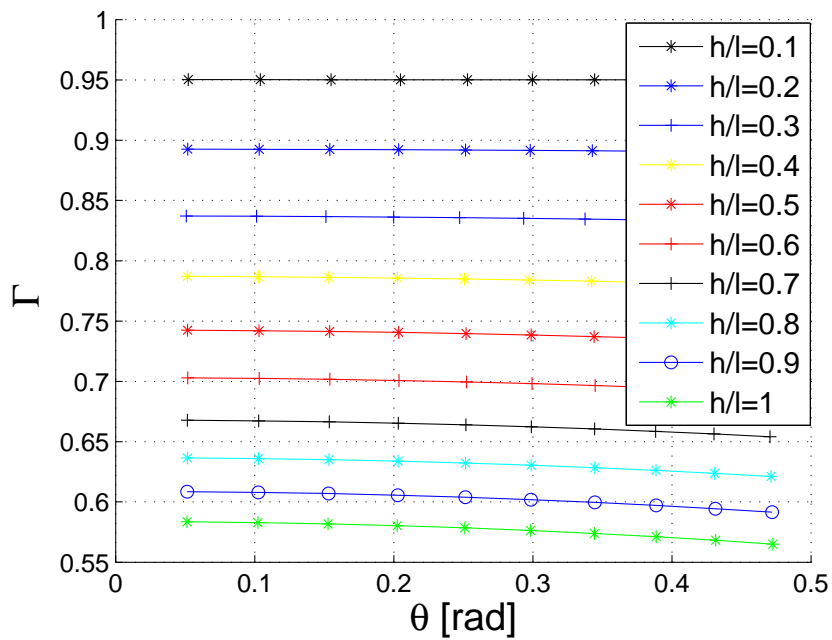


Figure 3.15: The $\Gamma - \theta$ relationship for corner-filletted flexure hinges

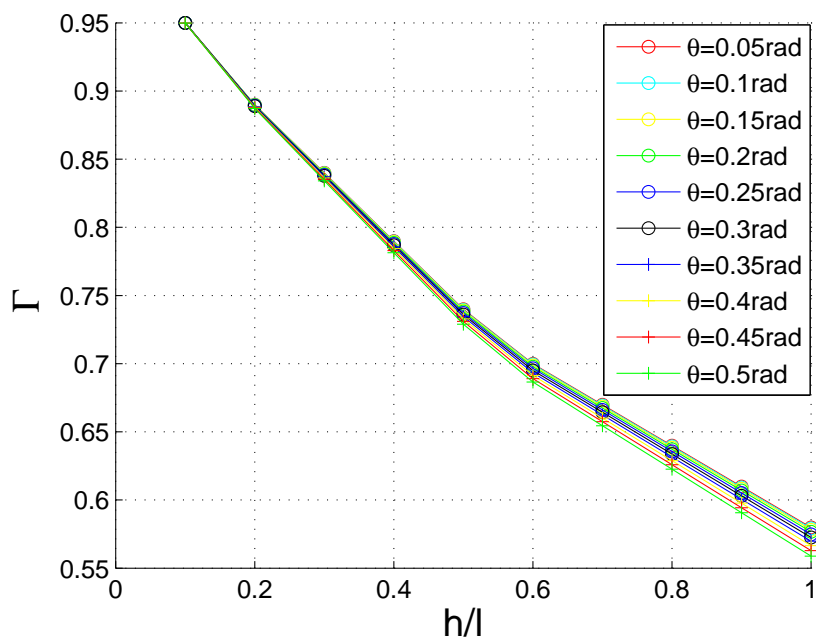


Figure 3.16: The $\Gamma - h/l$ relationship for corner-filletted flexure hinges

Chapter 4

Stress-Based Design of Flexure Hinges

This chapter studies the maximum stress characteristic for the three common types of flexure hinges by means of the FEA method. For each type of flexure hinges, there are three corresponding parameters, S_Y/E , h/l and the deflection rotation θ . Finally, three sets of generic design equations based on stress characteristics for each type of flexure hinges are proposed.

In FCMs, the flexure hinges are the first components to be failure prone, as they have the foremost exposure to loading, given their smaller dimensions. As previously reported, flexure hinges are capable of undergoing large deformations and entering the plastic domain before fracture occurs. Therefore, stress characteristics are the one of important design criteria for the design of flexure hinges.

The relationship between material characterized by a certain $\bar{\sigma} = S_Y/E$, where S_Y is the material yield strength, i.e. the bearable maximum stress of material, the maximum rotation θ bearable by the hinge at the limit of material failure and the geometry characterized by a maximum ratio h/l designable for the hinge following design requirements will be discussed in the chapter. Three types of flexure hinges studied in the chapter will be analyzed following three aspects:

- For a given material characterized by a $\bar{\sigma}$ ratio, the maximum rotation bearable by the hinge at the limit of material failure can be approximated. Beside the
-

principal stiffness, the results of the FEA simulations have been used to find an estimate for the maximum stress/strain that can be borne by the hinge. In engineering, there are main three theories that can be utilized to predict the critical condition in a body under a complex state of stress. The three theories are the maximum energy of deformation theory (Von Mises), the maximum shear stress theory (Tresca) and the maximum total strain energy theory (Beltrami-Haigh) [34]. This thesis will use the Von Mises strength theory;

- For a desired maximum rotation θ bearable by the hinge at the limit of material failure, the material of hinge can be chosen;
- For a desired geometry characterized by a maximum ratio h/l , the maximum rotation θ can be evaluated.

The above-mentioned items will be discussed in the following in more detail for the three types of flexure hinges.

4.1 Circular Flexure Hinges

Ten circular flexure hinges which are studied in Chapter 3 will be now analyzed, following the path presented above. As described in the following, the maximum stress for each studied model can be obtained according to Von Mises theory by a FEA software. Hence, the relationship between $\bar{\sigma}$, θ and h/l is shown in Figure 4.1.

According to the relationship, the closed-form equations describing the capacity of rotation for a flexure hinge, the material characteristic and the designable geometric characteristic are given next.

4.1.1 Capacity of rotation

The coordinates in Figure 4.1 are transformed, i.e. x-axis will denote $\bar{\sigma}$, and y-axis will denote θ , the new graph is shown in Figure 4.2. for a given material characterized by a certain $\bar{\sigma}$ and geometric characteristic h/l , the maximum rotation bearable by the hinge at the limit of material failure can be approximated by the following empirical relation:

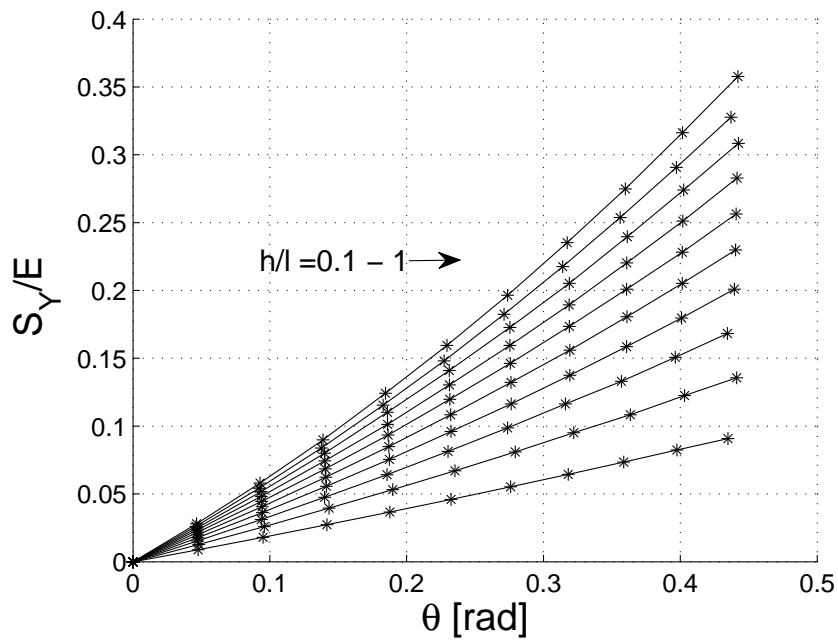


Figure 4.1: The relationship between $\bar{\sigma}$, θ and h/l for ten circular flexure hinges

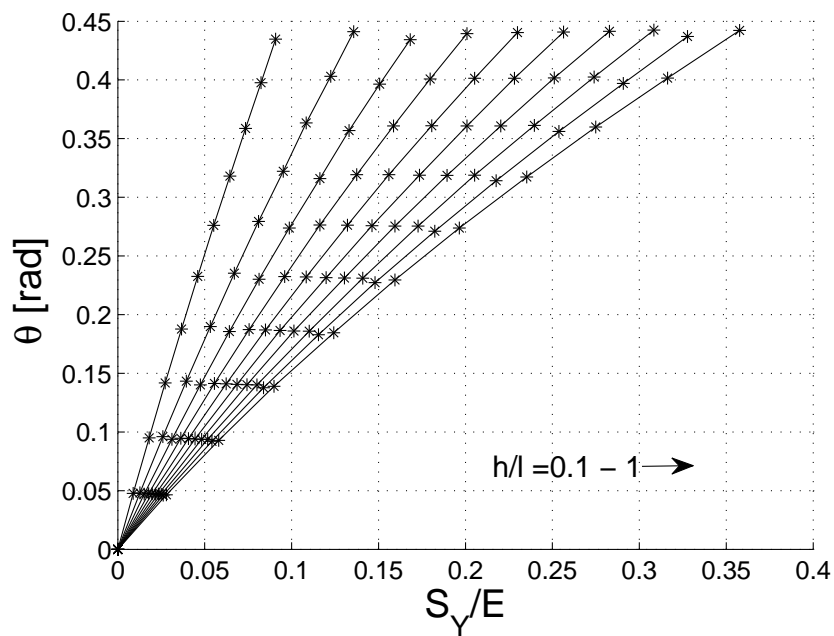


Figure 4.2: The relationship between θ , $\bar{\sigma}$ and h/l for ten circular flexure hinges

Table 4.1: Parameters for rotation design equation of circular flexure hinges

| Parameter | Value | Parameter | Value |
|------------|--------------|------------|--------------|
| ξ_{00} | -0.004891814 | ξ_{01} | -0.012458952 |
| ξ_{02} | -0.107789386 | ξ_{03} | 0.5750808338 |
| ξ_{10} | 0.1795051891 | ξ_{11} | 0.4709110597 |
| ξ_{12} | -0.630828220 | ξ_{20} | 0.5426186030 |
| ξ_{21} | 0.3773006620 | ξ_{30} | -0.141083131 |

Table 4.2: Parameters for material characteristic equation of circular flexure hinges

| Parameter | Value | Parameter | Value |
|-----------|---------------|-----------|---------------|
| a_{00} | 0.261241061 | a_{01} | 3.099213114 |
| a_{02} | -3.603327270 | a_{03} | 2.7856512330 |
| a_{04} | -0.8819542210 | a_{10} | 0.0011222362 |
| a_{11} | -1.395162109 | a_{12} | 0.5941891577 |
| a_{13} | 0.0240168305 | a_{14} | -0.1952204707 |

$$\theta_{z,max} = 1 \left/ \sum_{i,j=0}^3 \xi_{ij} \left(\frac{h}{l}\right)^{i-1} \bar{\sigma}^{j-1} \right. \text{ where } \xi_{ij} = 0 \text{ if } i + j \geq 4 \quad (4.1)$$

where the parameters ξ_{ij} , ($i, j = 0, 1, 2, 3$) are shown in Table 4.1.

4.1.2 Material characteristic

According to the relationship shown in Figure 4.1, for a desired maximum rotation θ_z and geometric characteristic h/l , the closed-form equation for material characteristic is:

$$\bar{\sigma} = \theta \left(\frac{h}{l}\right) \left/ \sum_{i,j=0}^4 a_{ij} \theta_{z,max}^i \left(\frac{h}{l}\right)^j \right. \text{ where } a_{ij} = 0 \text{ if } i \geq 2 \quad (4.2)$$

where the parameters a_{ij} , ($i, j = 0, 1, 2, 3, 4$) are shown in Table 4.2.

4.1.3 Geometric characteristic

The coordinates in Figure 4.1, i.e. x-axis will denote $\bar{\sigma}$, and y-axis will denote h/l , the new graph is shown in Figure 4.3. For a given material characterized by a

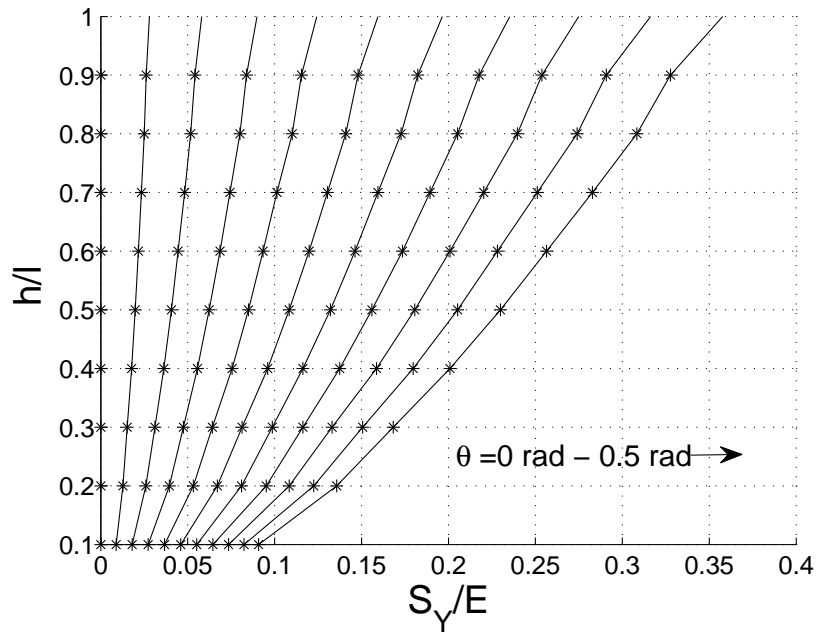


Figure 4.3: The relationship between h/l , θ and $\bar{\sigma}$ for ten circular flexure hinges

certain $\bar{\sigma}$ and the desired rotation θ , the maximum designable ratio of h/l can be approximated by the following empirical relation:

$$\left(\frac{h}{l}\right)_{max} = \chi^* + 1 \left/ \sum_{i,j=0}^2 \chi_{ij} \bar{\sigma}^{i-1} \theta_{z,max}^{j-1} \right. \quad (4.3)$$

where the parameters χ_{ij} , ($i, j = 0, 1, 2$) are shown in Table 4.3.

Table 4.3: Parameters for geometric characteristic equation of circular flexure hinges

| Parameter | Value | Parameter | Value |
|-------------|-------------|-------------|-------------|
| χ_{00} | 0.000077164 | χ_{01} | 0.001055602 |
| χ_{02} | 1.989063367 | χ_{10} | -0.00347776 |
| χ_{11} | -3.03144059 | χ_{12} | -2.36271139 |
| χ_{20} | 1.664255871 | χ_{21} | 2.533156330 |
| χ_{22} | 0.236181294 | χ^* | -0.06320109 |

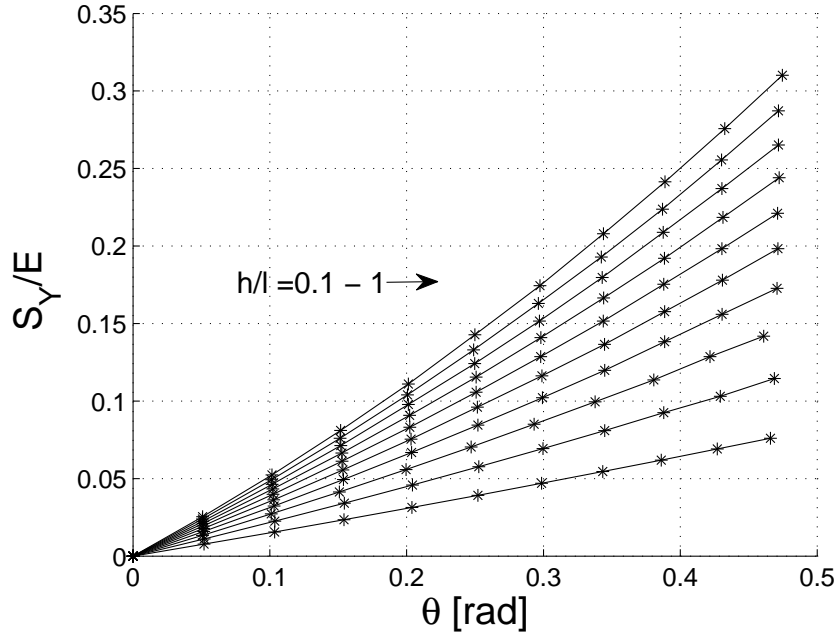


Figure 4.4: The relationship between $\bar{\sigma}$, θ and h/l for ten elliptical flexure hinges

4.2 Elliptical Flexure Hinges

Ten elliptical flexure hinges which are studied in Chapter 3 will be now analyzed, following the procedure used for circular flexure hinges. The relationship between $\bar{\sigma}$, θ and h/l for ten elliptical flexure hinges is shown in Figure 4.4. According to relationship, the closed-form equations describing the capacity of rotation for a flexure hinge, the material characteristic and the designable geometric characteristic are given next.

4.2.1 Capacity of rotation

The coordinates in Figure 4.4, i.e. x-axis will denote $\bar{\sigma}$, and y-axis will denote θ , the new graph is shown in Figure 4.5. For a given material characterized by a certain $\bar{\sigma}$ and geometric characteristic h/l , the maximum rotation bearable by the hinge at the limit of material failure can be approximated by the following empirical relation:

$$\theta_{z,max} = 1 \left/ \sum_{i,j=0}^3 \xi_{ij} \left(\frac{h}{l} \right)^{i-1} \bar{\sigma}^{j-1} \right. \text{ where } \xi_{ij} = 0 \text{ if } i + j \geq 4 \quad (4.4)$$

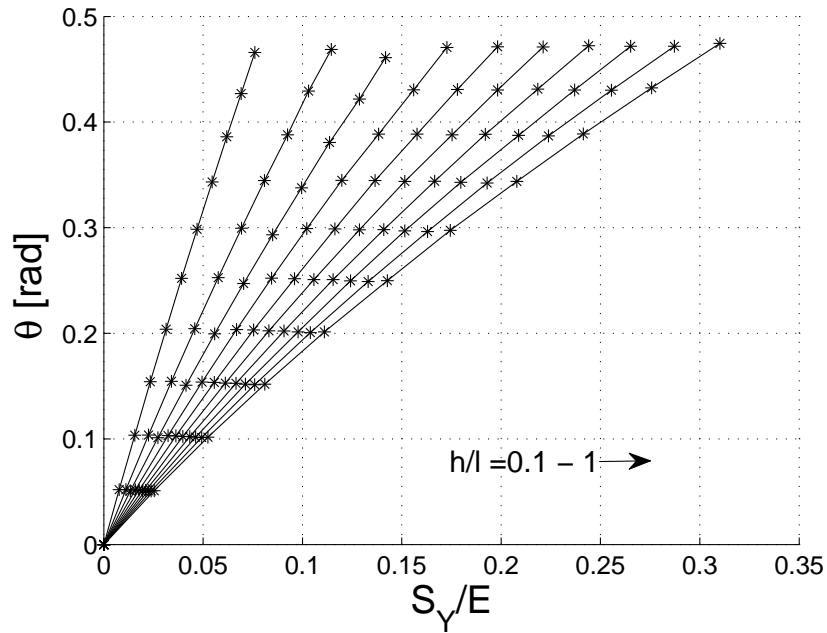


Figure 4.5: The relationship between θ , $\bar{\sigma}$ and h/l for ten elliptical flexure hinges

where the parameters ξ_{ij} , ($i, j = 0, 1, 2, 3$) are shown in Table 4.4.

4.2.2 Material characteristic

According to the relationship shown in Figure 4.4, for a desired maximum rotation θ_z and geometric characteristic h/l , the closed-form equation for material characteristic is:

Table 4.4: Parameters for rotation design equation of elliptical flexure hinges

| Parameter | Value | Parameter | Value |
|------------|--------------|------------|--------------|
| ξ_{00} | -0.003912317 | ξ_{01} | -0.014065652 |
| ξ_{02} | -0.047502868 | ξ_{03} | 0.3072218785 |
| ξ_{10} | 0.1396638150 | ξ_{11} | 0.3814235019 |
| ξ_{12} | -0.446640615 | ξ_{20} | 0.4702100794 |
| ξ_{21} | 0.3099882352 | ξ_{30} | -0.125977059 |

Table 4.5: Parameters for material characteristic equation of elliptical flexure hinges

| Parameter | Value | Parameter | Value |
|-----------|-------------|-----------|-------------|
| b_{00} | 0.411717398 | b_{01} | 3.071247682 |
| b_{02} | -2.18858763 | b_{03} | 0.780857329 |
| b_{10} | -0.04764814 | b_{11} | -1.59905558 |
| b_{12} | 0.216544677 | b_{20} | 0.115082225 |
| b_{21} | 0.575087469 | b_{30} | -0.17321061 |

Table 4.6: Parameters for geometric characteristic equation of elliptical flexure hinges

| Parameter | Value | Parameter | Value |
|-------------|-------------|-------------|-------------|
| χ_{00} | 0.000086190 | χ_{01} | -0.00052103 |
| χ_{02} | 2.256250214 | χ_{10} | -0.00270067 |
| χ_{11} | -2.86987560 | χ_{12} | -2.42279627 |
| χ_{20} | 1.343670651 | χ_{21} | 2.112534561 |
| χ_{22} | 0.309589658 | χ^* | -0.05527670 |

$$\bar{\sigma} = 1 \left/ \sum_{i,j=0}^3 b_{ij} \theta_{z,max}^{i-1} \left(\frac{h}{l} \right)^{j-1} \right. \quad \text{where } b_{ij} = 0 \text{ if } i + j \geq 4 \quad (4.5)$$

where the parameters b_{ij} , ($i, j = 0, 1, 2, 3$) are shown in Table 4.5.

4.2.3 Geometric characteristic

The coordinates in Figure 4.4, i.e. x-axis will denote $\bar{\sigma}$, and y-axis will denote h/l , the new graph is shown in Figure 4.6. For a given material characterized by a certain $\bar{\sigma}$ and the desired rotation θ , the maximum designable ratio of h/l can be approximated by the following empirical relation:

$$\left(\frac{h}{l} \right)_{max} = \chi^* + 1 \left/ \sum_{i,j=0}^2 \chi_{ij} \bar{\sigma}^{i-1} \theta_{z,max}^{j-1} \right. \quad (4.6)$$

where the parameters χ_{ij} , ($i, j = 0, 1, 2$) are shown in Table 4.6.

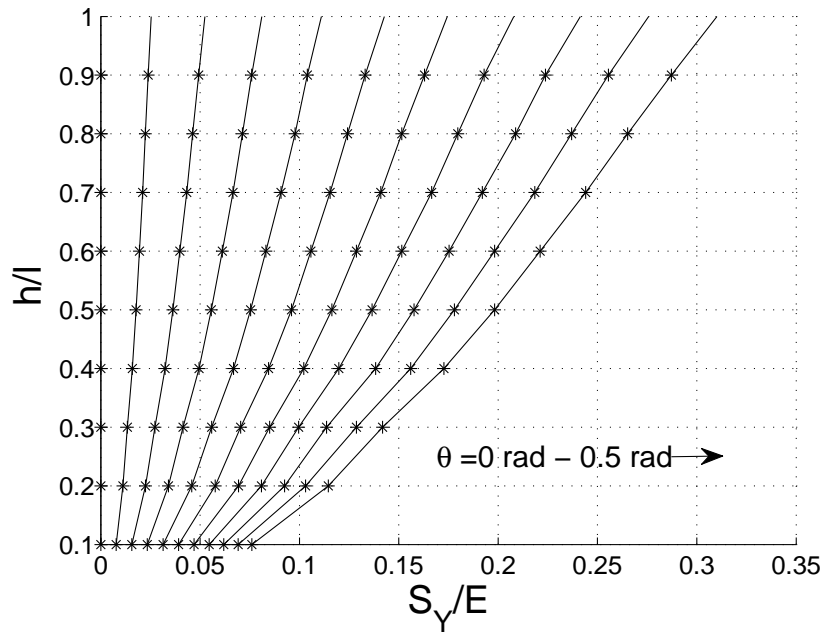


Figure 4.6: The relationship between h/l , θ and $\bar{\sigma}$ for ten elliptical flexure hinges

4.3 Corner-Filletted Flexure Hinges

Ten corner-filletted flexure hinges which are studied in Chapter 3 will be now analyzed, following the procedure used for circular flexure hinges. The relationship between $\bar{\sigma}$, θ and h/l for ten corner-filletted flexure hinges is shown in Figure 4.7. According to the relationship, the closed-form equations describing the capacity of rotation for a flexure hinge, the material characteristic and the designable geometric characteristics are given in the following.

4.3.1 Capacity of rotation

The coordinates in Figure 4.7, i.e. x-axis will denote $\bar{\sigma}$, and y-axis will denote θ , the new graph is shown in Figure 4.8. For a given material characterized by a certain $\bar{\sigma}$ and geometric characteristic h/l , the maximum rotation bearable by the hinge at the limit of material failure can be approximated by the following empirical relation:

$$\theta_{z,max} = 1 \left/ \sum_{i,j=0}^3 \xi_{ij} \left(\frac{h}{l} \right)^{i-1} \bar{\sigma}^{j-1} \right. \text{ where } \xi_{ij} = 0 \text{ if } i + j \geq 4 \quad (4.7)$$

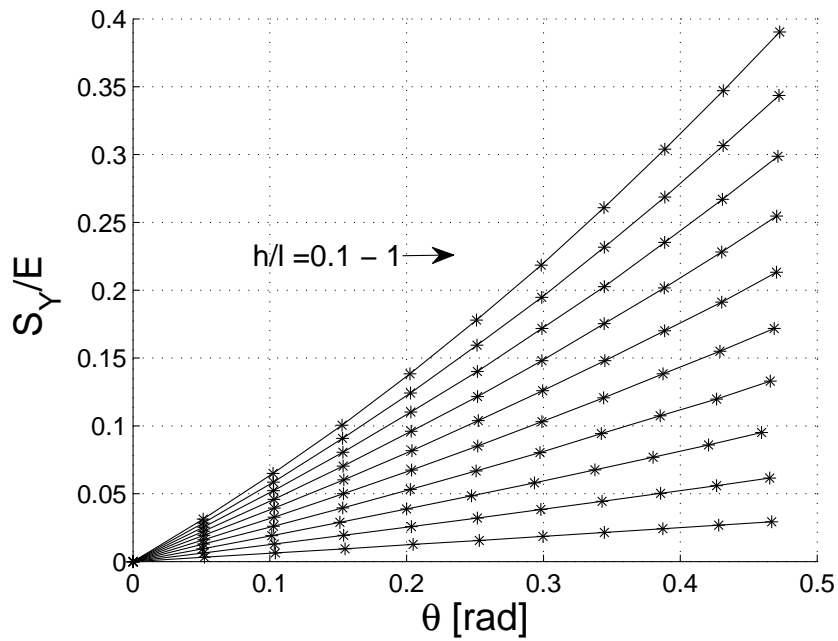


Figure 4.7: The relationship between $\bar{\sigma}$, θ and h/l for ten corner-filleted flexure hinges

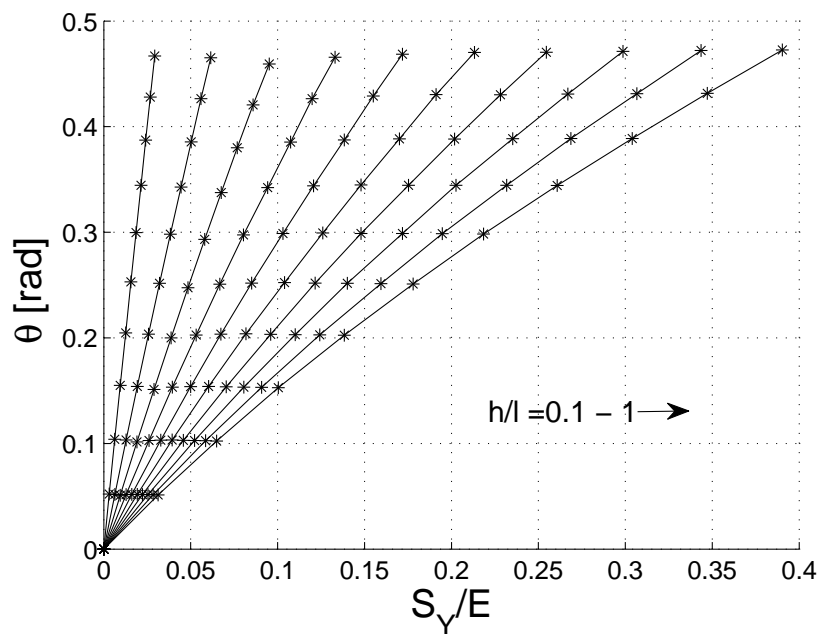


Figure 4.8: The relationship between θ , $\bar{\sigma}$ and h/l for ten corner-filleted flexure hinges

Table 4.7: Parameters for rotation design equation of corner-filletted flexure hinges

| Parameter | Value | Parameter | Value |
|------------|-------------|------------|-------------|
| ξ_{00} | 0.000854695 | ξ_{01} | -0.00863043 |
| ξ_{02} | 0.046516289 | ξ_{03} | 0.131309678 |
| ξ_{10} | -0.01469291 | ξ_{11} | 0.096624025 |
| ξ_{12} | -0.48645218 | ξ_{20} | -0.67373034 |
| ξ_{21} | 0.687140897 | ξ_{30} | -0.07608612 |

Table 4.8: Parameters for material characteristic equation of corner-filletted flexure hinges

| Parameter | Value | Parameter | Value |
|-----------|-------------|-----------|-------------|
| c_{00} | 0.000095893 | c_{01} | -0.00069024 |
| c_{02} | 0.000874360 | c_{10} | -0.00661849 |
| c_{11} | 0.661935750 | c_{12} | -0.08068387 |
| c_{20} | -0.00012609 | c_{21} | 0.008836010 |
| c_{22} | 0.523202666 | | |

where the parameters ξ_{ij} , ($i, j = 0, 1, 2, 3$) are shown in Table 4.7.

4.3.2 Material characteristic

According to the relationship shown in Figure 4.7, for a desired maximum rotation θ_z and geometric characteristic h/l , the closed-form equation for material characteristic is:

$$\bar{\sigma} = \sum_{i,j=0}^2 c_{ij} \theta_{z,max}^i \left(\frac{h}{l}\right)^j \quad (4.8)$$

where the parameters c_{ij} , ($i, j = 0, 1, 2$) are shown in Table 4.8.

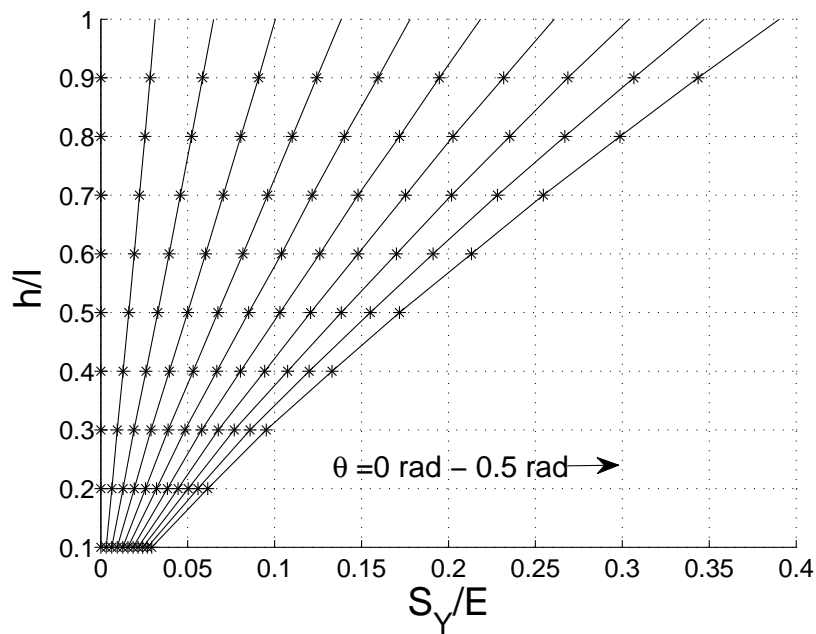
4.3.3 Geometric characteristic

The coordinates in Figure 4.7, i.e. x-axis will denote $\bar{\sigma}$, and y-axis will denote h/l , the new graph is shown in Figure 4.9.

For a given material characterized by a certain $\bar{\sigma}$ and the desired rotation θ , the maximum designable ratio of h/l can be approximated by the following empirical

Table 4.9: Parameters for geometric characteristic equation of corner-filleted flexure hinges

| Parameter | Value | Parameter | Value |
|-------------|--------------|-------------|--------------|
| χ_{00} | 0.0000466754 | χ_{01} | -0.000038222 |
| χ_{02} | -0.047474963 | χ_{10} | -0.001533606 |
| χ_{11} | -0.046694556 | χ_{12} | 0.0296131351 |
| χ_{20} | 0.6481165023 | χ_{21} | 0.7414768345 |
| χ_{22} | -0.280092045 | χ^* | 0.0057545458 |

Figure 4.9: The relationship between h/l , θ and $\bar{\sigma}$ for ten corner-filleted flexure hinges

relation:

$$\left(\frac{h}{l}\right)_{max} = \chi^* + 1 \left/ \sum_{i,j=0}^2 \chi_{ij} \bar{\sigma}^{i-1} \theta_{z,max}^{j-1} \right. \quad (4.9)$$

where the parameters χ_{ij} , ($i, j = 0, 1, 2$) are shown in Table 4.9.

Chapter 5

Discussion and Error Analysis

This chapter discusses the characteristics of the generic design equations proposed in Chapter 3 and Chapter 4 and analyzes the errors produced by these equations compared with the FEA results. Meantime, the correctness and applicability for these equations are evaluated.

Chapter 3 proposes nonlinear and linear modified coefficient equations for the small deformation stiffness equations of three types of flexure hinges. The generic stiffness design equations, which combined modified coefficient equations and small deflection stiffness equations, are proposed in the end. Chapter 4 proposes three sets of relation equations for material characteristic $\bar{\sigma}$, maximum bearable rotation $\theta_{z,max}$ and geometric characteristic h/l , which are three important parameters in design of flexure hinges. Hereafter, these relation equations will be called as stress generic design equations. Their application has been discussed in previous part of Chapter 4.

The correctness and applicability of these generic stiffness and stress design equations are very important in the reality applications. This chapter will discuss these problems for these proposed equations compared to their corresponding FEA results.

5.1 Evaluation of Stiffness Generic Design Equations

According to the work presented in Chapter 3, the nonlinear modified coefficient equations are more accurate than the linear modified coefficient equations. However, linear modified coefficient equations are more simple and easier to be used in the design of flexure hinges than the nonlinear modified coefficient equations. This section will discuss both the forms of generic stiffness design equations for each type of flexure hinges.

5.1.1 Circular flexure hinges

- Generic stiffness design equation with nonlinear modified coefficient equation.

According to Eq. 3.14, the comparison between the FEA results of the reality analysis models and the fitting results calculated by Eq. 3.14 is shown in Figure 5.1a. It can be seen from this figure that the fitting results are close to FEA results. In order to verify the fitting results, the errors for the proposed equation are analyzed according to the relation:

$$error = \frac{\theta_G - \theta_{FEA}}{\theta_{FEA}} \times 100\% \quad (5.1)$$

where θ_G is the rotation obtained by the proposed equation, and θ_{FEA} is the rotation obtained by FEA method. The error analysis results are shown in Figure 5.1 b. The maximum error is 0.0778%.

- Generic stiffness design equation with linear modified coefficient equation.

Linear modified coefficient equation is proposed in order to simplify the design equation and be easily used in design of flexure hinges. It can be seen that the linear modified equation Eq.3.16 is function of the geometric characteristic h/l only. The comparison between the FEA results of the reality analysis models and the fitting results calculated by Eq. 3.16 is shown in Figure 5.2(a). From this figure, it can be seen that the fitting results are close to FEA results. In order to verify the fitting results, the results of the errors analysis compared to the FEA results are shown in Figure 5.2(b). The maximum error is 2.2909%. It can be seen that the generic stiffness design equation with linear modified coefficient equation does not have the same precision as the design equation with nonlinear modified

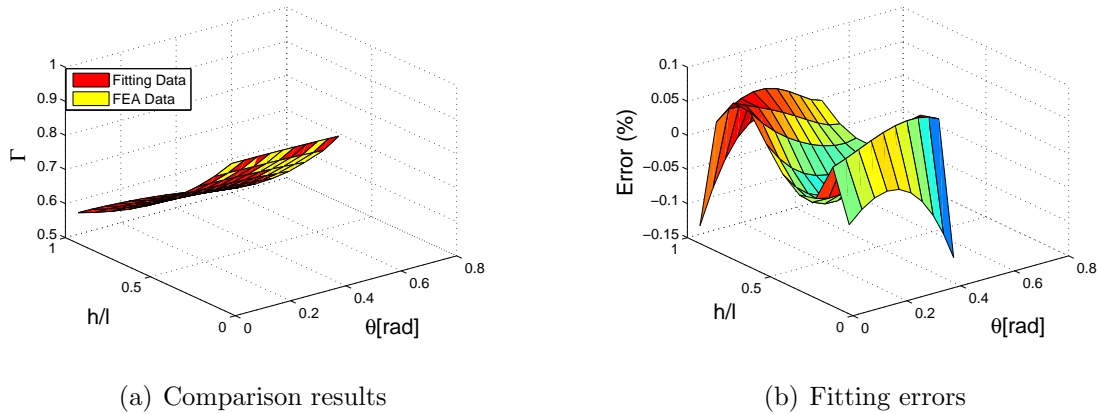


Figure 5.1: Comparison results and fitting errors for the generic stiffness design equation with nonlinear modified coefficient equation for circular flexure hinges

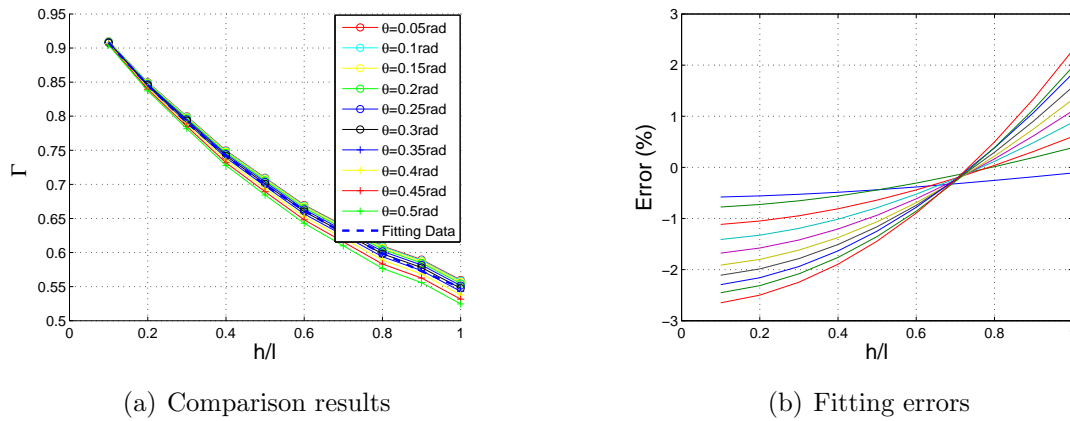


Figure 5.2: Comparison results and fitting errors for the generic stiffness design equation with linear modified coefficient equation for circular flexure hinges

coefficient equation but it is more accurate than the former studies.

5.1.2 Elliptical flexure hinges

- Generic stiffness design equation with nonlinear modified coefficient equation. According to the analysis method used in the evaluation of circular generic design equations, the comparison between the FEA results obtained by FEA method and those calculated by Eq. 3.19 is shown in Figure 5.3(a). It's easy to see from this figure, the fitting results are close to the FEA results. Further more, the errors analysis for fitting results is done following the error equation mentioned above

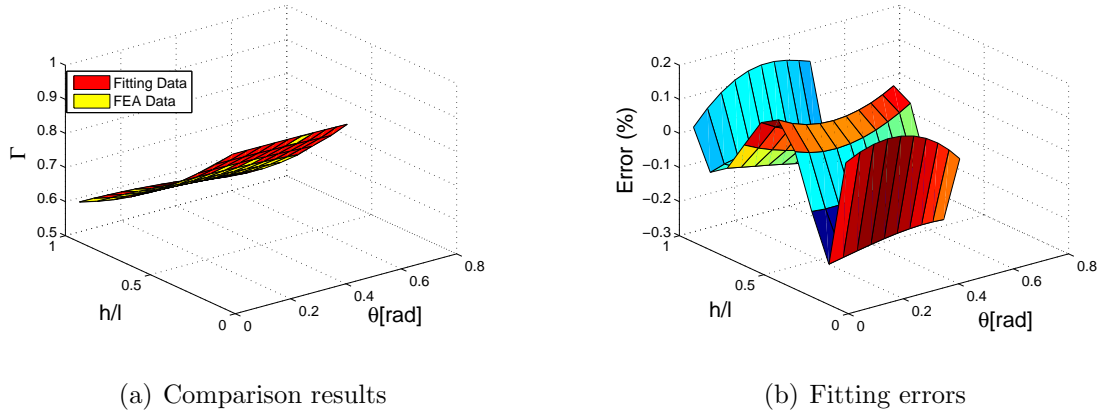


Figure 5.3: Comparison results and fitting errors for the generic stiffness design equation with nonlinear modified coefficient equation for elliptical flexure hinges

and the results are shown in Figure 5.3(b). The maximum error is 0.1509%.

- Generic stiffness design equation with linear modified coefficient equation. As described in the study of circular flexure hinges, a linear modified coefficient equation is proposed in order to simplify the design equation and be easily used in design of flexure hinges. It can be noted that the linear modified equation Eq.3.21 is a function of the geometric characteristic h/l only. The comparison result between the FEA results of the FEA models and the fitting results calculated by Eq. 3.21, it is shown in Figure 5.4(a). From this figure, it can be seen that the fitting results are close to the FEA results. In order to verify the fitting results, the results of the error analysis compared to the FEA results are shown in Figure 5.4(b). The maximum error is 2.8223%. Therefore, the error can be acceptable in engineering practice. It also states that the precision of the generic design equation with linear modified coefficient equation for elliptical flexure hinges is more accurate than the results proposed in the previous studies.

5.1.3 Corner-filletted flexure hinges

- Generic stiffness design equation with nonlinear modified coefficient equation. The same error analysis method has been used in the analysis for the generic design equation with nonlinear modified coefficient equation of corner-filletted flexure hinges. The generic design equation is proposed in Chapter 3. A comparison be-

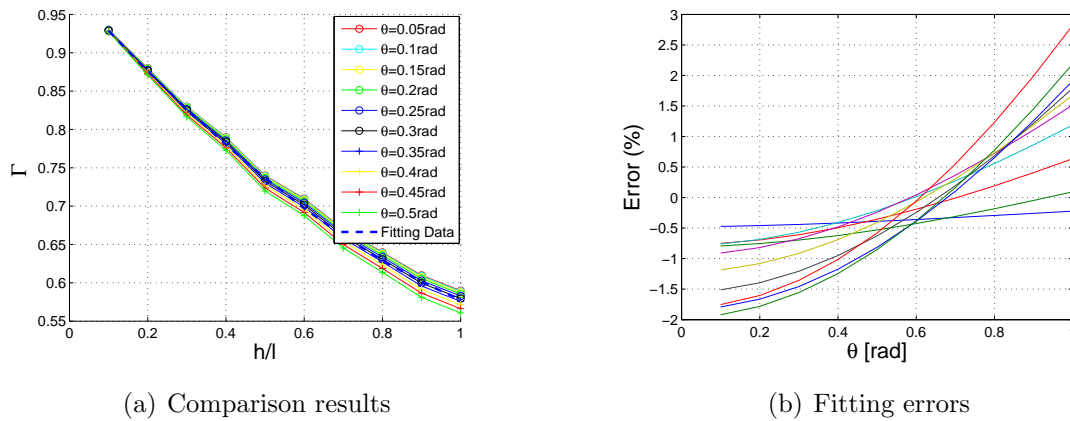


Figure 5.4: Comparison results and fitting errors for the generic stiffness design equation with linear modified coefficient equation for elliptical flexure hinges

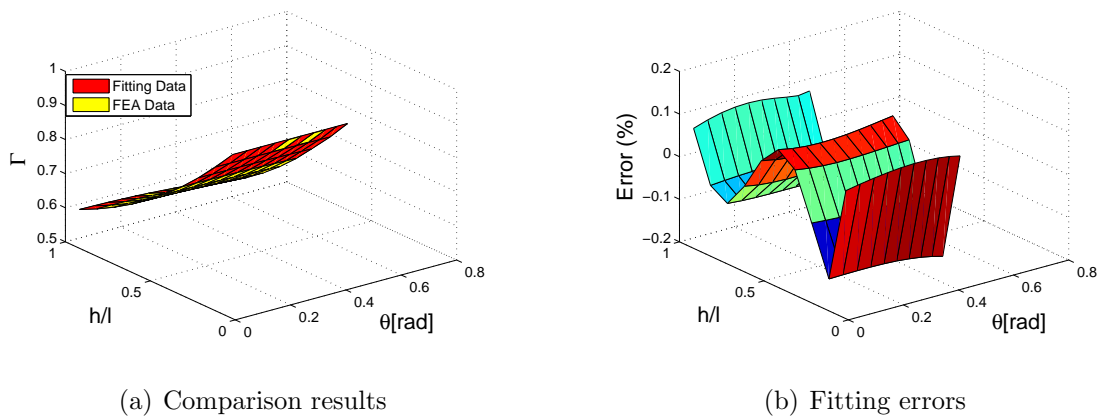


Figure 5.5: Comparison results and fitting errors for the generic stiffness design equation with nonlinear modified coefficient equation for corner-filleted flexure hinges

tween the results obtained by FEA method and the ones calculated by Eq. 3.24 is shown in Figure 5.5(a) at first. It can be seen that the fitting results are close to FEA results. The error compared with the results obtained by FEA method is shown in Figure 5.5(b). The maximum error is 0.105%.

- Generic stiffness design equation with linear modified coefficient equation.

The work of evaluating the generic design equation with linear modified coefficient equation for corner-filleted flexure hinges is also presented here. The comparison between the results respectively calculated by Eq. 3.26 and obtained by FEA method is presented in Figure 5.6(a). From this figure, it can be noted that

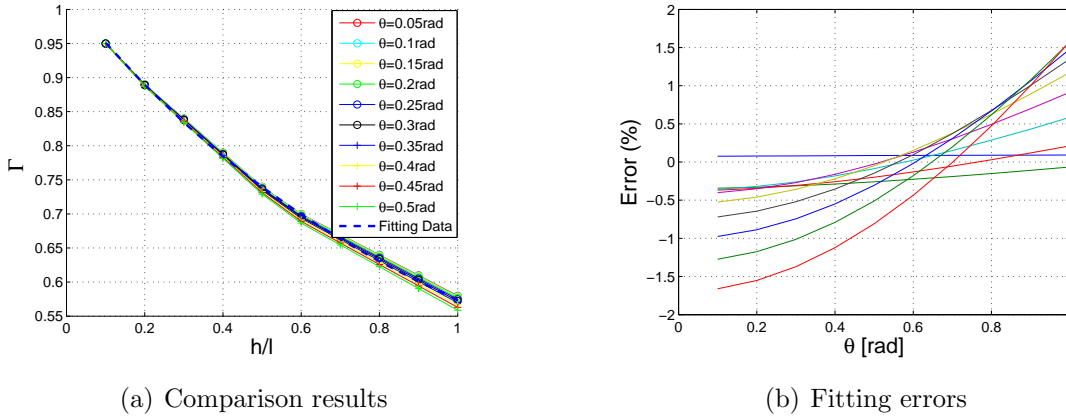


Figure 5.6: Comparison results and fitting errors for the generic stiffness design equation with linear modified coefficient equation for corner-filletted flexure hinges

the fitting results are close to the FEA results. In order to verify the fitting results, the results of errors analysis compared to those of the FEA are shown in Figure 5.6. The corresponding maximum error is 1.5799%. Thus it can be seen the generic stiffness design equation with linear modified coefficient equation for corner-filletted flexure hinges provide more accurate results than the former studies.

To sum up, both sets of stiffness design equations are precise. The nonlinear dimensionless stiffness design equations are more accurate than the linear dimensionless stiffness design equations. However, the errors produced by linear dimensionless stiffness design equations can be accepted, and the form of the equation is more simple and easier to be applied in applications of compliant mechanisms.

Concerning the three types of flexure hinges, the corner-filletted flexure hinges have the smallest stiffness of the three flexure hinges when they have identical geometric characteristic h/l , and are undergoing identical desired rotation. The circular flexure hinges have the largest stiffness under the same conditions.

5.2 Evaluation of Stress Generic Design Equations

As described in Chapter 4, the relation equations for material characteristic $\bar{\sigma}$, maximum bearable rotation $\theta_{z,max}$ and geometric characteristic h/l are fitted according to FEA results obtained in stress analysis. The meaning of the stress generic design equations have been presented in Chapter 4. This section will discuss the accuracy

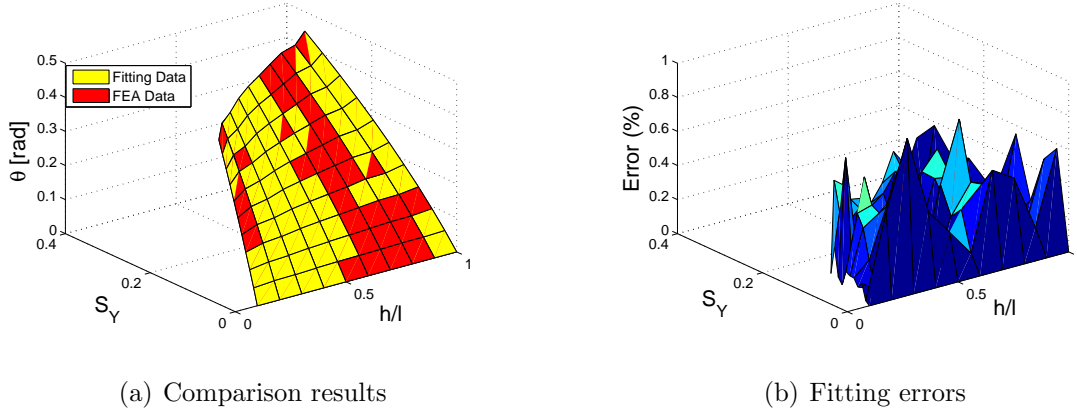


Figure 5.7: Comparison results and fitting errors for the $\theta_{z,max}$ design equation for circular flexure hinges

of these equations for each type of flexure hinges.

5.2.1 Circular flexure hinge

- Error analysis for the maximum bearable rotation $\theta_{z,max}$ design equation. Eq.4.1 is the fitting equation for obtaining the bearable maximum rotation by the hinge at the limit of material failure. The comparison result between fitting equation results and FEA real results is shown in Figure 5.7(a). The corresponding errors for the equation mentioned above are calculated according to:

$$error = \frac{\theta_{G,max} - \theta_{FEA,max}}{\theta_{FEA,max}} \times 100\% \quad (5.2)$$

where, the $\theta_{G,max}$ is calculated by Eq. 4.1. The $\theta_{FEA,max}$ is obtained by FEA method. The errors are shown in Figure 5.7(b). The maximum error of fitting results is obtained during the analysis, and it is 0.8954%.

- Error analysis for the material characteristic $\bar{\sigma}$ design equation. Eq.4.2 is obtained by fitting the FEA results of these circular flexure-hinge simulation models. The comparison between fitting equation results and FEA real results is shown in Figure 5.8(a). Its corresponding errors can be computed by

$$error = \frac{\bar{\sigma}_G - \bar{\sigma}_{FEA}}{\bar{\sigma}_{FEA}} \times 100\% \quad (5.3)$$

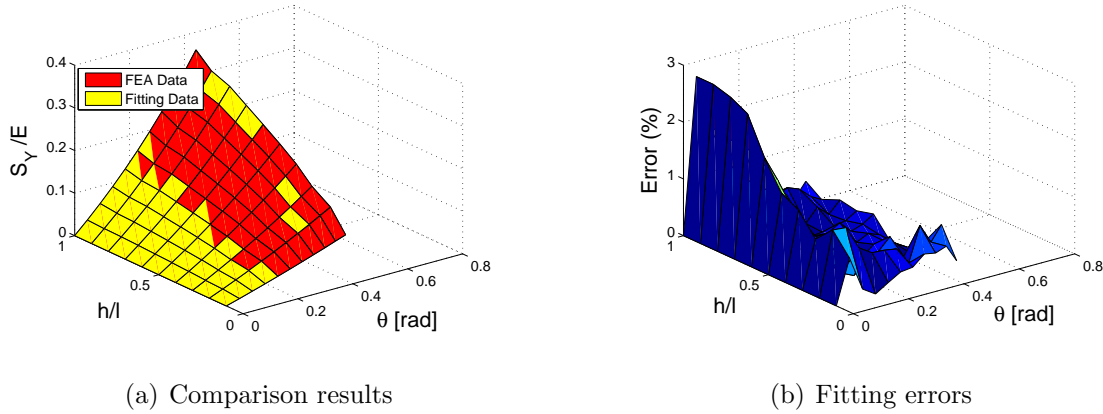


Figure 5.8: Comparison results and fitting errors for the $\bar{\sigma}$ design equation for circular flexure hinges

where, $\bar{\sigma}_G$ is calculated by Eq.4.2, and $\bar{\sigma}_{FEA}$ is obtained by FEA method. the corresponding result is shown in Figure 5.8(b). The maximum error of fitting equation is 2.7405%.

- Error analysis for the geometric characteristic h/l design equation.

Eq.4.3 is a fitting equation according to FEA results in order to obtain the maximum designable ratio h/l of a circular flexure hinge. The comparison between fitting equation results and FEA real results is shown in Figure 5.9(a). The errors can be calculated by the following relation:

$$error = \frac{(\frac{h}{l})_G - (\frac{h}{l})_{FEA}}{(\frac{h}{l})_{FEA}} \times 100\% \quad (5.4)$$

where, $(\frac{h}{l})_G$ is computed by Eq. 4.3, $(\frac{h}{l})_{FEA}$ is obtained by FEA method. the analysis result for the fitting equation is shown in Figure 5.9(b). The maximum error of fitting equation is 2.228%.

5.2.2 Elliptical flexure hinge

- Error analysis for the maximum bearable rotation $\theta_{z,max}$ design equation.

According to the procedure described in evaluation of circular flexure hinges. Eq. 4.4 is assessed here. The comparison between FEA results and the fitting equation results are shown in Figure 5.10(a) at first. Their corresponding errors

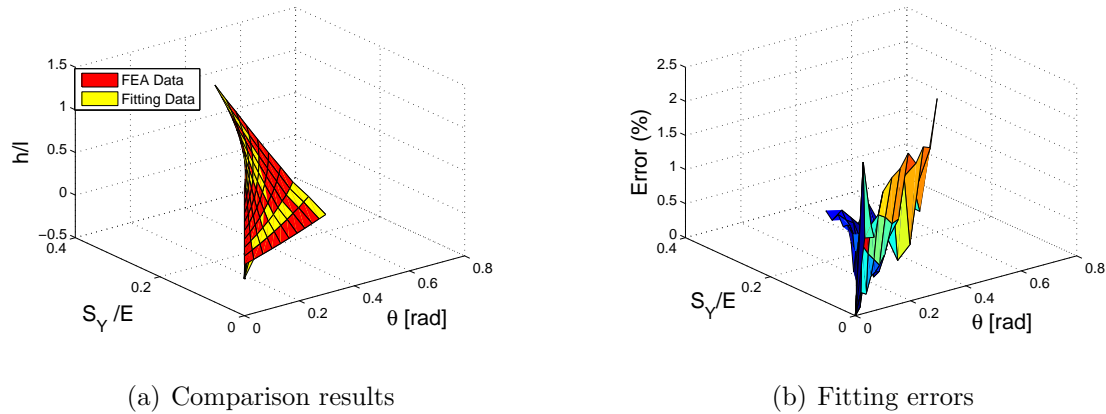


Figure 5.9: Comparison results and fitting errors for the h/l design equation for circular flexure hinges

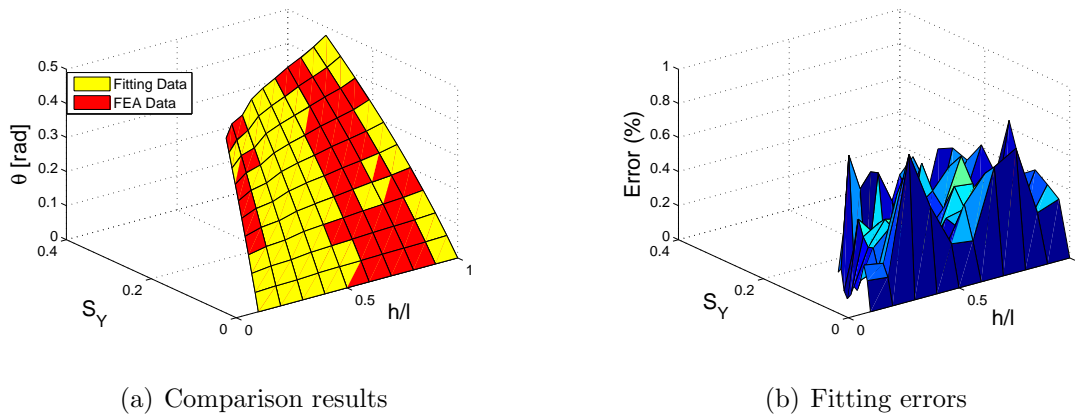


Figure 5.10: Comparison results and fitting errors for the $\theta_{z,max}$ design equation for elliptical flexure hinges

are expressed in Figure 5.10(b). The maximum error of fitting result is obtained during the analysis, and it is 0.8383%.

- Error analysis for the material characteristic $\bar{\sigma}$ design equation. Eq.4.5 is obtained by fitting the FEA results of these elliptical flexure hinges simulation models. The comparison between fitting equation results and FEA real results is shown in Figure 5.11(b). The error analysis results are shown in Figure 5.11(b). The maximum error of fitting equation is 2.157%.
- Error analysis for the geometric characteristic h/l design equation.

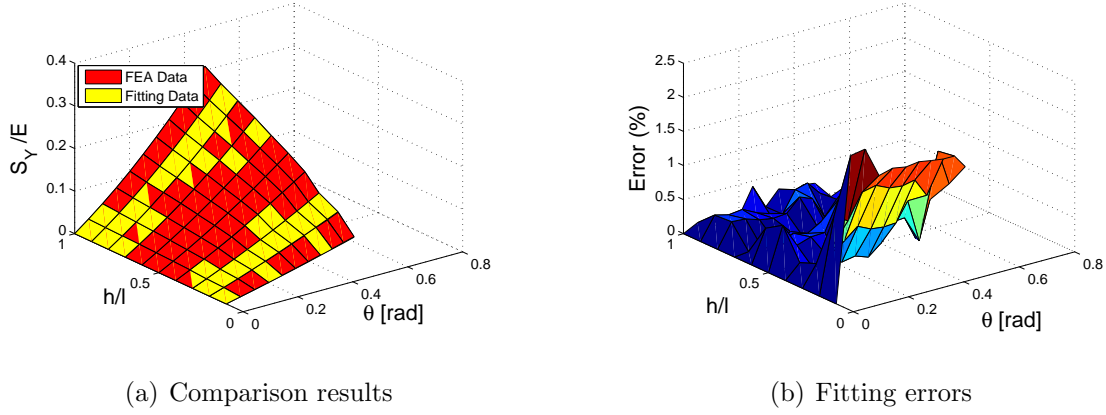


Figure 5.11: Comparison results and fitting errors for the $\bar{\sigma}$ design equation for elliptical flexure hinges

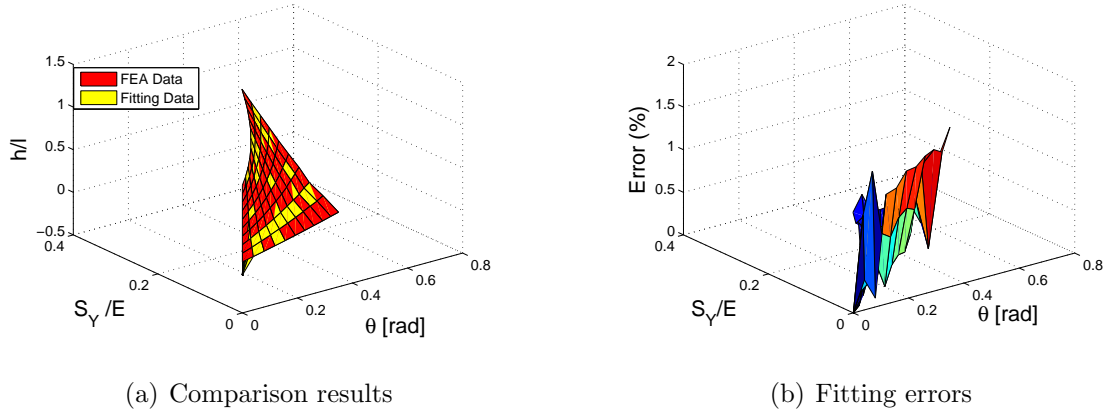


Figure 5.12: Comparison results and fitting errors for the h/l design equation for elliptical flexure hinges

Eq.4.6 is a fitting equation found according to FEA results in order to obtain the maximum designable ratio h/l of an elliptical flexure hinge. The comparison between fitting equation results and FEA real results is shown in Figure 5.12(a). The error analysis results for the fitting equation are shown in Figure 5.12(b). The maximum error of fitting equation is 1.5976%.

5.2.3 Corner-filletted flexure hinge

- Error analysis for the maximum bearable rotation $\theta_{z,max}$ design equation.
Eq.4.7 is the fitting equation for obtaining the bearable maximum rotation by the

hinge at the limit of material failure. The comparison between fitting equation results and FEA real results is shown in Figure 5.13(a). The error analysis results for the equation mentioned above are shown in Figure 5.13(b). The maximum error of fitting result is obtained during the analysis, is 0.6665%.

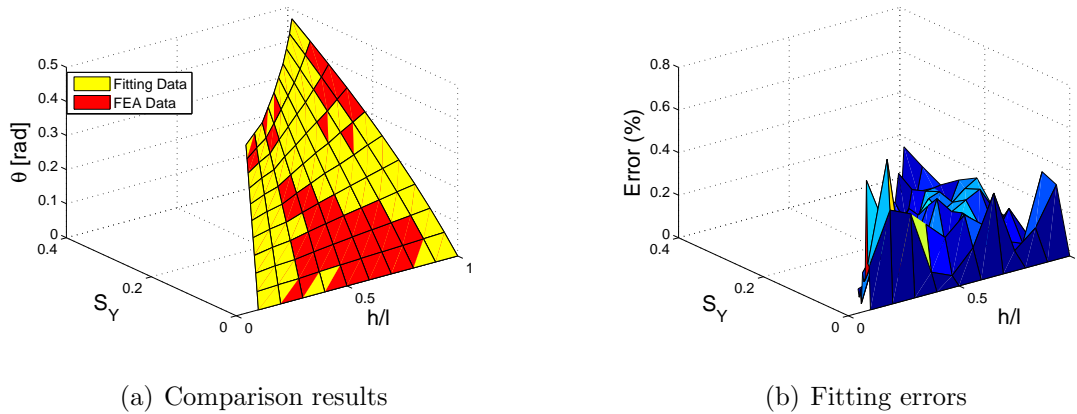


Figure 5.13: Comparison results and fitting errors for the $\theta_{z,max}$ design equation for corner-filleted flexure hinges

- Error analysis for the material characteristic $\bar{\sigma}$ design equation.
Eq.4.8 is the obtained by fitting the FEA result of these corner-filleted flexure hinges simulation models. The comparison between fitting equation results and FEA real results is shown in Figure 5.14(a). The error analysis results are shown in Figure 5.14(b). The maximum error of fitting equation is 2.2278%.
- Error analysis for the geometric characteristic h/l design equation.
Eq.4.9 is a fitting equation found according to FEA results in order to obtain the maximum designable ratio h/l of a corner-filleted flexure hinge. The comparison between fitting equation results and FEA real results is shown in Figure 5.15(a). The error analysis results for the fitting equation are shown in Figure 5.15(b). The maximum error of fitting equation is 1.1528%.

From what reported above, the generic stress design equations of the three types of flexure hinges are accurate.

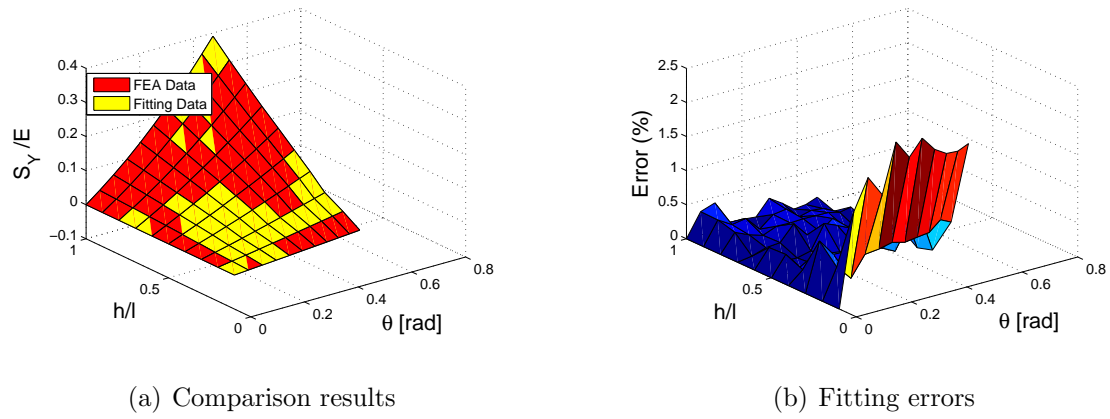


Figure 5.14: Comparison results and fitting errors for the $\bar{\sigma}$ design equation for corner-filletted flexure hinges

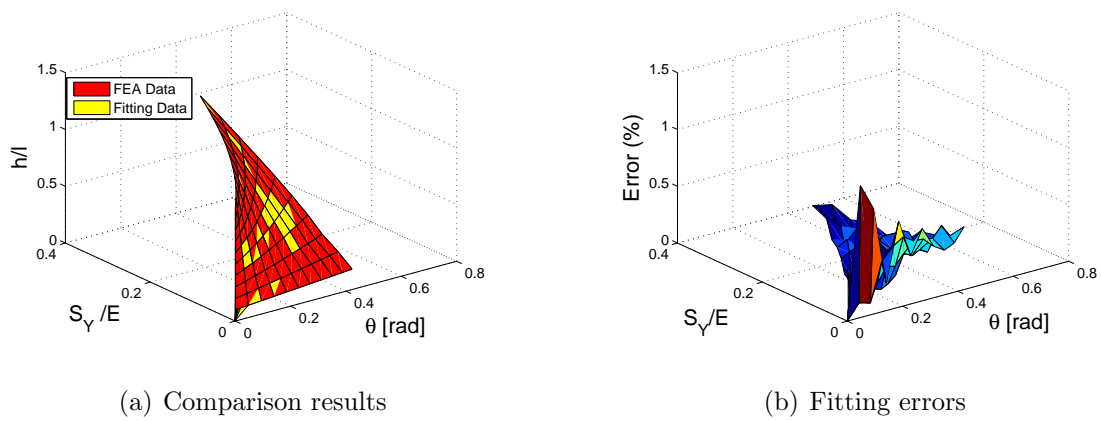


Figure 5.15: Comparison results and fitting errors for the h/l design equation for corner-filletted flexure hinges

Chapter 6

Flexure-Based Compliant Mechanisms

This chapter briefly presents the design procedure for designing a FCM. By reporting this procedure, this chapter introduces in detail the application method of the generic design equations proposed in the previous chapters by designing a four-bar compliant mechanism. Moreover, these generic design equations are assessed again in order to verify their applicability in FCM design. Finally, a numerical example of designing a flexure-based four-bar compliant mechanism (FFCM) is presented.

6.1 Design of a Flexure-Based Compliant Mechanism

Howell [24] proposed that a compliant mechanism could be transformed into a rigid body mechanism with springs at the link points, i.e. PRBM technique is used in analysis and synthesis of compliant mechanisms. A PRBM is a rigid counterpart of a compliant mechanism which contains not only the rigid linkages and kinematic pairs, but includes appropriate discrete springs for modeling the compliance of flexible members. This thesis will use PRBM technology to design a FCM. The flexure hinges used as joints will be transformed into revolute pairs plus springs.

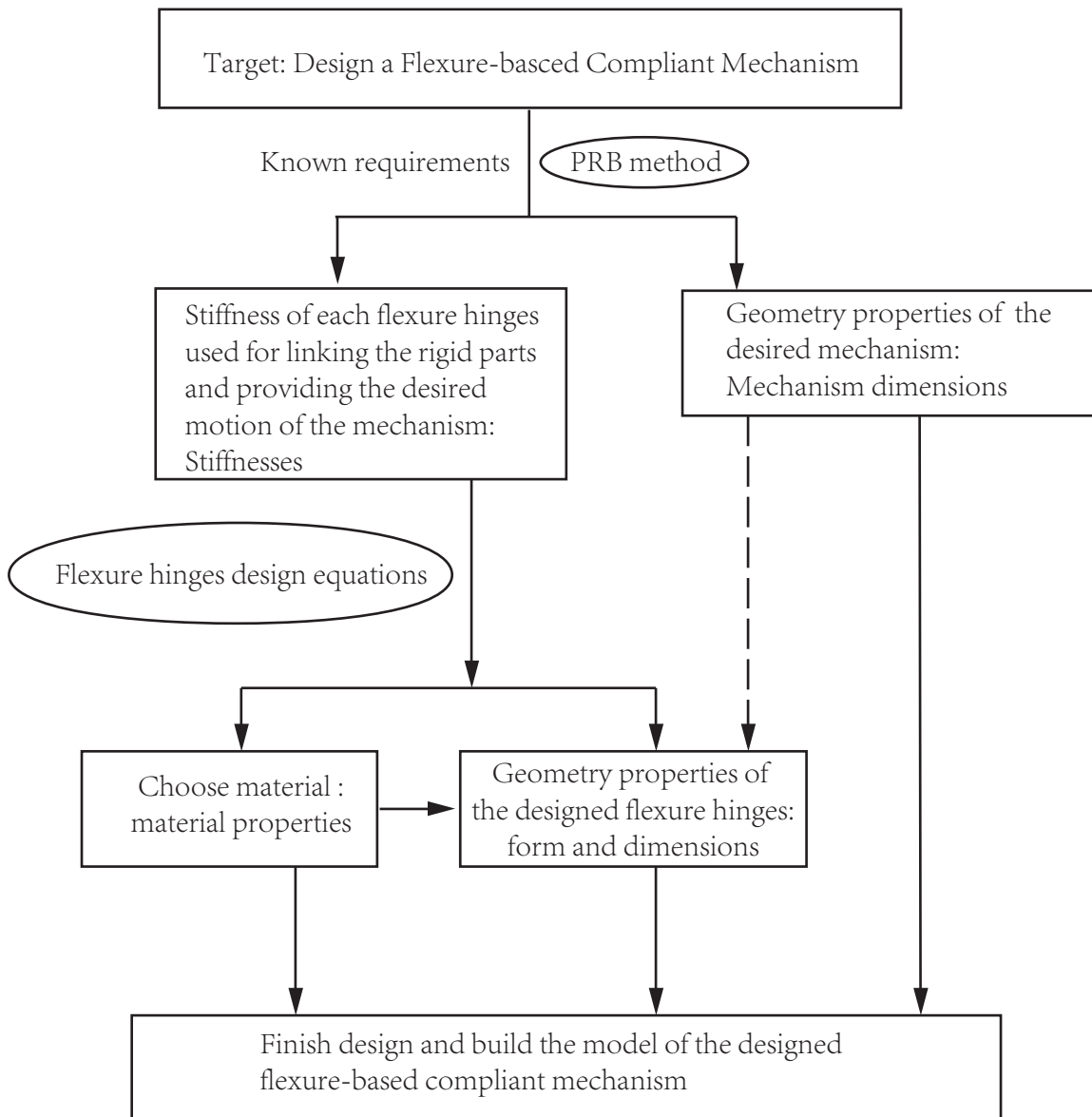


Figure 6.1: Design flow chart for designing a FCM

The design procedure for designing a FCM is described by the flow chart reported in Figure 6.1. There are two important technologies which are used in the design procedure. The first one is PRBM mentioned above. The second one is the flexure hinge design equations which are used in design of flexure hinges. The generic design equations obtained in Chapters 3 and 4 can be recalled here. The dotted line in Figure 6.1 means that the mechanism dimensions can act as a reference condition for flexure hinges design. For a FCM, the stiffness of rigid parts must be assumed.

The key point in the procedure of designing a FCM is to design the flexure hinges

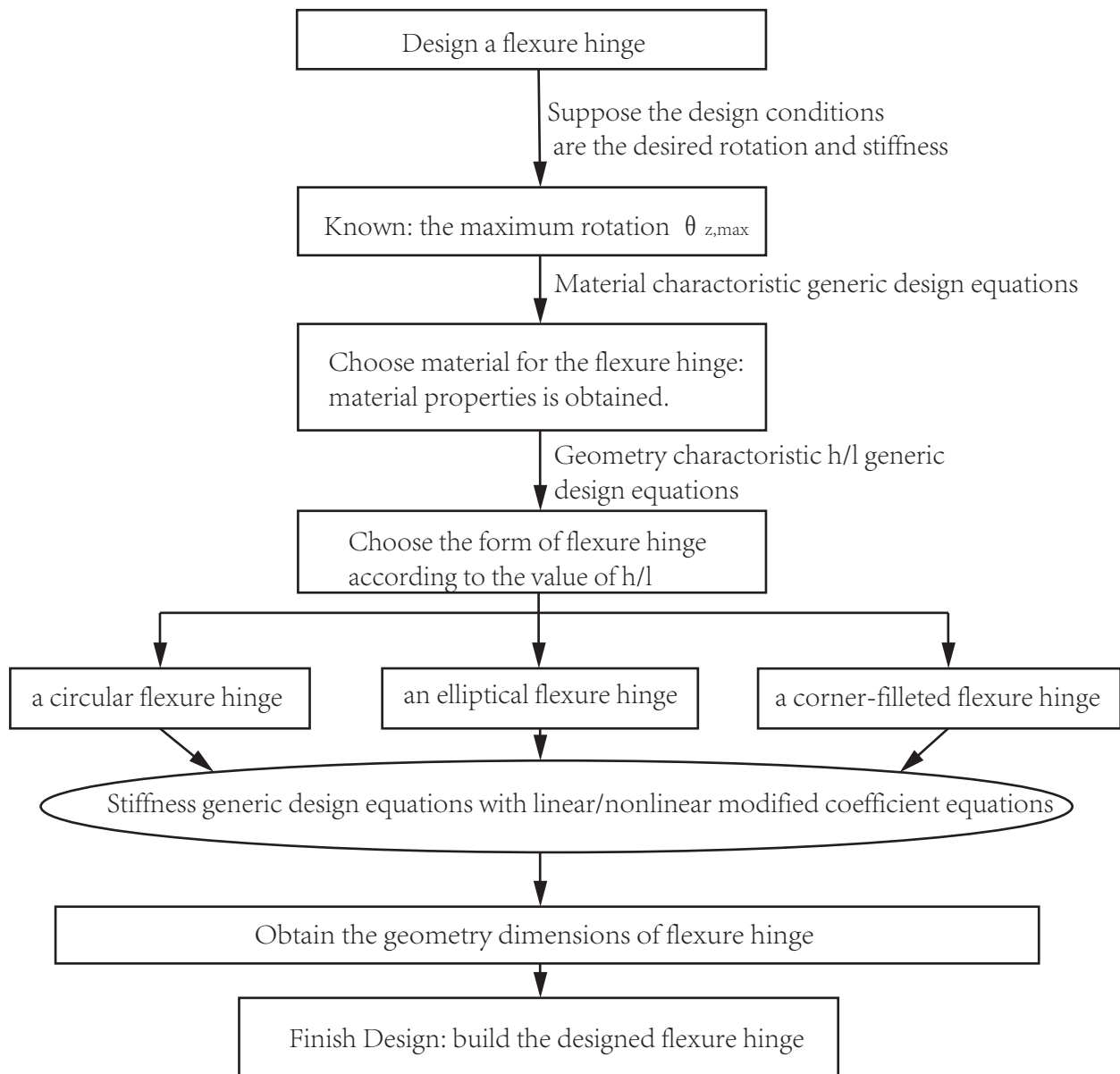


Figure 6.2: Design flow chart for designing a flexure hinge

of the mechanism. The related design procedure for designing a flexure hinge is presented in Figure 6.2. In addition, the method using the generic design equations is also described in the flow chart of Figure 6.2.

6.2 Analysis and Evaluation for the Generic Design Equations in FFCMs

6.2.1 Flexure-based four-bar compliant mechanisms(FFCMs)

FFCMs are utilized widely in various applications. In order to demonstrate the use of the proposed design equations and verify their applicability and precision, a flexure-based four-bar compliant mechanism(FFCM) is studied here (Figure 6.3). In Figure 6.3, links 1, 2, 3, 4 are the rigid parts of the FFCM, link 1 is chosen as the base of the mechanism. The flexible parts, hinges 1, 2, 3, 4, are the connecting joints to make the mechanism movable by using their elastic deformation instead of traditional revolute pairs. In addition, the horizontal axis of hinge 1 is perpendicular to the end plane of link 1 or link 2, respectively. The horizontal axis of hinge 2 is perpendicular to the end plane of link 2 or link 3, also it lies in the direction of the horizontal axis of hinge 1. The horizontal axis of hinge 3 is perpendicular to the end plane of link 3 or link 4, respectively. The horizontal axis of hinge 4 is perpendicular to the end plane of link 4 or link 1, as well it lies in the horizontal axis of hinge 3.

Following the procedure presented above, the study of the FFCM will start from

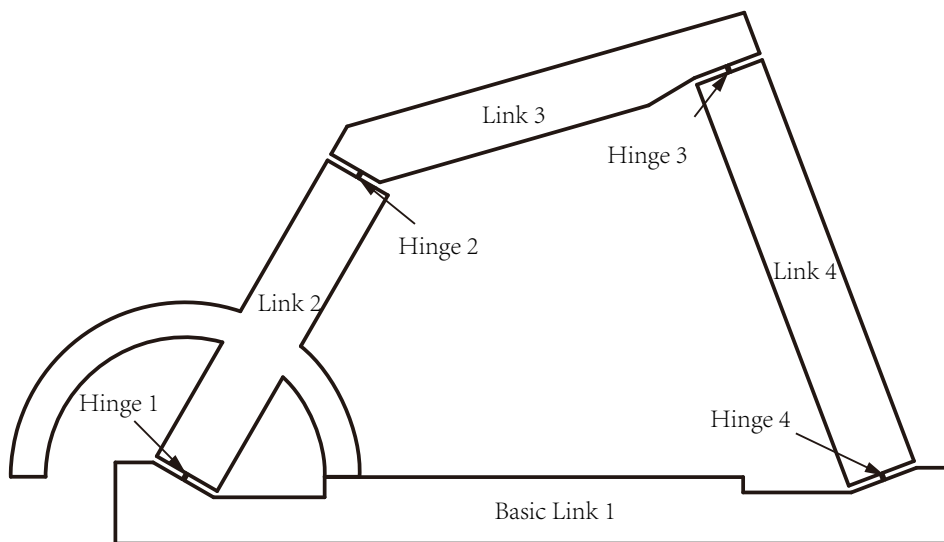


Figure 6.3: A FFCM

its PRBM according to the work by Howell et al. who presented closed-form equations describing force-displacement relationship for FFCMs by means of PRBM. The equivalent PRBM of the FFCM as mentioned above is shown in Figure 6.4. In

this chapter, the coordinate system is defined as follows. The origin of the global coordinate system XY is chosen at the geometric center point of hinge 1, i.e. the point O in the Figure 6.4. The X axis is designed along the link 1. In Figure 6.4, $K_i, (i = 1, 2, 3, 4)$ is the stiffness of hinge i , $r_i, (i = 1, 2, 3, 4)$ describes the length of link i , $\theta_i, (i = 1, 2, 3, 4)$ is the angle between each adjacent links.

As concerning such a FFCM, the moment-rotation relationship is studied in order

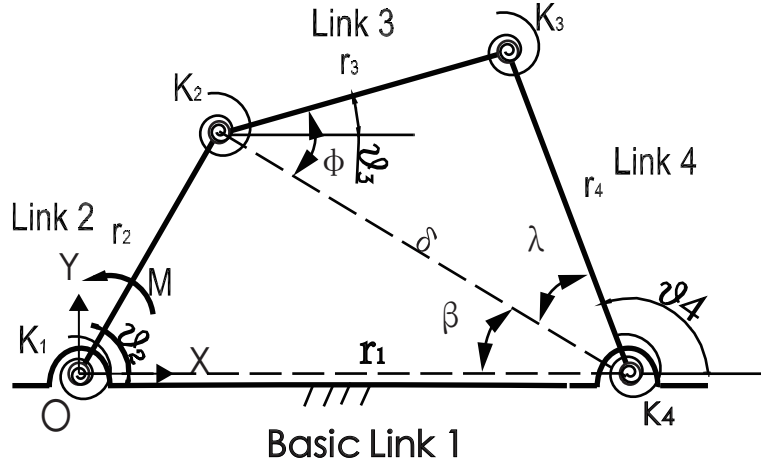


Figure 6.4: The equivalent pseudo rigid body model for the FFCM

to analyze and evaluate a FFCM. The relationship equation is proposed in [24] as shown in Eq.6.1.

$$M + T_1 + T_2 - (T_2 + T_3)h_{32} + (T_3 + T_4)h_{42} = 0 \quad (6.1)$$

where, M is the moment applied to the link 2 as shown in Figure 6.4. $T_i, (i = 1, 2, 3, 4)$ is the torque provided by the flexure hinges, hinges 1, 2,3,4, which can be obtained by using Eq.6.6.

$$T_1 = -K_1\Psi_1 \quad (6.2)$$

$$T_2 = -K_2\Psi_2 \quad (6.3)$$

$$T_3 = -K_3\Psi_3 \quad (6.4)$$

$$T_4 = -K_4\Psi_4 \quad (6.5)$$

$$(6.6)$$

where, $K_i, (i = 1, 2, 3, 4)$, is the stiffness of hinge i . In particular, as for a slender beam with geometric dimensions, h (height), l (length) and w (width), which are

defined in [24], the stiffness is calculated by $K = EI/l$. Here, E is the Young's modulus of material, I is the moment of inertia of the slender beam that can be calculated by $I = wh^3/12$. Also, Ψ_i , ($i = 1, 2, 3, 4$) is the deformation rotation of hinge i . These deformation rotation can be calculated according to Eq.6.10.

$$\Psi_1 = \theta_2 - \theta_{20} \quad (6.7)$$

$$\Psi_2 = (\theta_2 - \theta_{20}) - (\theta_3 - \theta_{30}) \quad (6.8)$$

$$\Psi_3 = (\theta_4 - \theta_{40}) - (\theta_3 - \theta_{30}) \quad (6.9)$$

$$\Psi_4 = \theta_4 - \theta_{40} \quad (6.10)$$

where, θ_i , ($i = 1, 2, 3, 4$) is the angle as shown in Figure 6.4, θ_{i0} , $i = 1, 2, 3, 4$ is the initial angle of θ_i . The relation equations for these angles are presented here, as shown in Eqs.6.11, 6.12 and 6.13.

$$\delta = \sqrt{r_1^2 + r_2^2 - 2r_1r_2 \cos \theta_2}, \quad \beta = \arccos \frac{r_1^2 + \delta^2 - r_2^2}{2r_1\delta} \quad (6.11)$$

$$\phi = \arccos \frac{r_3^2 + \delta^2 - r_4^2}{2r_3\delta}, \quad \lambda = \arccos \frac{r_4^2 + \delta^2 - r_3^2}{2r_4\delta}$$

$$\theta_3 = \phi - \beta \quad (6.12)$$

$$\theta_4 = \pi - \lambda - \beta \quad (6.13)$$

where θ_3 and θ_4 define the position of links r_3 and r_4 with respect to the frame. Finally, in Eq.6.1, h_{32} and h_{42} can be calculated following Eq.6.16.

$$h_{32} = \frac{r_2 \sin(\theta_4 - \theta_2)}{r_3 \sin(\theta_3 - \theta_4)} \quad (6.14)$$

$$h_{42} = \frac{r_2 \sin(\theta_3 - \theta_2)}{r_4 \sin(\theta_3 - \theta_4)} \quad (6.15)$$

$$(6.16)$$

In the design of a FFCM, an optimal design method is presented here for designing the configuration of the FFCM. With reference to Figure 6.4, for given links length r_1 , r_2 , r_3 and r_4 , the uninflected configuration of the FFCM is described by $\theta_2 = \theta_{20}$ (which is the FFCM rest configuration). The desired moment-rotation (or, torque-angle) profile is the relation between the angle θ_2 and the input torque, M (i.e. a pure moment acting on the rocker arm r_2) (Figures 6.4). Here, the following quadratic torque-angle profile is considered:

$$T_d(\theta_2) = A_2\theta_2^2 + A_1\theta_2 \quad (6.17)$$

where A_1 , A_2 , and θ_2 will be defined according to the design requirements. Given Eqs. 6.17 and 6.1, the parameters that characterize the considered FFCM will be obtained by means of the following optimization process. Here, the following cost function is used:

$$J = \int_{\theta_{2min}}^{\theta_{2max}} [T(\theta_2) - T_d(\theta_2)]^2 d\theta_2 \quad (6.18)$$

where $\theta_{2min,max}$ are the FFCM limiting angular positions. By defining the vector $\Lambda = [\theta_{20}, r_1, r_2, r_3, r_4, K_1, K_2, K_3, K_4]$ containing the characteristic FFCM parameters, the design optimization process consists of finding the optimal value of Λ , which minimizes the cost function:

$$\min_{\Lambda} J : \Lambda_{min} < \Lambda < \Lambda_{max} \quad (6.19)$$

where Λ_{min} and Λ_{max} are suitable bounds of the FFCM geometric parameters, which are necessary to avoid unfeasible architectural solutions. The proposed optimization process has been implemented in MATLAB, and solved numerically by means of the `lsqnonlin` algorithm, which requires an initial guess for the parameter vector θ_{20} .

6.2.2 Analysis and evaluation of the generic design equations

This section will combine FEA method to analyze and to evaluate the proposed generic design equations when used to design a FFCM. The procedure is presented by referring to both the procedure of designing a FCM and the procedure of designing a flexure hinge presented in the previous section of this chapter.

- Define the configuration of the desired FFCM.

The configuration of the desired FFCM is presented in Table.6.1. The analysis and the use of the generic design equations will be discussed.

- Design the flexure hinges.

Based on the conditions obtained in the previous step, design the flexure hinges following the procedure described in the earlier part of this chapter. In stiffness generic design equations, at first, four slender beams are designed in order to verify the optimal method used for obtaining the configuration of the desired FFCM. Second, four corner-filleted flexure hinges, two sets of four circular flexure hinges and two sets of four elliptical flexure hinges are designed based on the corresponding generic design equations. In the same way, in order to check the reliability of

Table 6.1: Configuration of the desired FFCM

| | | | |
|---------------|-----------------|------------------|-----------------|
| r_1 | 200mm | K_1 | 44.97Nmm |
| r_2 | 100mm | K_2 | 44.97Nmm |
| r_3 | 110mm | K_3 | 44.97Nmm |
| r_4 | 125mm | K_4 | 44.97Nmm |
| θ_{20} | $\frac{\pi}{3}$ | $\Delta\theta_2$ | $\frac{\pi}{6}$ |

the stiffness and stress generic design equations, four corner-filleted flexure hinges, four circular flexure hinges and four elliptical flexure hinges are sized on the basis of the corresponding equations.

- Build models.

According to the geometric dimensions of these designed flexure hinges, which are obtained in the last step, seven FFCM models are built in the commercial software SOLIDWORKS.

- Analyzing these models by means of FEA method.

The commercial FEA software COMSOL is used in simulating these models. At first, the model is input into COMSOL workspace. Second, the material parameters, such as Young's modulus E and Poisson's ratio μ (Young's modulus $E = 1.135e3MPa$ and Poisson's ratio $\mu = 0.33$) are chose for these FEA models. Third, the boundary conditions are set up. According to the defined condition before, link 1 is the basic link and fixed. Hence, the boundary constrain of link 1 is chose as fixed. In addition, a couple of forces are loaded on arc part of link 2 as shown in Figure 6.5. The couple of forces are loaded here in order to produce a pure moment loaded on link 2 as shown in Figure 6.4.

The next, as for FEA method, the mesh generated for the analysis model plays a key role on the precision of analysis results. Therefore, refined mesh is needed for the analysis as shown in Figure 6.6. At the end, the analysis is run and obtained from the FEA result.

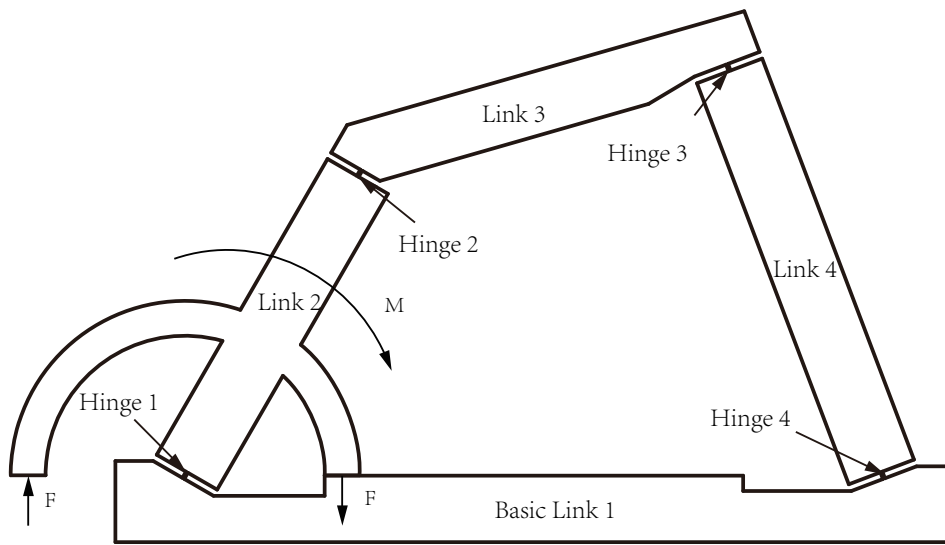


Figure 6.5: A couple of forces loaded on FCM

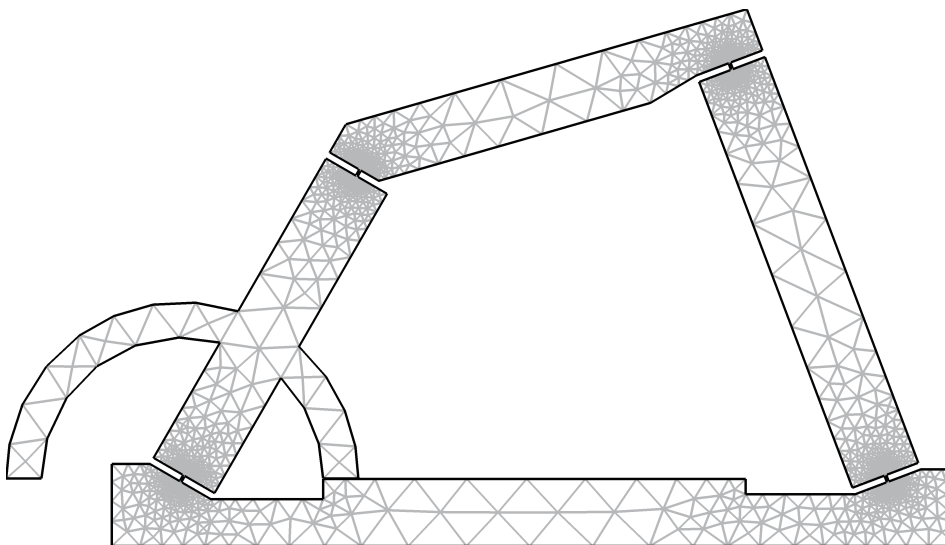


Figure 6.6: Refined mesh for a FFCM

- Postprocessing of results.

As mentioned above, the moment-rotation relationship of link 2 is an evaluation criteria for verifying the applicability and precision of the generic design equations. Therefore, the results obtained in FEA method need to be processed in the commercial software MATLAB. The computing process has been programmed, which is easier to be used.

- Error analysis and Evaluation.

Analyze the results obtained in the last step, calculate the error for these seven moment-rotation profiles obtained by FEA method compared to the desired moment-rotation profile. In the end, evaluate the applicability and precision of these proposed generic design equations by comparing their results with those obtained by the small deformation design equations.

A FFCM with four slender beams analysis model

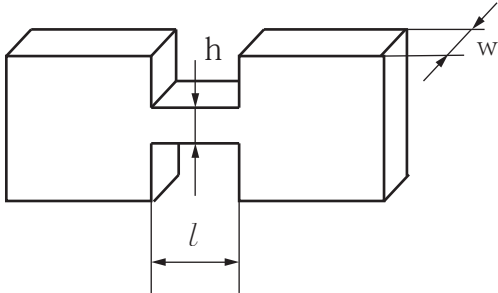
The aim of designing a FFCM with four slender beams is to test the accuracy of this testing procedure. According to Table 6.1, the stiffness of four flexure hinges has identical value. Therefore, four identical slender beams are designed referring to $K = EI/l$. Its form and geometric dimensions are shown in Table 6.2.

Following the analysis method mentioned above, the moment-rotation profile based on the FEA results is plotted in blue line in Figure 6.7 with the green line as the desired moment-rotation relationship. It can be seen that the blue line is very close to the green line. Such a result implies that the moment-rotation profile of the designed FFCM is as the desired profile. Therefore, the testing procedure is correct. It can be convinced in analysis and evaluation of the proposed generic design equations.

Discussion about generality for the generic design equations

The aim of proposing stiffness generic design equations is to eliminate the limitations of small deformation design equations and to ensure their accuracy and applicability in analysis and synthesis of FFCMs. Therefore, the geometric characteristic h/l to be for each type of flexure hinges. As for a FFCM with four corner-filletted flexure

Table 6.2: Geometries of a flexure hinge(slender beam)

| | | |
|---|---|------|
|  | h | 1mm |
| | l | 10mm |
| | w | 5mm |

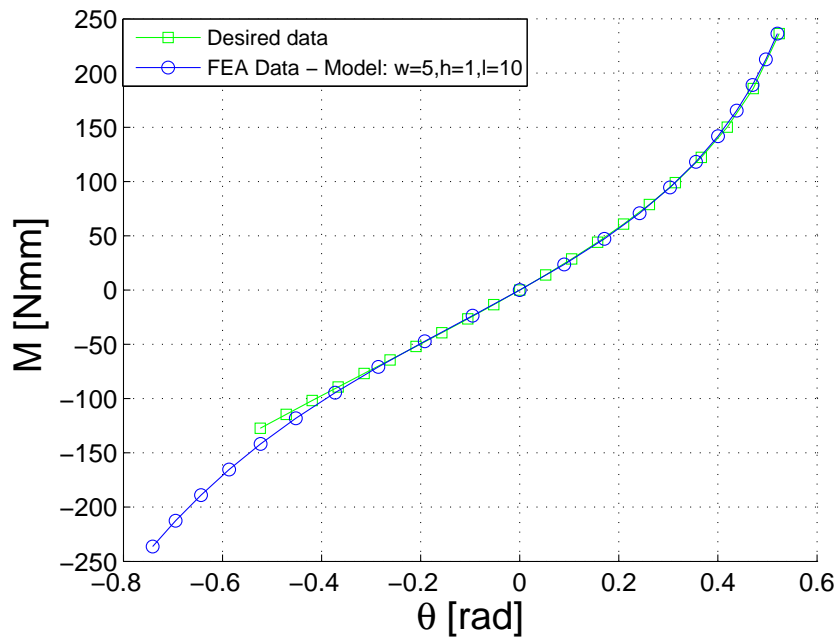


Figure 6.7: The moment-rotation relationship of link 2

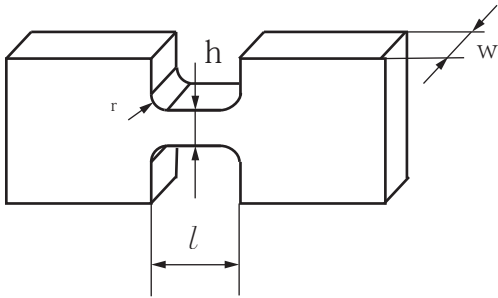
hinges, the ratio $h/l = 0.1$ will not be discussed here as the results are similar to those of a FECM with four slender beams.

- A FFCM with four corner-filletted flexure hinges analysis model.
Four identical corner-filletted flexure hinges with the ratio $h/l = 0.3$ are de-

signed by the proposed stiffness design equations of corner-filletted flexure hinges and shown in Table 6.3

Using the FEA method as aforementioned, the relationship between moment

Table 6.3: Geometries of a corner-filletted flexure hinge

| | | |
|---|---|------------|
|  | h | 0.61646mm |
| | l | 2.05487mm |
| | r | 0.205487mm |
| | w | 5mm |

and rotation angle of link 2 is obtained. Figure 6.8 shows two moment-rotation relationships. The red line is obtained based on the FEA method, the green line is the desired one.

It can be seen that the red line is very close to green line. i.e. the moment-rotation profile of the designed FFCM is the desired profile. Therefore, the corner-filletted generic design equations are accurate enough for design purposes. The accuracy and applicability of the corner-filletted generic design equations are considered as verified.

- Model of a FFCM with four circular flexure hinges.

Two sets of four identical circular flexure hinges with the ratio $h/l = 0.1$ and $h/l = 0.3$ are designed by the proposed stiffness design equations of circular flexure hinges and shown in Table 6.4.

Following the analysis method mentioned above, the moment-rotation profile based on FEA results is plotted as the blue line with stars and the black line with stars as shown in Figure 6.9, where the blue line with stars denotes the moment-rotation relationship of the analysis model with $h/l = 0.1$, and the black line with stars describes the moment-rotation relationship of the analysis model with $h/l = 0.3$. The green line with squares in the figure is the desired moment-rotation relationship. It can be seen that both the line with stars are

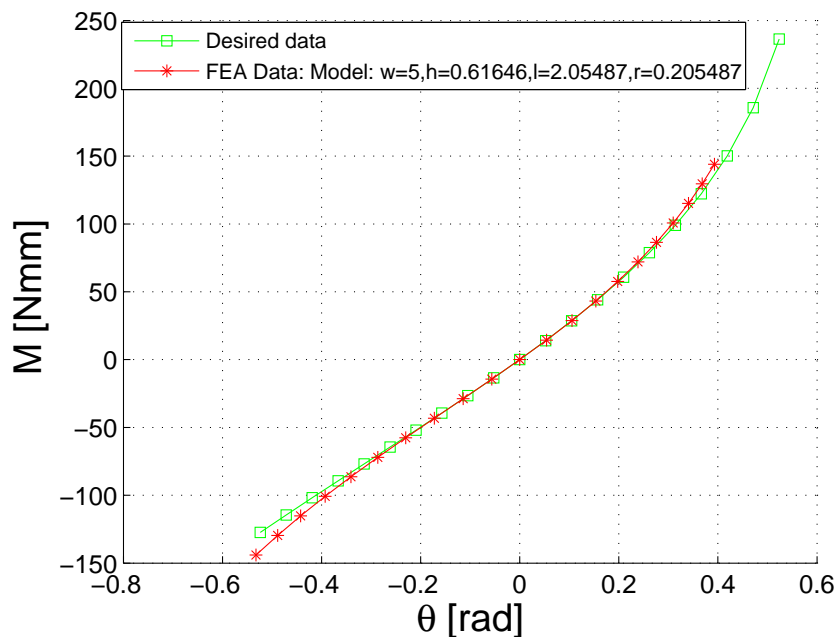
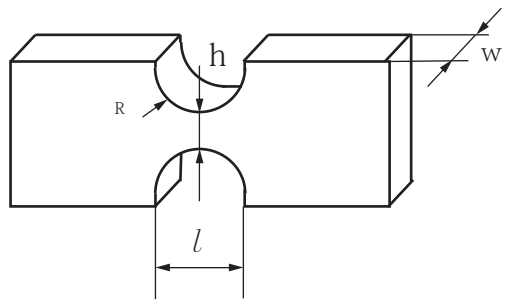


Figure 6.8: The moment-rotation profile of FFCM with four corner-filleted flexure hinges

Table 6.4: Geometries of a circular flexure hinge

|  | $h/l=0.1$ | | $h/l=0.3$ | |
|---|-----------|----------|-----------|-----------|
| | h | 0.5185mm | h | 0.41107mm |
| l | 5.185mm | l | 1.37024mm | |
| R | 2.5925mm | R | 0.68512mm | |
| w | 5mm | w | 5mm | |

very close to the line with squares. Such a result shows that the moment-rotation profiles of the designed FFCMs act as the desired profile. Therefore, this fact proves that the circular generic design equations can be generally utilized in analysis and synthesis of FFCMs. Especially, the result precision can be guarantee.

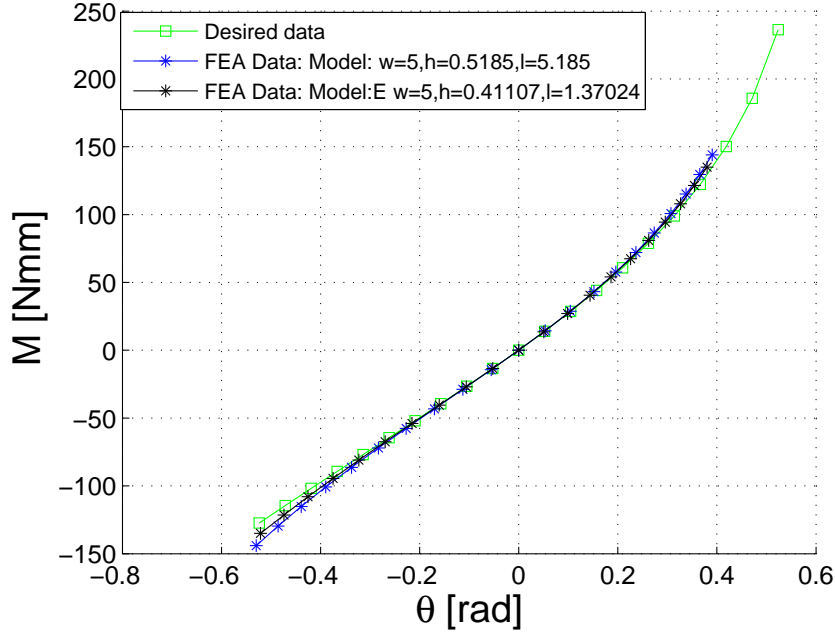


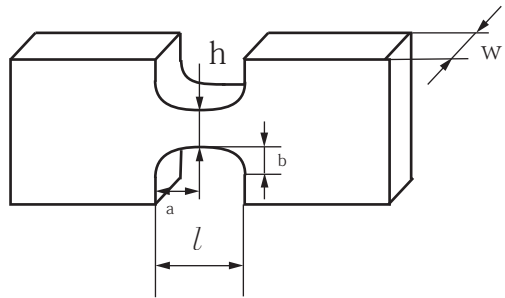
Figure 6.9: The moment-rotation relationship of link 2

- Model a FFCM with four elliptical flexure hinges.

Two sets of four identical elliptical flexure hinges with the ratio $h/l = 0.1$ and $h/l = 0.3$ are designed by the proposed stiffness design equations of elliptical flexure hinges and shown in Table 6.5. In the table, b is the semi-axis of the profile of an elliptical flexure hinge.

Following the analysis method mentioned above, the moment-rotation profile based on FEA results is plotted as the green line with stars and the black line with triangles as shown in Figure 6.10, where the green line with stars denotes the moment-rotation relationship of the analysis model with $h/l = 0.1$, and the black line with triangles describes the moment-rotation relationship of the analysis model with $h/l = 0.3$. The green line with squares in the figure is the desired moment-rotation relationship. It can be seen that both the green line with stars and black line with triangles are very close to the green line with squares. Such a result shows that the moment-rotation profiles of the designed FFCMs act as the desired profile. Therefore, this fact proves that the elliptical generic design equations can be generally utilized in analysis and synthesis of

Table 6.5: Geometries of an elliptical flexure hinge

| | | | | |
|---|-----------|------------|-----------|------------|
|  | $h/l=0.1$ | | $h/l=0.3$ | |
| | h | 0.575923mm | h | 0.44196mm |
| | l | 5.75923mm | l | 1.480652mm |
| | a | 2.87961mm | a | 0.74326mm |
| | b | 1.727769mm | b | 0.44196mm |
| | w | 5mm | w | 5mm |

FFCMs. Especially, the result precision can be guaranteed.

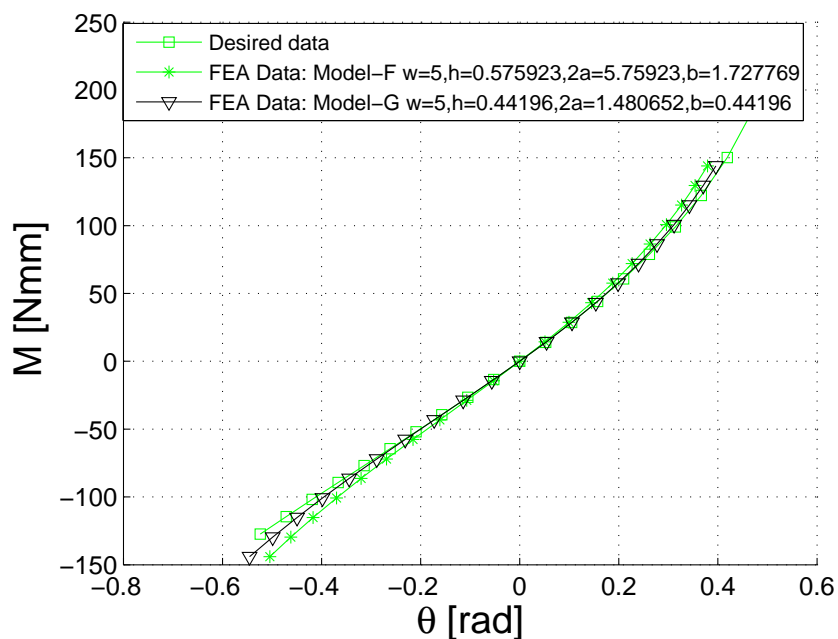


Figure 6.10: The moment-rotation relationship of link 2

To sum up the above discussion, the stiffness generic design equations proposed in the thesis can be used in the analysis and synthesis of FFCMs with a careful con-

sideration for shear force produced in the flexure hinge. In addition, the accuracy of analysis and synthesis results can be guaranteed.

In the discussion about stiffness design equations, the stress influence is not be considered in analysis and synthesis of FFCMs. In practice, however, the designed FFCM perhaps cannot be implemented because the mechanism can fail when the stress produced in the deformation exceeds the yield strength of the material. Hence, the geometric characteristic h/l and material characteristic $\bar{\sigma}$ must be selected reasonably. The stress generic design equations are easier to be used in finding the material and the ratio h/l for a flexure hinge design. For a given maximum rotation, the material for flexure hinges can be chosen by using the material characteristic design equations. Then, according to the given maximum rotation and the selected material, the geometric characteristic can be obtained by utilizing the geometric characteristic design equations. The error analysis have been done in Chapter 5.

Comparison with the small deformation design equations

At the first, three FFCMs are designed by following the procedure of designing a FFCM and a flexure hinge. They are respectively the FFCM with four corner-filletted flexure hinges, the FFCM with three circular flexure hinges and one corner-filletted flexure hinge (i.e. hinge 2, because the deflection angle is so large that the corner-filletted flexure hinge can be used here only. The configuration of hinge 2 used in the other two models is the same as the model of FFCM with four corner-filletted flexure hinge.) and the FFCM with three elliptical flexure hinges and one corner-filletted flexure hinge (this one has the same situation as the previously described.). The proposed generic design equations are used in the case. The geometric dimensions of these designed flexure hinges are shown in Table 6.6. Thereinto, θ_{max} is defined using three values for each type of flexure hinges according to the position of the hinge in the FFCM.

Three FFCMs are then designed by following the procedure of designing a FFCM and a flexure hinge, they are respective FFCM with four corner-filletted flexure hinges, FFCM with three circular flexure hinges and one corner-filletted flexure hinge, and FFCM with three elliptical flexure hinges and one corner-filletted flexure hinge. The small deformation design equations described in chapter 3 are used in this case. The geometric dimensions of these designed flexure hinges are shown in Table 6.7. Thereinto, θ_{max} coincides with the last one.

Table 6.6: Designed flexure hinges (Generic design equations)

| Corner-filletted flexure hinges | | | |
|--|------------|----------------|-------------|
| | hinge4 | hinge 1,hinge3 | hinge2 |
| h | 1.06336mm | 1.21046mm | 1.1.46827mm |
| l | 3.34535mm | 5.28856 | 10.17395mm |
| r | 0.334535mm | 0.528856 | 1.017395mm |
| w | 5mm | 5mm | 5mm |
| $\frac{h}{l}$ | 0.31786 | 0.22888 | 0.14432 |
| θ_{max} | 18° | 25° | 40° |
| Circular flexure hinges | | | |
| | hinge4 | hinge 1,hinge3 | hinge2 |
| h | 1.12113mm | 0.79642mm | |
| l | 23.81mm | 3.70212 | |
| w | 5mm | 5mm | |
| $\frac{h}{l}$ | 0.04709 | 0.21512 | |
| θ_{max} | 25° | 13° | |
| Elliptical flexure hinges | | | |
| | hinge4 | hinge 1,hinge3 | hinge2 |
| h | 0.79491mm | 1.08129mm | |
| l | 2.46745mm | 12.333mm | |
| b | 0.7402mm | 3.6999mm | |
| w | 5mm | 5mm | |
| $\frac{h}{l}$ | 0.32216 | 0.08767 | |
| θ_{max} | 13° | 25° | |

Finally, the moment-rotation relationship for the analysis models (Tables 6.6 and 6.7) are obtained by following the procedure presented in the section. The comparison results for these moment-rotation relationships are show in Figure 6.11.

In Figure 6.11, the green line with squares describes the desired moment-rotation relationship. The black, green and blue lines with triangles describe the moment-rotation relationship for the FFCM with four corner-filletted flexure hinges (Model 1), the FFCM with three circular flexure hinges and one corner-filletted flexure hinge (Model 2) and the FFCM with three elliptical flexure hinges and one corner-filletted flexure hinge (Model 3), respectively, which are designed by using the generic design equations. The black, green and blue lines with stars describe the moment-rotation

Table 6.7: Designed flexure hinges (Small deflection design equations)

| Corner-filletted flexure hinges | | | |
|--|------------|----------------|-----------|
| | hinge4 | hinge 1,hinge3 | hinge2 |
| h | 0.96571mm | 1.13091mm | 1.41054mm |
| l | 3.03816mm | 4.941 | 9.7739mm |
| r | 0.303816mm | 0.4941 | 0.97739mm |
| w | 5mm | 5mm | 5mm |
| $\frac{h}{l}$ | 0.31786 | 0.22888 | 0.14432 |
| θ | 18° | 25° | 40° |
| Circular flexure hinges | | | |
| | hinge4 | hinge 1,hinge3 | hinge2 |
| h | 1.08930mm | 0.72860mm | |
| l | 23.1341mm | 3.38686 | |
| w | 5mm | 5mm | |
| $\frac{h}{D}$ | 0.04709 | 0.21512 | |
| θ | 25° | 13° | |
| Elliptical flexure hinges | | | |
| | hinge4 | hinge 1,hinge3 | hinge2 |
| h | 0.71805mm | 1.04571mm | |
| l | 2.22886mm | 11.9272mm | |
| b | 0.6687mm | 3.5782mm | |
| w | 5mm | 5mm | |
| $\frac{h}{l}$ | 0.32216 | 0.08767 | |
| θ | 13° | 25° | |

relationship for the FFCM with four corner-filletted flexure hinges (Model 4), the FFCM with three circular flexure hinges and one corner-filletted flexure hinge (Model 5) and the FFCM with three elliptical flexure hinges and one corner-filletted flexure hinge (Model 6), respectively, which are designed by using the small deformation design equations. From this figure, it can be seen that the relationship for these models designed by generic design equations are more close to the desired relationship than the ones designed by small deformation design equations. The error analysis diagram is shown in Figure 6.12.

The maximum error for the relationships referring to the generic design equations is 5%, while the maximum error for the ones referring to the small design equations is

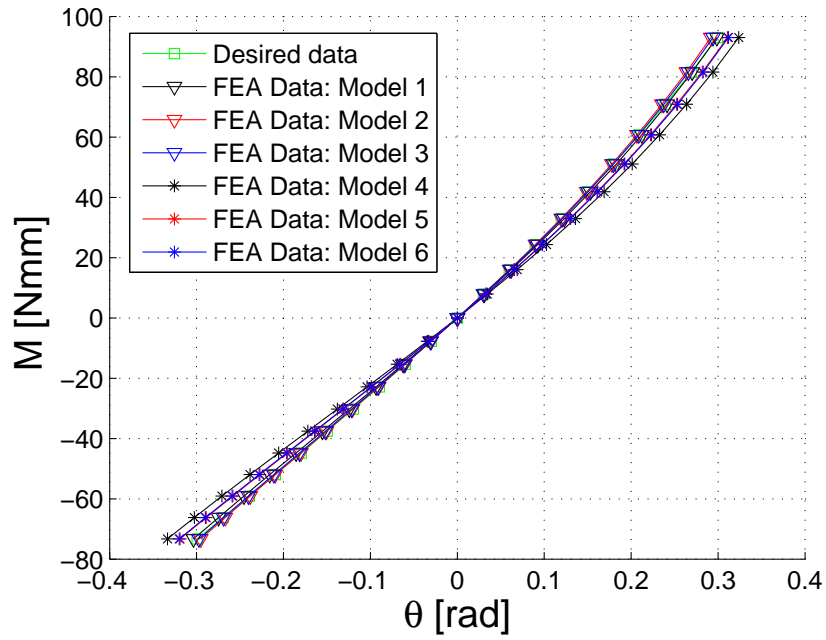


Figure 6.11: Comparison for the obtained moment-rotation relationship

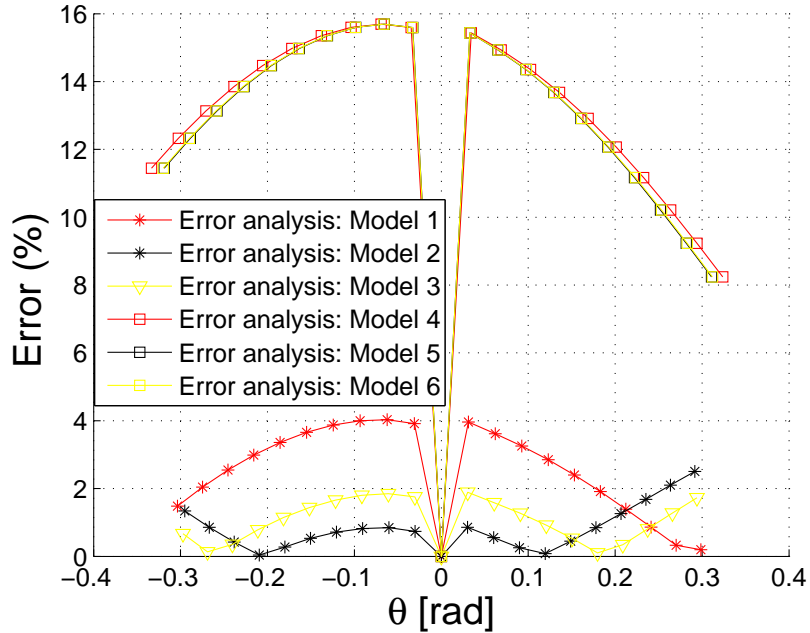


Figure 6.12: Error analysis diagram

20%. Therefore, the generic design equations are better than the small deformation

design equations.

Chapter 7

Conclusions

This thesis has presented a design method for flexure-based compliant mechanisms on the basis of their stiffness and stress characteristics. In particular, the effects of large-deflections and shear induced deformations have been addressed.

Within this scenario, three sets of design equations have been proposed for the first time, concerning three types of flexures, namely corner-filletted, circular and elliptical flexures.

As for the flexure stiffness, the proposed equations, are either function of both hinge rotational deformation and height to length ratio or function of the sole height to length ratio. In the first case, a more accurate model is achieved. In the second case, the model is more convenient for design purposes but less accurate.

As for the flexure stress, another set of design equations have been derived. For each kind of geometry, once the flexure material is chosen, these relations can be conveniently used for predicting the maximum achievable rotation before failure.

At last, as a case study, a flexure-based four bar compliant mechanism (FFCM) has been synthesized and simulated by means of finite element analysis. Numerical results confirm that the proposed design equations outperform previously published results when modeling thick cross-section hinges undergoing large deflections.

In conclusion, both the stiffness and the stress equations presented in this thesis might contribute to the fields of compliant mechanisms by conveniently simplifying their conceptual design and synthesis.

Bibliography

- [1] A.K. Mallik A. Banerjee, B. Bhattacharya. Large deflection of cantilever beams with geometric non-linearity: analytical and numerical approaches. *International Journal of Non-Linear Mechanics*, 43:366–376, 2008.
 - [2] S. N. Kramer A. Saxena. A simple and accurate method for determining large deflections in compliant mechanisms subjected to end forces and moments. *Transactions of the ASME*, 120:392–400, 1998.
 - [3] S. Awtar. *Syntheis and analysis of parallel kinematic XY flexure mechanisms*. PhD thesis, Massachusetts Institute of Technology, 2004.
 - [4] L. L. Howell B. D. Jensen. The modeling of cross-axis flexural pivots. *Mechanism and Machine Theory*, 37:461–476, 2001.
 - [5] B. D. Jensen A. R. Hawkins S. M. Schultz B. J. Hansen, C. J. Carron. Plastic latching accelerometer based on bistable compliant mechanisms. *Smart Materials and Structures*, 16:1967–1972, 2007.
 - [6] E. Garcia B. J. Pokines. A smart material microamplification mechanism fabricated using liga. *Smart Mater. Struct.*, 7:105–112, 1998.
 - [7] N. G. Dagalakis J. J. Gorman B. Kang, J. T. Wen. Analysis and design of parallel mechanisms with flexure joints. *IEEE Transactions on Robotics*, 21:1179–1185, 2005.
 - [8] S. Kota B. P. Trease, Y. Moon. Design of large-displacement compliant joints. *Transactions of the ASME*, 127:788–798, 2005.
 - [9] G. B. Chung W. K. Kim H. Suh B. Yi, H. Na. Design and experiment of a 3-dof parallel micro-mechanism utilizing flexure hinges. In *Proceedings of the 2002 IEEE Intemational Conference on Robotics & Automation Washington, DC May 2002*, 2002.
-

-
- [10] G. Berselli. *On designing compliant actuators based on dielectric elastomers*. PhD thesis, University of Bologna, 2009.
- [11] Sridhar Kota Charles Kim, editor. *Design of a novel compliant transmission for secondary microactuators in disk drives*. Proceedings of DETC 02 2002 ASME Design Engineering Technical Conference September 29–October 2, 2002, Montreal, Canada, 2002.
- [12] J. Njuguna D. Bandopadhyaya. Estimation of bending resistance of ionic polymer metal composite (ipmc) actuator following variable parameters pseudo-rigid body model. *Materials Letters*, 63:745–747, 2009.
- [13] H. M. J. R. Soemers D. M. Brouwer, B. R. de Jong. Design and modeling of a six dofs mems-based precision manipulator. *Precision Engineering 34 (2010) 307319*, 34:307–319, 2010.
- [14] X. Liu Y. Tian D. Zhang, D.G. Chetwynd. Investigation of a 3-dof micro-positioning table for surface grinding. *Mechanical Sciences*, 48:1401–1408, 2006.
- [15] J. Cai G. Xiao D. Zhu, Y. Feng. Kinematic analysis of 3-dof perpendicular parallel manipulator with flexure hinge. In *2010 Third International Conference on Knowledge Discovery and Data Mining*, 2010.
- [16] Y. Du G. Chen, X. Liu. Elliptical-arc-fillet flexure hinges: toward a generalized model for commonly used flexure hinges. *Journal of Mechanical Design*, 133:081002, 2011.
- [17] Z. Li G. Chen, J. Jia. On hybrid flexure hinges. *IEEE Networking, Sensing and Control*:700–704, 2005.
- [18] Z. Li G. Chen, J. Jia. Right-circular corner-fillet flexure hinges. In *the 2005 IEEE International Conference on Automation Science and Engineering*, 2005.
- [19] B. D. Jensen L. L. Howell G. Chen Q. T. Aten, S. Zirbel. A tristable mechanism configuration employing orthogonal compliant mechanisms. *Journal of Mechanisms and Robotics*, 2:014501, 2010, Vol. 2 / 014501-1.
- [20] G. K. Ananthasuresh G. Krishnan. Evaluation and design of displacement-amplifying compliant mechanisms for sensor applications. *Journal of Mechanical Design*, 130:102304, 2008.
-

-
- [21] U. Goebelue. Beam theories: the difference between euler-bernoulli and timoschenko. Like a lecture.
- [22] L. Wang Z. Zhong H. Ma, S. Yao. Analysis of the displacement amplification ratio of bridge-type flexure hinge. *Sensors and Actuators*, 132:730–736, 2006.
- [23] S. Bi H. Zhao. Stiffness and stress characteristics of the generalized cross-spring pivot. *Mechanism and Machine Theory*, 45:378–391, 2010. about constant stiffness, I kneed to read it carefully.
- [24] L. L. Howell. *Compliant mechanisms*. A Wiley-Interscience Publicationb, 2002.
- [25] H. Kunzmann J. Hesselbach, A. Raatza. Performance of pseudo-elastic flexure hinges in parallel robots for micro-assembly tasks. *CIRP Annals - Manufacturing Technology*, 53:329–332, 2004.
- [26] A. J. Bard J. Kwak. Scanning electrochemical microscopy. apparatus and two-dimensional scans of conductive and insulating substrates. *American Chemical Society*, 61:1794–1799, 1989.
- [27] D. Gweon K. S. Moon J. W. Ryu, S. Lee. Inverse kinematic modeling of a coupled flexure hinge mechanism. *Mechatronics*, 9:657–674, 1999.
- [28] K. S. Moon J. W. Ryu, D. Gweon. Optimal design of a flexure hinge based xy wafer stage. *Precision Engineering*, 21:18–28, 1997.
- [29] A. Midha L. L. Howell. A method for the design of compliant mechanisms with small-length flexural pivots. *Transactions of the ASME*, 116:280–290, 1994.
- [30] A. Midha L. L. Howell. Parametric deflection approximations for end-loaded, large-deflection beams in compliant mechanisms. *Transactions of the ASME*, 117:156–165, 1995.
- [31] T. W. Norton L. L. Howell, A. Midha. Evaluation of equivalent spring stiffness for use in a pseudo-rigid-body model of large-deflection compliant mechanisms. *Transactions of the ASME*, 118:126–131, 1996.
- [32] J. TSAY L. LIN, J. SHEU. Modeling and hierachical neuro-fuzzy control for flexure-based micropositioning systems. *Journal of Intelligent and Robotic Systems*, 32:411–435, 2001.
-

-
- [33] J. Li. *Electrostatic zipping actuators and their application to MEMS*. PhD thesis, Massachusetts Institute of Technology, 2004.
- [34] N. Lobontiu. *Compliant mechanisms: design of flexure hinges*. CRC Press, 2002.
- [35] Y. Luo. An efficient 3d timoshenko beam element with consistent shape functions. *Theor. Appl. Mech.*, 1:95–106, 2008.
- [36] A. Cardona M. A. Pucheta. Design of bistable compliant mechanisms using precisionposition and rigid-body replacement methods. *Mechanism and Machine Theory*, 45:304–326, 2010.
- [37] D. Trumper M. Holmes, R. Hocken. The long-range scanning stage: a novel platform for scanned-probe microscopy. *Precision Engineering*, 24:191–209, 2000.
- [38] B. Shirinzadeh M. N. M. Zubir. Development of a high precision flexure-based microgripper. *Precision Engineering*, 33:362–370, 2009.
- [39] Y. Tian M. N. M. Zubir, B. Shirinzadeh. Development of a novel flexure-based microgripper for high precision micro-object manipulation. *Sensors and Actuators A: Physical*, 150:257–266, 2009.
- [40] Y. Tian M. N. M. Zubir, B. Shirinzadeh. Development of novel hybrid flexure-based microgrippers for precision micro-object manipulation. *Review of Scientific Instruments*, 80:065106, 2009.
- [41] Y. Tian M. N. M. Zubir, B. Shirinzadeh. A new design of piezoelectric driven compliant-based microgripper for micromanipulation. *Mechanism and Machine Theory*, 44:2248–2264, 2009.
- [42] X. Wang Y. Mei M. Yu Wang, S. Chen. Design of multi-material compliant mechanisms using level set methods. *Journal of Mechanical Design*, 127:941–956, 2005.
- [43] E. Garcia N. Lobontiu. Analytical model of displacement amplification and stiffness optimization for a class of flexure-based compliant mechanisms. *Computers & Structures*, 81:2797–2810, 2003.
-

-
- [44] E. Garcia N. Lobontiu. Static response of planar compliant devices with small-deformation flexure hinges. *Mechanics Based Design of Structures and Machines*, 32:459–490, 2004.
- [45] E. Garcia N. Lobontiu. Stiffness characterization of corner-filletted flexure hinges. *Review of Scientific Instruments*, 75:4896–4905, 2004.
- [46] E. Garcia M. Goldfarb N. Lobontiu, J. S. N. Paine. Corner-filletted flexure hinges. *Transactions of the ASME*, 123:346–352, 2001.
- [47] E. Garcia M. Goldfarb N. Lobontiu, J. S. N. Paine. Design of symmetric conic-section flexure hinges based on closed-form compliance equations. *Mechanism and Machine Theory*, 37:477498, 2002.
- [48] E. O' Malley M. Samuelson N. Lobontiu, J. S.N. Paine. Parabolic and hyperbolic flexure hinges: flexibility, motion precision and stress characterization based on compliance closed-form equations. *Precision Engineering*, 26:183–192, 2002.
- [49] J. S. N. Paine N. Lobontiu. Design of circular cross-section corner-filletted flexure hinges for three-dimensional compliant mechanisms. *Journal of Mechanical Design*, 124:479–484, 2002.
- [50] Y. Takase N.i Noda. Generalized stress intensity factors of v-shaped notch in a round bar under torsion, tension, and bending. *Engineering Fracture Mechanics*, 70:1447–1466, 2003.
- [51] T. Sinh O. J. Aldraihem, R. C. Wetherhold. Intelligent beam structures: Timoshenko theory vs. euler bernoulli theory. In *the 1996 IEEE International Conference on Control Applications*, 1996.
- [52] M. M. Gupta P. R. Ouyang, W. J. Zhang. A new compliant mechanical amplifier based on a symmetric five-bar topology. *Journal of Mechanical Design*, 130:104501, 2008.
- [53] P. M. Ferreira Q. Yao, J. Dong. Design, analysis, fabrication and testing of a parallel-kinematic micropositioning xy stage. *International Journal of Machine Tools & Manufacture*, 47:946–961, 2007.
- [54] E. R. Marsh R. R. Vallance, B. Haghghian. A unified geometric model for designing elastic pivots. *Precision Engineering*, 32:278–288, 2008.
-

-
- [55] A. H. Slocum S. Awtar. Constraint-based design of parallel kinematic xy flexure mechanisms. *Transactions of the ASME*, 129:816–830, 2007.
- [56] J. Yu S. Bi, H. Zhao. Modeling of a cartwheel flexural pivot. *Journal of Mechanical Design*, 131:061010, 2009.
- [57] M. Y. Wang S. Chen. Design distributed compliant mechanisms with characteristic stiffness. In *The ASME 2007 International Design Engineering Technical Conferences & Computers and Information in Engineering Conference*, 2007.
- [58] S. S. Li S. H. Chang. A high resolution long travel friction-drive micropositioner with programmable step size. *Review of Scientific Instruments*, 70:2776–2782, 1999.
- [59] G. Liu S. K. Koh. Optimal plane beams modelling elastic linear objects. *Robotica: Cambridge University Press*, Robotica:1–14, 2009.
- [60] Z. Kreiner B. Trease J. Arenas J. Geiger S. Kota, K. J. Lu. Design and application of compliant mechanisms for surgical tools. *Journal of Biomechanical Engineering*, 127:981–989, 2005.
- [61] J. Dong S. Polit. Design of high-bandwidth high-precision flexure-based nanopositioning modules. *Journal of Manufacturing Systems*, 28:71–77, 2009.
- [62] J. S. Dale Y. Xu S. T. Smith, V. G. Badami. Elliptical flexure hinges. *Review of Scientific Instruments*, 68:1474–1483, 1997.
- [63] J. B. Lee S.H Chang. Design of a long range nano-scale resolution mechanism. *Journal of Zhejiang University-SCIENCE A (Applied Physics & Engineering)*, 11(4):250–254, 2010.
- [64] M. Chen C. Lin Li-Chen Fu S.h Huang, S. Hung. A novel six-dof electromagnetic precision positioner utilizing hybrid magnetic and fluid mechanism. In *The 33rd Annual Conference of the IEEE Industrial Electronics Society (IECON)*, 2007.
- [65] H. Su. A load independent pseudo-rigid-body 3r model for determining large deflection of beams in compliant mechanisms. In *The ASME 2008 International Design Engineering Technical Conference & Computer and Information in Engineering Conference*, 2008.
-

-
- [66] A. Belendez T. Belendez, C. Neipp. Large and small deflections of a cantilever beam. *European Journal of Physics*, 23:371–379, 2002.
- [67] S. KURANISHI T. IWAKUMA. How much contribution does the shear deformation have in a beam theory. *Structural Eng./Earthquake Eng.*, 344:141–151, 1984.
- [68] B. D. Jensen T. M. Pendleton. Compliant wireform mechanisms. *Journal of Mechanical Design*, 130:122302, 2008.
- [69] Y. M. Tseytlin. Notch flexure hinges: An effective theory. *Review of Scientific Instruments*, 73:3363–3368, 2002.
- [70] C. C. Tutum U. Snmez. A compliant bistable mechanism design incorporating elastica buckling beam theory and pseudo-rigid-body model. *Journal of Mechanical Design*, 130:042304, 2008.
- [71] Z.J. Du W. Dong, L.N. Sun. Design of a precision compliant parallel positioner driven by dual piezoelectric actuators. *Sensors and Actuators A: Physical*, 135:250256, 2007.
- [72] H. Tragter F. J. A. M. van Houten W. O. Schotborgh, F. G.M. Kokkeler. Dimensionless design graphs for flexure elements and a comparison between three flexure elements. *Precision Engineering*, 29:41–47, 2005.
- [73] C. M. Wang. Timoshenko beam-bending solutions in terms of euler bernoulli solutions. *Journal of Engineering Mechanics*, June:763–765, 1995.
- [74] G. Zong S. Bi X. Pei, J. Yu. An effective pseudo-rigid-body method for beam-based compliant mechanisms. *Precision Engineering*, 32:634–639, 2010.
- [75] G. Zong S. Bi X. Pei, J. Yu. The stiffness model of leaf-type isosceles-trapezoidal flexural pivots. *Journal of Mechanical Design*, 130:082303, 2008.
- [76] G. Zong S. Bi H. Su X. Pei, J. Yu. The modeling of cartwheel flexural hinges. *Mechanism and Machine Theory*, 44:1900–1909, 2009.
- [77] G. Zong S. Bi Z. Yu X. Pei, J. Yu. Analysis of rotational precision for an isosceles-trapezoidal flexural pivot. *Journal of Mechanical Design*, 130:052302, 2008.
-

-
- [78] H. S. Yang X. S. Sua. Design of compliant microleverage mechanisms. *Sensors and Actuators*, 87:146–156, 2001.
- [79] M. Wang Y. Gao. The refined theory of deep rectangular beams for symmetrical deformation. *Science in China Series G: Physics, Mechanics & Astronomy*, 52:919–925, 2009.
- [80] D.I C. Handley Y. K. Yong, T. Lu. Review of circular flexure hinge design equations and derivation of empirical formulations. *Precision Engineering*, 32:63–70, 2008.
- [81] Q. Xu Y. Li. Development and assessment of a novel decoupled xy parallel micropositioning platform. *Transactions on Mechatronics*, 15:125–135, 2010.
- [82] D. Zhang Y. Tian, B. Shirinzadeh. A flexure-based five-bar mechanism for micro/nano manipulation. *Sensors and Actuators A: Physical*, 153:96–104, 2009.
- [83] D. Zhang Y. Tian, B. Shirinzadeh. Closed-form compliance equations of filleted v-shaped flexure hinges for compliant mechanism design. *Precision Engineering*, 34:92–100, 2010.
- [84] D. Zhang Y. Tian, B. Shirinzadeh. Design and dynamics of a 3-dof flexure-based parallel mechanism for micro/nano manipulation. *Microelectronic Engineering*, 87:230–241, 2010.
- [85] D. Zhang G.Alici Y. Tian, B. Shirinzadeh. Development and dynamic modelling of a flexure-based scottrussell mechanism for nano-manipulation. *Mechanical Systems and Signal Processing*, 23:957–978, 2009.
- [86] D. Zhang X. Liu D. Chetwynd Y. Tian, B. Shirinzadeh. Design and forward kinematics of the compliant micro-manipulator with lever mechanisms. *Precision Engineering*, 3:466–475, 2009.
- [87] D. Zhang Y. Zhong Y. Tian, B. Shirinzadeh. Three flexure hinges for compliant mechanism designs based on dimensionless graph analysis. *Precision Engineering*, 34:92–100, 2010.
- [88] X. Zhao Q. J. Ge Y. Yue, F. Gao. Relationship among input-force, payload, stiffness and displacement of a 3-dof perpendicular parallel micro-manipulator. *Mechanism and Machine Theory*, 45:756771, 2010.
-

Acknowledgment

First of all, I would like to thank my supervisor: Prof. Vincenzo Parenti Castelli, who has not only given me the opportunity to work in this doctoral project and supervised me throughout my three-year PhD studying and research, but also has cared about me, encouraged me continuously and helped me to solve any problems what he could do for me. His academic professional ability, patient and spirits have deeply moved me. It is my greatly honor to learn from him. I would also like to thank Dr. Giovanni Berselli for his selfless help, patient and guidance on my research for three years, and Dr. Rocco Vertechy for every fruitful conversation about my research. The period of working with them will be a great memories to me.

I would like to give my acknowledgement to Dr. Guangbo Hao, a lecturer in University College Cork, who has given me great help on my work and my final thesis. An acknowledgement goes specially to his wife, my lovely friend, Xiuyun He, a PhD student in Heriot-Watt University for her encouragement, support and understanding to me. In addition, I would like to thank Prof. Shunjun Li for his kind help and supports. I couldn't't realize my dream without his help.

I would also like to thank my colleagues in GRAB, especially, Marco Carricato and Benedetta Baldiselli who gave me huge help and warmth when I just arrived at Bologna. I will never forget you. In addition, I would like to thank my friend, Miss Dan Li for her support, her heart and tolerance. I thank all of my friends in China for their understanding and supporting. I also thank all of my friends in Italy, I couldn't't always be such happiness without all of you.

At last, many thanks go to my great mother, Mrs. Jingxue Xu, I can be me because of you. I also would like to thank my lovely sister Jiamei Meng and her husband, Yimin Zhao. I can do what I want because of your support and help. Thanks a lot for your unconditioned help and support throughout the years. What you have done for me is huge and will be in my heart forever.
